

12-1-2013

## Experimental and Finite Element Studies of Shock Transmission

Eldon Jerry Goddard

University of Nevada, Las Vegas, eldongoddard@gmail.com

Follow this and additional works at: <https://digitalscholarship.unlv.edu/thesesdissertations>



Part of the [Applied Mechanics Commons](#)

---

### Repository Citation

Goddard, Eldon Jerry, "Experimental and Finite Element Studies of Shock Transmission" (2013). *UNLV Theses, Dissertations, Professional Papers, and Capstones*. 1990.

<https://digitalscholarship.unlv.edu/thesesdissertations/1990>

This Thesis is protected by copyright and/or related rights. It has been brought to you by Digital Scholarship@UNLV with permission from the rights-holder(s). You are free to use this Thesis in any way that is permitted by the copyright and related rights legislation that applies to your use. For other uses you need to obtain permission from the rights-holder(s) directly, unless additional rights are indicated by a Creative Commons license in the record and/or on the work itself.

This Thesis has been accepted for inclusion in UNLV Theses, Dissertations, Professional Papers, and Capstones by an authorized administrator of Digital Scholarship@UNLV. For more information, please contact [digitalscholarship@unlv.edu](mailto:digitalscholarship@unlv.edu).

EXPERIMENTAL AND FINITE ELEMENT STUDIES OF SHOCK TRANSMISSION  
THROUGH COMPOSITE STRUCTURES

by

Eldon Jerry Goddard

Bachelor of Science  
University of Nevada Las Vegas  
December 2009

A thesis submitted in partial fulfillment  
of the requirements for the

Master of Science - Mechanical Engineering

Department of Mechanical Engineering  
Howard R. Hughes College of Engineering  
The Graduate College

University of Nevada Las Vegas  
December 2013



THE GRADUATE COLLEGE

We recommend the thesis prepared under our supervision by

**Eldon Goddard**

entitled

**Experimental and Finite Element Studies of Shock Transmission  
through Composite Structures**

is approved in partial fulfillment of the requirements for the degree of

**Master of Science in Engineering - Mechanical Engineering  
Department of Mechanical Engineering**

Brendan O'Toole, Ph.D., Committee Chair

Yi-Tung Chen, Ph.D., Committee Member

Mohamed B. Trabia, Ph.D., Committee Member

Samaan G. Ladkany, Ph.D., Graduate College Representative

Kathryn Hausbeck Korgan, Ph.D., Interim Dean of the Graduate College

**December 2013**

## ABSTRACT

Composite materials are more widely used today in engineering products than ever before. Shock transmission in jointed composite sections needs to be investigated to understand the affect of composite materials on the dynamic response of the system. There exists limited published work on transient shock propagation through composite sections. The aim of this study is to analyze the transient behavior of joints in composite materials subjected to low impact loads and to develop a computational model that provides an improved physics based shock model. The jointed connection will be investigated experimentally and using Finite Element Analysis (FEA). The bolted joint will be the type of connection investigated. This is a commonly used joint for composite assemblies. For simplicity a simple hat section and cantilever beam structure are chosen for investigation. The initial case study verifies the experimental and finite element results on the individual cantilever beam structure by comparing the accuracy of the finite element results of an aluminum cantilever beam to the composite cantilever beams. The second study investigates the composite bolted hat structure response to low impact shock loading. Two different composite lamina orientations were chosen, a 0/90 plain weave bidirectional composite and a 0° unidirectional composite. The structures are subjected to low impact loading (nondestructive) using a modally tuned impact hammer. Accelerations and impact force are recorded using an accelerometer and the modally tuned impact hammer respectively. A Normalized Root Mean Square Difference (NRMSD) criterion was used to compare the experimental results to the FEA results.

## ACKNOWLEDGEMENTS

I would like to thank Dr. Brendan O'Toole, my advisor, for his help, knowledge, and patience throughout this project. I would also like to thank those on my committee Dr. Mohamed Trabia, Dr. Yi-tung Chen, and Dr. Samaan Ladkany. There are many I would like to mention for their technical help and expertise including Dr. Jagadeep Thota, Deepak Sankar, and Shawoon Roy. I would like to thank Dr. Douglas Reynolds for his generosity in lending me experimental equipment. I also like to thank Jeffery Markle and Jon Becker for their assistance. I would like to make special mention of Joan Conway for all her help, it is greatly appreciated. Thank you.

To my friends who made the years of work and research at UNLV enjoyable I thank you. To Benjamin Mead, Siul Ruiz, Adam Kessler, Sebastian Uppapalli, and Chris Salisbury my friends and companions through the long hours in the lab, meeting you guys was the highlight of my graduate career. To my long time friends Chris Ryan, Ben Stoner, Cory "Quincy" Roundy, Derrick "Beardrick" Yates, Logan Battles, and Kyle Carlson thank you for keeping my spirits up. Finally I would like to thank my family for their support and encouragement.

## DEDICATION

To my mother and father,

thank you for all your love and support.

## TABLE OF CONTENTS

ABSTRACT.....	iii
ACKNOWLEDGEMENTS.....	iv
TABLE OF CONTENTS.....	vi
LIST OF TABLES.....	viii
LIST OF FIGURES.....	x
CHAPTER 1 INTRODUCTION.....	1
1.1 Background.....	1
1.2 Literature Review.....	3
1.3 Thesis Objectives.....	10
CHAPTER 2 COMPOSITE MATERIALS AND FABRICATION & PROPERTIES .	12
2.1 Introduction.....	12
2.2 Composite Fabrication Procedure.....	13
2.3 Determination of Fiber Volume Fraction.....	14
2.4 Analytical Determination of Woven Fabric Composite Elastic Properties.....	16
2.5 Analytical Determination of Unidirectional Composite Elastic Properties.....	21
2.6 Estimated Physical and Elastic Properties.....	22
CHAPTER 3 DYNAMIC EXPERIMENTAL PROCEDURES.....	23
3.1 Introduction.....	23
3.2 Experimental Equipment.....	23
3.3 Experimental Set-up for Cantilever Beam Structures.....	26
3.4 Experimental Set-up of Unconstrained Structures without Joints.....	32
CHAPTER 4 ANALYSIS OF COMPOSITE CANTILEVER BEAM.....	39
4.1 Background.....	39
4.2 Experimental Calibration of Equipment.....	40
4.3 Repeatability and Consistency Test.....	40
4.4 Experimental, Analytical, and Finite Element Analysis of Cantilever Beam Natural Frequencies.....	48
4.5 Mode Shapes of Cantilever Beams.....	61
4.6 Transient Analysis of Cantilever Beam.....	62

CHAPTER 5 ANALYSIS OF BOLTED HAT STRUCTURE .....	78
5.1 Background .....	78
5.2 Natural Frequency Analysis of Hat Section .....	79
5.3 Mode Shapes of Hat Section .....	85
5.4 Preload on Bolt.....	85
5.5 Time History Analysis of Composite Bolted Hat Structure.....	87
5.6 Summary of Results .....	104
CHAPTER 6 CONCLUSIONS AND FUTURE WORK.....	105
APPENDIX A: MODE SHAPES OF ALUMINUM CANTILEVER BEAM (277, 720, 1392, 1607, and 2307 Hz).....	107
APPENDIX B: MODE SHAPES OF UNIDIRECTIONAL COMPOSITE CANTILEVER BEAM (198, 476, 940, 1514, and 2430 Hz).....	109
APPENDIX C: MODE SHAPES OF WOVEN FABRIC COMPOSITE CANTILEVER BEAM (137, 330, 647, and 1074 Hz).....	111
APPENDIX D: MODE SHAPES OF UNIDIRECTIONAL COMPOSITE HAT (127, 410, and 623 Hz).....	113
APPENDIX E: MODE SHAPES OF WOVEN FABRIC COMPOSITE HAT (86, 264, 418, 1149 and 1241 Hz).....	115
REFERENCES .....	117
VITA.....	120



## LIST OF TABLES

Table 1: Properties of Carbon Fiber Fabrics.....	14
Table 2: Fiber Mass Fraction .....	14
Table 3: Measure Density .....	15
Table 4: Fiber Volume Fraction.....	16
Table 5: Elastic Properties of Yarn Materials.....	17
Table 6: Estimated Physical and Elastic Properties .....	22
Table 7: Fundamental Frequency of Cantilever Beams.....	55
Table 8: Comparison of Analytical and Experimental Natural Frequencies of Cantilever Beams.....	55
Table 9: Mass Test for Cantilever Beams.....	59
Table 10: Total Number of Elements and Nodes for Mesh Optimization.....	59
Table 11: Natural Frequencies of Aluminum Cantilever Beam .....	59
Table 12: Natural Frequencies of Unidirectional Composite Cantilever Beam .....	60
Table 13: Natural Frequencies of Woven Fabric Composite Cantilever Beam.....	60
Table 14: Aluminum Cantilever Beam Natural Frequency Error of FEA.....	60
Table 15: Unidirectional Composite Cantilever Beam Natural Frequency Error of FEA	60
Table 16: Woven Fabric Composite Cantilever Beam Natural Frequency Error of FEA	61
Table 17: NRMSD of Experimental and FEA Cantilever Beam Time History .....	69
Table 18: Damping Factor for Composite Cantilever Beams.....	71
Table 19: Stiffness Reduction from *DAMPING_FREQUENCY_RANGE.....	72
Table 20: NRMSD of Experimental and FEA with Damping Cantilever Beam Time History.....	76

Table 21: Mass Test of Hat.....	83
Table 22: Mass Test of Improved Hat .....	83
Table 23: Nodes and Elements of Finite Element Model of Hat.....	84
Table 24: Natural Frequencies of Unidirectional and Woven Fabric Hat .....	84
Table 25: Nodes and Elements of Unidirectional Finite Element Model and Woven Fabric Finite Element Model .....	96
Table 26: NRMSD of Time History of Accelerometer 1 and Accelerometer 2 Unidirectional Composite Bolted Hat Structure and Woven Fabric Composite Bolted Hat Structure.....	101

## LIST OF FIGURES

Figure 1: Non-Hybrid Weaves.....	6
Figure 2: Idealization of Woven Fabric Composite Using Mosiac Model.....	17
Figure 3: Accelerometer .....	24
Figure 4: Impact Hammer.....	25
Figure 5: Current Source.....	25
Figure 6: Handheld Shaker Calibrator .....	26
Figure 7: Experimental Set-up for Cantilever Beam Test .....	27
Figure 8: Aluminum Cantilever Beam.....	28
Figure 9: Unidirectional Composite Cantilever Beam.....	28
Figure 10: Woven Fabric Composite Cantilever Beam .....	29
Figure 11: Experimental Cantilever Beam Fixture.....	31
Figure 12: Cantilever Beam Experiment Layout (X marks Hammer Impact and O Marks Accelerometer).....	31
Figure 13: Unidirectional Composite Hat.....	33
Figure 14: Woven Fabric Composite Hat .....	33
Figure 15: Hanging Mass Structure for Unconstrained Structure without Joints Experiment.....	34
Figure 16: Experimental Set-up for Unconstrained Structure without Joints Experiment	34
Figure 17: Bolted Hat Structure.....	36
Figure 18: Hanging Mass Structure for Unconstrained Bolted Hat Structure Experiment .....	36
Figure 19: Experimental Set-up for Unconstrained Bolted Hat Structure Experiment ....	37

Figure 20: Location of Accelerometers (O) and Impact (X) on Unconstrained Bolted Hat Structure.....	37
Figure 21: Time History Response of Aluminum Cantilever Beam Repeatability Test ..	42
Figure 22: Frequency Response of Aluminum Cantilever Beam Repeatability Test.....	42
Figure 23: Impact Force of Aluminum Cantilever Beam Repeatability Test.....	43
Figure 24: Frequency Response of Impact Force of Aluminum Cantilever Beam Repeatability Test .....	43
Figure 25: Time History Response Unidirectional Composite Cantilever Beam Repeatability Test .....	44
Figure 26: Frequency Response of Unidirectional Composite Cantilever Beam Repeatability Test .....	44
Figure 27: Impact Force of Unidirectional Composite Cantilever Beam Repeatability Test .....	45
Figure 28: Frequency Response of Impact Force of Unidirectional Composite Cantilever Beam Repeatability Test.....	45
Figure 29: Time History Response of Woven Fabric Cantilever Beam Repeatability Test .....	46
Figure 30: Frequency Response of Woven Fabric Composite Cantilever Beam Repeatability Test .....	46
Figure 31: Impact Force of Woven Fabric Composite Cantilever Beam Repeatability Test .....	47
Figure 32: Frequency Response of Impact force of Woven Fabric Composite Repeatability Test .....	47

Figure 33: Impact Force for Aluminum Cantilever Beam Analysis.....	49
Figure 34: Time History Response of Aluminum Cantilever Beam.....	50
Figure 35: Frequency Response of Aluminum Cantilever Beam .....	50
Figure 36: Impact Force for Unidirectional Composite Cantilever Beam.....	51
Figure 37: Time History Response of Unidirectional Composite Cantilever Beam .....	51
Figure 38: Frequency Response of Unidirectional Composite Cantilever Beam .....	52
Figure 39: Impact Force of Woven Fabric Composite Cantilever Beam .....	52
Figure 40: Time History Response of Woven Fabric Composite Cantilever Beam.....	53
Figure 41: Frequency Response of Woven Fabric Composite Cantilever Beam .....	53
Figure 42: Cantilever Beam Meshed with Shell Elements (Coarse, Medium, Fine) .....	57
Figure 43: Cantilever Beam with Solid Mesh 2, 4, and 6 Elements along the Thickness	58
Figure 44: Finite Element Model of Cantilever Beam Experiment Showing Constraints, Impact Force, and Accelerometer Placement .....	63
Figure 45: Time History Plot of Aluminum Cantilever Beam Experimental and FEA....	66
Figure 46: Frequency Domain of Aluminum Cantilever Beam Experimental and FEA..	67
Figure 47: Time History Plot of Unidirectional Composite Cantilever Beam Experimental and FEA .....	67
Figure 48: Frequency Domain of Unidirectional Composite Cantilever Beam Experimental and FEA.....	68
Figure 49: Time History Plot of Woven Fabric Composite Cantilever Beam Experimental and FEA .....	68
Figure 50: Frequency Domain of Woven Fabric Composite Cantilever Beam Experimental and FEA.....	69

Figure 51: Time History Plot of Unidirectional Composite Cantilever Beam FEA with Damping.....	74
Figure 52: Frequency Domain of Unidirectional Composite Cantilever Beam FEA with Damping.....	75
Figure 53: Time History Plot of Woven Fabric Composite Cantilever Beam FEA with Damping.....	75
Figure 54: Frequency Domain of Woven Fabric Composite Cantilever Beam FEA with Damping.....	76
Figure 55: Force Impact Curve Unidirectional Hat .....	80
Figure 56: Time History Plot of Unidirectional Hat Experimental Unfiltered and Filtered .....	80
Figure 57: Frequency Domain of Unidirectional Composite Hat.....	81
Figure 58: Impact Force Curve of Woven Fabric Hat .....	81
Figure 59: Time History Plot of Woven Fabric Composite Hat Experimental Unfiltered and Filtered .....	82
Figure 60: Frequency Domain Plot of Woven Fabric Composite Hat.....	82
Figure 61: Finite Element Model of Hat.....	84
Figure 62: Bolt Preload.....	87
Figure 63: Impact Force Curve for Unidirectional Composite Bolted Hat Structure.....	88
Figure 64: Time History of Accelerometer 1 Unidirectional Composite Bolted Hat Structure Experimental Unfiltered and Filtered.....	88
Figure 65: Frequency Domain of Accelerometer 1 Unidirectional Composite Bolted Hat Structure .....	89

Figure 66: Time History of Accelerometer 1 Unidirectional Composite Bolted Hat Structure Experimental Unfiltered and Filtered.....	89
Figure 67: Frequency Domain of Accelerometer 2 Unidirectional Composite Bolted Hat Structure.....	90
Figure 68: Impact Force Curve for Woven Fabric Composite Bolted Hat Structure .....	90
Figure 69: Time History of Accelerometer 1 Woven Fabric Composite Bolted Hat Structure Experimental Unfiltered and Filtered.....	91
Figure 70: Frequency Domain of Accelerometer 1 Woven Fabric Composite Bolted Hat Structure.....	91
Figure 71: Time History of Accelerometer 2 Woven Fabric Composite Bolted Hat Structure Experimental Unfiltered and Filtered.....	92
Figure 72: Frequency Domain of Accelerometer 2 Woven Fabric Composite Bolted Hat Structure.....	92
Figure 73: Finite Element Model of Unidirectional Composite Bolted Hat Structure Showing Impact, Accelerometer 1, and Accelerometer 2 Location ↑, 313142, and 356942 respectively. ....	95
Figure 74: Finite Element Model of Woven Fabric Composite Bolted Hat Structure Showing Impact, Accelerometer1, and Accelerometer 2 Location↑, 247474, and 248632 respectively. ....	96
Figure 75: Time History Plot of Accelerometer 1 Unidirectional Composite Bolted Hat Structure.....	97
Figure 76: Frequency Domain of Accelerometer 1 Unidirectional Composite Bolted Hat Structure.....	97

Figure 77: Time History Plot of Accelerometer 2 Unidirectional Composite Bolted Hat Structure.....	98
Figure 78: Frequency Domain of Accelerometer 2 Unidirectional Composite Bolted Hat Structure.....	98
Figure 79: Time History Plot of Accelerometer 1 Woven Fabric Composite Bolted Hat Structure.....	99
Figure 80: Frequency Domain of Accelerometer 1 Woven Fabric Composite Bolted Hat Structure.....	99
Figure 81: Time History Plot of Accelerometer 2 Woven Fabric Composite Bolted Hat Structure.....	100
Figure 82: Frequency Domain Plot of Accelerometer 2 Woven Fabric Composite Bolted Hat Structure Experimental and FEA .....	100
Figure 83: Time History Plot of Accelerometer 2 Woven Fabric Composite Bolted Hat Structure for 10 milliseconds.....	101
Figure 84: Plot of Accelerometer 1 Unidirectional Composite Bolted Hat Structure Initial Peaks .....	103
Figure 85: Plot of Accelerometer 1 Woven Fabric Composite Bolted Hat Structure Initial Peaks .....	103



## CHAPTER 1

### INTRODUCTION

#### 1.1 Background

Every product will be subjected to low shock impacts during its operational life. Many components of the system can suffer damage from these impacts. Shock propagation is therefore important to consider when designing an engineered product. Joints are integral to how the overall system reacts to these impacts as they provide damping to the system. The most common types of joints used in the manufacture of composite assemblies are bolted and adhesive. Transient dynamic response of joints is a complex nonlinear event and is difficult to analyze analytically. A numerical solution is often chosen to analyze transient dynamic responses. The Finite Element Method (FEM) in particular is commonly used to solve these problems. The FEM is a numerical technique that gives approximate solutions to differential equations. The problem must be defined in geometrical space, which it subdivides into a finite number of smaller regions. Over each of the regions a known function is used to solve for the unknown variables. The advantage of the FEM over others is that the elements do not have to be orthogonal [1]. The FEM is not without its limitations. Many parameters must be defined in the FEA and what is chosen and how they are defined can greatly affect the result of the simulation. Joints in particular can cause problem in the FEA as they are a discontinuity of the structure and can cause errors in the result. The FEM can also be computationally demanding for complex structures for this reason the hat section and cantilever beam are used as they represent the simplest structure for the testing of shock transmission through joints.

Composite materials are materials in which one or more individual materials are made into a single material. There exist many different types of composite materials. For this study only fiber-reinforced composite materials will be used. Fiber-Reinforced composites are made of a high strength high modulus fiber embedded in or bonded to a matrix with distinct interfaces between [2]. Fiber-Reinforced composite materials are used when a high strength to weight or modulus to weight ratio are needed. Fiber-Reinforced composites are not isotropic materials, but instead their material properties vary with direction. This characteristic of fiber-reinforced composite arises from how they are made. Composite lamina can be arranged in any direction to give the best properties for product that it is designed for. This study looks at two common configurations for a composite lamina. A unidirectional  $0^\circ$  laminate and a bidirectional  $0/90^\circ$  laminate. They are also the common building blocks of more complex laminates. Carbon is a typical material used for fiber in a fiber-reinforced composite. Carbon fiber has a very high modulus to weight ratio and tensile strength to weight ratio, very low coefficient of thermal expansion, high fatigue strength, and high thermal conductivity and this makes it ideal for aerospace and special automotive applications. Carbon fibers drawbacks include its low failure strain, high electrical conductivity, and most importantly for this work its low impact resistance. Carbon fiber gets its high tensile strength from its graphite form. The graphite forms crystallographic structure of parallel interconnecting planes. The strong covalent bonds between these carbon atoms in the planes and the weaker van der Waals forces between the planes give carbon fiber its anisotropic mechanical properties. Carbon fiber is created by first using a precursor material, either Polyacrylonitrile (PAN) or Pitch filament. PAN being the most commonly used

precursor. The precursor is carefully heated at different stages, using changing temperatures and conditions, until graphitization occurs. During this processes many alterations can be made to the crystalline structure to achieve desired material properties [2]. Carbon fiber is used in many industries where shock from impact loading is of high interest. The prohibitive cost of materials and production have limited the used of carbon fiber composites to these applications. High costs of manufacture of carbon fiber composites further the need to understand how they react to impact loading. Epoxy is a widely used matrix material in fiber-reinforced composites. The main advantages of epoxy are its wide variety of properties, absence of volatile matters during curing, low shrinkage during curing, corrosion resistant to chemical solvents, and excellent adhesion to a wide variety of fillers, fibers, and other substrates. Epoxy is a thermoset polymer. A thermoset polymer is a polymer whose molecules are joined together by cross-links formed during polymerization [2]. Carbon fiber and an epoxy matrix were chosen as the materials used to create the fiber-reinforced composites in this study.

## 1.2 Literature Review

The effect of low impact shock transmission through joints is of interest to manufacturers of composite products. There is a need to protect components within these composite products. Joints provide a large amount of damping to the structure and are subject to failures from impact. This occurs due to the joint being a discontinuity that results in high stress concentration that leads to the failure of the structure [3]. Two of the most commonly used joints in composite structures are adhesive and bolted joints. Bolted joints are the most commonly used joint today yet there transient dynamic behavior is still not very well understood. Adhesive joints are more commonly used for composite

structures than any other as the materials lend themselves to be easily connected using this method. There has been little published work on the subject of shock propagation through joints. Doppola has done work with jointed double hat sections under low impact loading showing that both adhesive and bolted connections can be modeled with marginal error with the bolted connection showing higher margins of error than adhesive [4]. Doppola's work showed that for both adhesive and bolted connection solid models provide improved results over those of the shell element models. Fegghi worked on a bolted hat section and flat plate subject to low impact loading showed that altering various parameters of the finite element analysis had little or no effect on the results. Fegghi conducted a parametric study on the parameters, including constant types, contact surface areas, friction between parts, preload, mesh refinement, spacer and material properties and finite element output frequency. Fegghi also presented several ways to compare transient time signals [5]. Kumarswamy showed that accurate modeling of shock transmission due to high and low impact can be achieved by experimentally measuring the damping properties of the bolted connection. The measurement is placed into the finite element model through stiffness proportional damping as SPD damps out the high frequencies which are seen in the finite element models. Kumarswamy also showed several techniques for imparting pre-load on the bolt for the finite element model. Kumarswamy showed that the most accurate model for FEA of shock propagation across bolts is a 3-D model including contacts, friction, and bolt preload. This model is however more computationally demanding than the other models used in his research [3]. Semke et al investigated the dynamic structural response of piping system with bolted flanges. A simple model was used that did not include friction, preload on bolts, nor was the gasket

modeled. Results showed good correlation with natural frequencies from experimental data [6]. Kim used bolted lap joints and investigated the static stresses using FEA. Four different models were used and it was determined that the solid model provided the best results, but with approximately twice as long computational time over a spider bolt model(bolt modeled as beam elements) [7].

Much work has been done on static analysis of bolted joints. Stocchi, C. looked at bolted joints with countersunk fasteners. The effect of clearance, friction coefficient, and preload on the five states of joint behavior and numerical results were compared to experimental data. The results showed good agreement with experimental load-displacement curves. Clearance is related to the length of the Slip stage and increasing clearance leads to lower stiffness in the No-Slip stage. Friction and preload define the maximum force transmitted during the No-Slip stage [8]. Croccolo presents findings on how coatings, lubrication, manufacturing process, and spoiled/unspoiled bolted connections affect friction coefficients. It was found that with the exception of manufacturing process all of the factors play an important role in defining the friction coefficient of the bolted connection. There is no difference in joints that use forged or cast components [9].

The elastic properties of woven fabric composites are not orthotropic as unidirectional fabric composites. The interlocking of yarns leads to a transfer of stress between them. This helps woven fabrics to have higher moduli in the out of fiber direction compared to composite made with unidirectional fabrics and they exhibit elastic properties that are closer to isotropic materials. A woven fabric composite will have lower moduli in the fiber direction than a composite made from unidirectional fabric.

Several analytical and numerical solutions have been given for finding the elastic properties of woven fabric composites. Woven fabrics are made in a great number of different patterns [10]. A simple definition for a weave begins by defining a hybrid and a non-hybrid fabric, where in a non-hybrid fabric the number of interlaced warp and fill threads are equal. For non-hybrid fabrics an “ng” number can be defined where a square is made of the interlaced region and the number of warp threads represent the ng number. For a plain weave  $ng=2$ , twill  $ng=3$ , 4 harness satin  $ng=4$ .

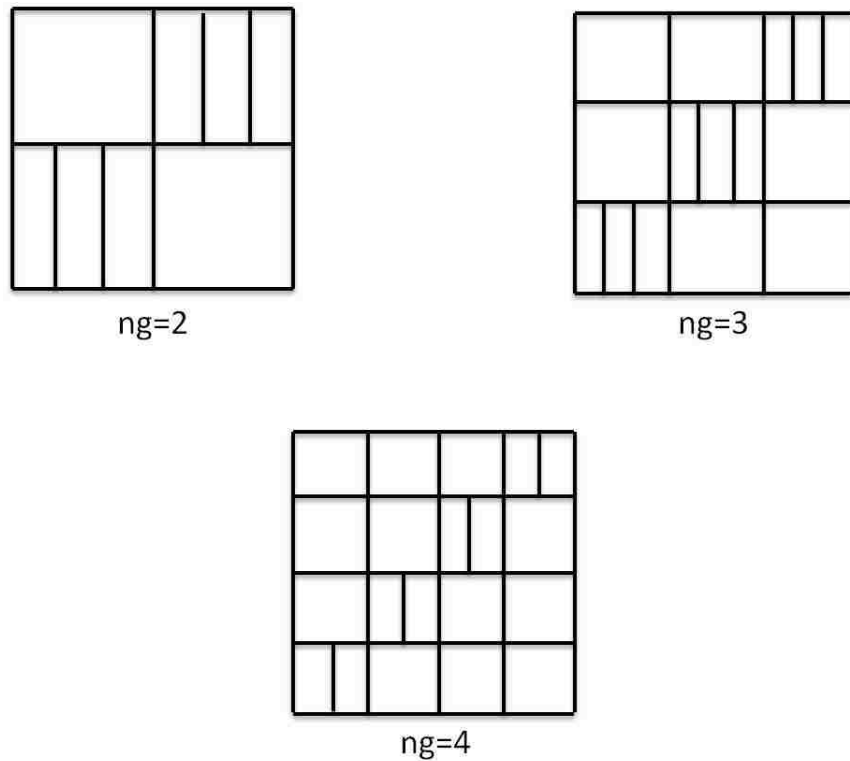


**Figure 1: Non-Hybrid Weaves**

Ishikawa, et al. provide several models for prediction of elastic properties of woven fabrics: an idealized mosaic model, a fiber undulation model, and a bridge model for weaves with  $ng \geq 4$ . The mosaic model idealizes the weave by replacing the fiber undulation with a 2-D model that has a discontinuity in the yarn at an intersection. The fiber undulation model assumes that the classical lamination theory applies to infinitesimal piece of thread wise strip and an analytical solution is found for the fiber undulation in one direction. The fiber undulation model can be used to look at the knee phenomenon of woven fabric composites. The “knee phenomenon” is the nonlinear elastic response caused by the initial failure of the fabric. The mosaic model is compared to the fiber undulation model (1-D) for plain weave fabrics. As expected the idealized mosaic model gives higher moduli as the fibers remain straight in an idealized moduli. As a result the mosaic model overestimates elastic moduli. Using 1-d fiber undulation model for “knee phenomenon” analysis shows good correlation with stress-strain results from a FEA of woven fabrics. The bridging model is used for weaves  $ng \geq 4$  satin weaves as satin weaves have spaces between interlaced regions. The bridging model shows excellent agreement with initial elastic stiffness and “knee phenomenon” from experimental results [10]. Naik, et al. investigates several methods for determining elastic material properties for woven fabric composites. Two analytical models of 2-D woven fabric composites are presented: a Series-Parallel (SP) model in which the infinitesimal pieces of a section along the loading direction are assembled with an iso-stress conditions then all sections along the loading direction are assembled with an iso-strain condition and a Parallel-Series model where all infinitesimal pieces of a sections across loading direction are assembled in an iso-strain condition and then all the sections across the

loading direction are assembled under the iso-stress condition. These models are compared to the 1-D Series model and the Crimp (Fiber Undulation) model given by Ishikawa. The new models show improved prediction of elastic properties over previous models. The P-S model is recommended for in-plane elastic properties [11]. 3-D weaves are designed for increasing the out of plane or through thickness mechanical properties. 3-D weaves are made by interlocking layers of woven fabrics and like 2-D weaves there exist multiple 3-D weaves. 3-D weaves will not be investigated in this work, but it is important to understand the physical characteristics and how they are modeled analytically as the 2-d woven fabric is a specific form of the more generalized 3-D woven fabric [12]. Hallal, et al. create an analytical three stage homogenized model (3SHM) that achieves good results for elastic material properties when compared to numerical FEM. The 3SHM shows improved results in predicting several elastic properties of 3-D woven fabric composites over the homogenized Voigt-Ruesss model [12]. Abot, et al show that for elastic properties in the through thickness direction unidirectional and woven fabric composites can be assumed to be the same with marginal error. With only compressive and shear strengths having a noticeable change between the two composites [13].

Little research has been done on the effect of joints on the shock propagation of composites, but other aspects of shock propagation in composites like the effect of fiber orientation in respect to impact have been researched in detail. Millet shows that the fiber orientation, in respect to impact direction, of the composite affects the shock response [14]. For impact in the through thickness direction the composite acts as a monolithic polymer as has been suggested by Zaretsky [15]. The response in this case is dominated by the matrix. For a composite that is impacted in a direction with fibers running parallel



to the impact direction an elastic precursor wave is seen in the fibers. For low velocity impacts the composites with fibers parallel to the impact load show a stiffer Hugoniot, but converge with composites that have fibers normal to impact at higher velocities [14]. Lukyanov gives an analytical model for an equation of state for an anisotropic material that accounts for the damage softening processing in composites.  $0^\circ$  fiber direction impact shows a decrease in shock velocity with an increasing pressure. This implies that the shock front brakes into two or more waves. A single wave and two wave structure was investigated. A composite with impact normal to fiber direction gives good correlation to experimental data with the single wave model, but the composite with impact parallel to fiber direction have poor correlation is seen with the single wave model. Both show agreement using the two wave structure model, proving that the composite with fibers parallel to the impact direction has both isotropic elastic waves and non-linear anisotropic waves due to the epoxy-carbon layers [16]. Allix, et al. proposed a meso-scale model (yarns and matrix) of a composite to model both static stresses and transient dynamic loading. Comparisons of the analytical meso-scale model were compared to experimental results, with good results being achieved for measured shock velocity in constituents and the location of the spalling plane [17]. Marshall made a 3-D Finite Element model to investigate the effect of clamping ratio, contact friction, and staking sequence. The results show that an increase in clamping ratio improves the stress state at a joint, but causes an increase in interlaminar shear stresses around the washer edge. Increasing friction decreased bearing stress in the pin joint and staking sequence effects the interlaminar normal stresses [18].

### 1.3 Thesis Objectives

This project is conducted to better understand how joints affect the overall dynamic response of composite structures to low impact loading both experimentally and numerically. It is important to have simple and accurate finite element models of shock propagation through joints so that it can be used in design of the overall model or assembly. This thesis focuses on the shock propagation through bolted joints in composite structures due to low impact loading. The objective is to obtain a simple finite element model that can give accurate results when used to simulate the shock propagation through joints of composite materials due to low impact loading.

To accomplish the objective the thesis is broken into several smaller objectives. The thesis was broken down as follows:

- Determine a simple process to compare transient signals.
- Obtain accurate material properties of the composite structures.
- Establish an experiment to calibrate the finite element method for composites.
- Conduct experiments on composite structures without joints and compare experimental and finite element results.
- Verify that finite element results can give satisfactory results for composite structures.
- Conduct experiments on composite structures with bolted connections and compare experimental and finite element results.
- Verify that finite element results can give satisfactory results for composite structures with bolted joints.

- Analyze results and make conclusions on results and what work should be done in the future.

## CHAPTER 2

### COMPOSITE MATERIALS AND FABRICATION & PROPERTIES

#### 2.1 Introduction

Composite materials, due to the nature of their production, are not isotropic. There are some composites that exhibit planar isotropic properties such as plain weave fiber reinforced composites and randomly oriented non continuous fiber reinforced composites. The two composites used in this study are a unidirectional carbon fiber reinforced composite and a plain weave woven fabric carbon fiber reinforced composite. The unidirectional composite is transversely orthotropic, where the elastic properties are equal in the directions that are not the fiber direction. The plain weave woven fabric composite is planar isotropic where in the lamina plane the elastic properties are equal.

To define the elastic properties of the composite used in this study several properties must be determined. The elastic properties of both the carbon fiber and of the epoxy resin are known. The range of densities for epoxy resin varies so it was necessary to determine the density of the specific epoxy resin used in to make the composites. From the mass measurement and density measurement taken from the composites it is possible to obtain the fiber volume fraction. With the elastic properties of the components and the fiber volume fraction of the composite the elastic properties of the unidirectional composite can be found. The woven fabric composite elastic properties are more difficult to obtain. In a woven fabric lamina the yarns of fiber undulate, which causes the elastic properties to be reduced from that of an idealized lamina with no undulation.

## 2.2 Composite Fabrication Procedure

There are several methods that are used in the fabrication of fiber reinforced composites. Carbon fiber reinforced composites are made in the same way as other fiber reinforced composites. The most common methods for the preparation of industrial composites include bag-molding, compression molding, filament winding, and liquid composite molding. For the geometries and designs of these experiments the bag-molding process is ideal. The bag-molding process is commonly used in the aerospace industry for the creation of carbon fiber composites. The bag-molding process uses impregnated carbon fiber sheets which are placed under a vacuum and heated in an autoclave. Although not commonly used for the production of carbon fiber composites a hand lay-up was used as access to an autoclave was not available. The hand lay-up method consists of wetting out individual layers of fiber with a matrix until the desired dimensions are met. A simple hand layup was used for creation of all carbon fiber composite specimens used in this study. All composites were fabricated under atmospheric pressure.

The fabrication process included two cantilever beams and four hat sections. The epoxy used in the fabrication of all composites is U.S Composites 635 Thin Epoxy Resin 3:1 Medium Epoxy Hardener. The two composite cantilever beams include a unidirectional carbon fiber reinforced composite and a plain weave woven fabric carbon fiber reinforced composite. The unidirectional carbon fiber fabric used is Soller Composites T700 Carbon Fiber Uni-directional fabric. All unidirectional carbon fiber composites were constructed using 6 layers of fabric. The woven fabric carbon fiber fabric used is Fiberglast 3k Plain Weave Carbon Fiber. All woven fabric carbon fiber composites were constructed using 9 layers of fabric. The unidirectional composites were

slightly larger than the woven fabric composites due to the increased thickness of the unidirectional fabric. The properties of the carbon fiber fabrics used to fabricate the unidirectional carbon fiber reinforced composite and the woven fabric composite are given in Table 1.

**Table 1: Properties of Carbon Fiber Fabrics**

Carbon Fiber	Tensile Modulus	Fabric Thickness	Fabric Width	Areal Weight
Unidirectional	234.4 GPa	.3556 mm	.6096 m	305 g/m <sup>2</sup>
Woven Fabric	227.5-240.6 Gpa	.3048 mm	1.27 m	193 g/m <sup>2</sup>

### 2.3 Determination of Fiber Volume Fraction

In order to determine the overall fiber volume fraction of the composite the mass of the fiber used to construct the composite is measured before the composite is made. After the composite has cured the finished part is measured for the total mass of the composite. Dividing the finished composite mass by the fiber mass a fiber mass fraction can be estimated. This gives an average mass fraction over the composite, which does not account for the local differences in mass fraction. The resulting fiber mass fraction for the composites is given in Table 2.

**Table 2: Fiber Mass Fraction**

	Cant Beam Uni	Cant Beam WF	Hat 1 Uni	Hat 2 Uni	Hat 1 WF	Hat 2 WF
Fiber Mass (%)	51.34	47.87	53.8	49.85	47.43	49.3

To get the fiber volume fractions from the fiber mass fractions both the density of epoxy and the density of the carbon fiber must be known. The density of carbon fiber can be looked up depending on what type of carbon fiber is used. The density of epoxy varies and the epoxy used to make the composites did not have a listed density. To find the density a submersion test is conducted. The test procedure is outlined in the ASTM standard D792-91 [19]. The density of the epoxy resin, carbon fiber, and the finished composites is given in Table 3.

**Table 3: Measure Density**

	Cant Beam Uni	Cant Beam WF	Hat 1 Uni	Hat 2 Uni	Hat 1 WF	Hat 2 WF	Epoxy	Carbon Fiber
Density $kg/m^3$	1.311	1.351	1.287	1.3	1.31	1.36	1.125	1.76

The fiber volume fraction can be determined by a simple equation using the fiber mass fraction and the known densities [2].

$$v_f = \frac{Vol\ Fiber}{Vol\ Composite} = \frac{Mass\ Fiber * \rho_f}{Mass\ Fiber * \rho_f + Mass\ Epoxy * \rho_E}$$

The fiber volume fractions for all of the carbon fiber structures are given in Table 4. It is important to have good estimates of fiber volume fraction as all elastic properties of the composite are dependent on it. The resulting fiber volume fraction is much lower than industry standards. The process used for these experiments is not a reliable method for industrial processes.

**Table 4: Fiber Volume Fraction**

	Cant Beam Uni	Cant Beam WF	Hat 1 Uni	Hat 2 Uni	Hat 1 WF	Hat 2 WF
Vf (%)	40.28	36.99	42.67	38.85	36.58	38

#### 2.4 Analytical Determination of Woven Fabric Composite Elastic Properties

There are many analytical models that can be used to determine the elastic properties of woven fabric composites. Ishikawa gave three analytical models for determining the elastic properties including the mosaic model, undulation model, and the bridging model. For this model the simple mosaic model was used to determine the upper bounds of the elastic properties by assuming an iso-strain condition for all the infinitesimal pieces along the loading direction this is referred to as a parallel model. The mosaic model is an idealization of the weave in which no undulation occurs. The idealized configuration is shown in Figures 2. The fiber volume fraction in the yarn is approximated as a unidirectional laminate. To find the yarn fiber volume fraction the overall fiber volume fraction is used and the geometry of the weave. The yarn fiber volume fraction is then used in the mosaic model to determine the upper bounds of the elastic properties of the woven fabric composites.



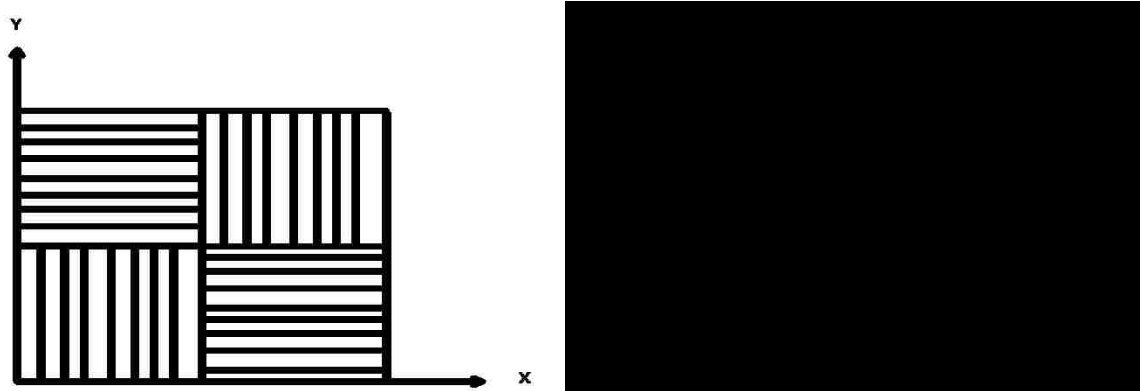


**Figure 2: Idealization of Woven Fabric Composite Using Mosaic Model**

The composite cylinder assemblage outlined by Naik et al is then used to get the elastic properties of the yarn [11]. The properties of the individual materials used to make the composite must be defined as shown in Table 5, where  $E_L$  is the modulus of elasticity in the fiber direction,  $E_T$  is the modulus in the transverse direction,  $G_{TT}$  is the shear modulus in the plane perpendicular to the fibers, and  $\nu_{LT}$  is the major Poisson's ratio. The carbon fiber properties are the similar for both the unidirectional carbon fiber fabric and the woven fabric carbon fiber.

**Table 5: Elastic Properties of Yarn Materials**

	$E_L$	$E_T$	$G_{LT}$	$G_{TT}$	$\nu_{LT}$
Carbon Fiber	230 GPa	40 GPa	24 GPa	14 GPa	.26
Epoxy	3.5 GPa	3.5 GPa	1.3 GPa	1.3 GPa	.35

The Composite Cylinder Assemblage (CCA) gives a closed form analytic solution for the yarn elastic properties  $E_L$ ,  $G_{LT}$ ,  $\nu_{LT}$ , and  $k$ . It gives bounded expressions for  $G_{TT}$  and  $E_T$ . The Composite Cylinder Assemblage is a variational bonding method based on the classic principles of minimum potential energy and minimum complementary energy.

The five material properties that define a transversely orthotropic material are rigorously bounded for a case of composite cylinders of infinite length and different cross sections with diameters ranging from finite to infinite size. For this case four of the five elastic moduli have coinciding bounds providing an exact expression, however the transverse shear modulus does not have coinciding bounds and hence does not provide a closed form solution [20].

$$k = \frac{k^m(k^f + G_{TT}^M)(1 - V_f) + k^f(k^m + G_{TT}^M)V_f}{(k^f + G_{TT}^M)(1 - V_f) + (k^m + G_{TT}^M)V_f}$$

$$\frac{1}{k^f} = -\frac{1}{G_{TT}^f} - \frac{4v_{LT}^{f2}}{E_L^f} + \frac{4}{E_T^f}$$

$$\frac{1}{k^m} = -\frac{1}{G_{TT}^m} - \frac{4v_{LT}^{m2}}{E_L^m} + \frac{4}{E_T^m}$$

$$E_L = E_L^f V_f + E_L^m V_m + \frac{4(v_{LT}^f - v_{LT}^m)^2 V_m V_f}{\frac{V_m}{k^f} + \frac{V_f}{k^m} + \frac{1}{G_{TT}^m}}$$

$$v_{LT} = v_{LT}^f V_f + v_{LT}^m V_m + \frac{(v_{LT}^f - v_{LT}^m) \left( \frac{1}{k^m} - \frac{1}{k^f} \right) V_f V_m}{\frac{V_m}{k^f} + \frac{V_f}{k^m} + \frac{1}{G_{TT}^m}}$$

$$G_{LT} = G_{LT}^m \frac{G_{LT}^m V_m + G_{LT}^f (1 + V_f)}{G_{LT}^m (1 + V_f) + G_{LT}^f V_m}$$

$$G_{TT(-)} = G_{TT}^m + \frac{V_f}{\left[ \frac{1}{(G_{TT}^f - G_{TT}^m)} + \frac{(k^m + 2G_{TT}^m)V_m}{2G_{TT}^m(k^m + G_{TT}^m)} \right]}$$

$$G_{TT(+)} = G_{TT}^m \left( 1 + \frac{(1 + \beta_1)V_f}{\rho - V_f \left[ 1 + \frac{3\beta_1^2 V_m^2}{\alpha V_F^3 - \beta_1} \right]} \right)$$

$$\beta_1 = \frac{k^m}{k^m + 2G_{TT}^m} \quad \beta_2 = \frac{k^f}{k^f + 2G_{TT}^f}$$

$$\gamma = \frac{G_{TT}^f}{G_{TT}^m} \quad V_m = 1 - V_f$$

$$\alpha = \frac{\beta_1 - \gamma\beta_2}{1 + \gamma\beta_2} \quad \rho = \frac{\gamma + \beta_1}{(\gamma - 1)}$$

$$E_{T(\pm)} = \frac{4kG_{TT(\pm)}}{k + mG_{TT(\pm)}}$$

$$m = 1 + \frac{4k\nu_{LT}^2}{E_L}$$

The steps for the obtaining the elastic properties are given in the following equations.

$$Q_{ij} = \begin{matrix} \frac{E_x}{D_v} & \frac{\nu_{xy}E_x}{D_v} & 0 \\ \frac{\nu_{xy}E_y}{D_v} & \frac{E_y}{D_v} & 0 \\ 0 & 0 & G_{xy} \end{matrix}$$

The Qij matrix is assembled for the warp yarn, fill yarn, and matrix. In the case of non hybrid fabrics with the same material for warp and fill the Qij matrix will be the same. The in plane stiffness constants are then determined by integrating over the area of the weave. For the mosaic model the Qij matrix is constant along the x and y axis and the in plane stiffness constants given by the Aij matrix is the stiffness matrix multiplied by the height of the yarn.

$$A_{ij} = Q_{ijw} * h_w + Q_{ijf} * h_f$$

The in plane stiffness constants can then be inverted to get the in plane compliance constants.

$$a_{ij} = A_{ij}^{-1}$$

The elastic constants are then found from the in plane compliance constants.

$$E_x = \frac{1}{a_{11} * h}$$

$$G_{xy} = \frac{1}{a_{66} * h}$$

$$\nu_{xy} = -\frac{a_{12}}{a_{11}}$$

The out of plane properties must then be determined for the woven fabric composite. Abbot and Daniel show that the out of plane properties of a woven fabric composite are equivalent to the out of plane properties of a unidirectional composite with the same fiber volume fraction [13]. The out of plane properties of a unidirectional composite are equal to those of the transverse direction [2]. To find the elastic properties in the out of plane direction of the woven fabric composite the properties of a unidirectional composite of the same fiber volume fraction is determined and then the out of plane properties are then used for the out of plane woven fabric composite elastic properties. The elastic properties of a unidirectional composite can be found in the following equations. The underscore u implying that the properties came from the unidirectional composite model.

$$E_z = E_{yu}$$

$$\nu_{13} = \nu_{12u}$$

$$\nu_{23} = \nu_{12u} * \left( \frac{1 - \nu_{21u}}{1 - \nu_{12u}} \right)$$

$$G_{33} = G_{22u}$$

$$G_{23} = \frac{E_{yu}}{2 * (1 + \nu_{23})}$$

## 2.5 Analytical Determination of Unidirectional Composite Elastic Properties

The elastic properties of the unidirectional composite can be found by the CCA previously described. The elastic properties of the carbon fiber and the epoxy matrix are the same as those used in the woven fabric composite and are given in Table 4. The unidirectional composite is a transversely isotropic material with the elastic properties being the same in the out of plane and non fiber direction. The CCA gives the in plane elastic properties for the unidirectional composite the transverse elastic modulus and the transverse shear modulus are bounded, while the longitudinal elastic modulus and the longitudinal shear modulus are given in a closed form analytical solution.

The out of plane elastic properties of a unidirectional composite are the same as the transverse elastic properties due to the geometry of the unidirectional composite. The transverse elastic properties are found in the CCA above. The equations for the out of plane elastic properties are also given above.

## 2.6 Estimated Physical and Elastic Properties

The physical and elastic properties of the composites are estimated from the fiber volume fraction of the composite using the methods discussed in the previous section. Estimates of the physical and elastic properties are necessary to obtain results from the FEA. The composites fabricated have various fiber volume fractions and hence different physical and elastic properties. In order to reduce the number of different physical and elastic properties that need to be calculated and to reduce the number simulations needed an average fiber volume fraction is chosen for both the unidirectional composites and the woven fabric composites. A fiber volume fraction of 40% and 37% are chosen for the unidirectional carbon fiber composites and the woven fabric carbon fiber composites respectively. The physical and elastic properties calculated are used as the initial properties in the FEA, often properties must be adjusted to obtain more satisfactory results from the FEA. The physical and elastic properties of the composites are given in Table 6 where  $E_L$  is the longitudinal (fiber direction) elastic modulus,  $E_T$  is the transverse modulus,  $E_O$  is the out of plane modulus,  $G_{LT}$  is the shear modulus, and  $\nu_{LT}$  is the major Poisson's ratio.

**Table 6: Estimated Physical and Elastic Properties**

Composite	$E_L$	$E_T$	$E_O$	$G_{LT}$	$\nu_{LT}$	P
Unidirectional	94.1 GPa	7.5 GPa	7.5 GPa	2.8 GPa	.31	1.3 g/cm <sup>3</sup>
Woven Fabric	52.4	52.4	7.1 GPa	2.8	.045	1.35 g/cm <sup>3</sup>

## CHAPTER 3

### DYNAMIC EXPERIMENTAL PROCEDURES

#### 3.1 Introduction

To better understand the process of shock propagation in composites a series of experiments are implemented. The first set of experiments is used to validate the finite element method for determining the transient dynamic response of composite materials. This experiment compares the experimental data from three different specimens: an aluminum rectangular beam, a unidirectional carbon fiber composite beam, and a carbon fiber woven fabric composite beam. The second set of experiments involves structures without joints. The structures are hanged on a frame to simulate a structure without joints or constraints. The structures include a unidirectional carbon fiber composite hat and a woven fabric carbon fiber composite hat. The last set of experiments involves bolted structures. The hat sections are bolted together and the tests are conducted by hanging them from a frame to simulate the condition with no constraints. The two bolted sections will be made by attaching the two unidirectional carbon fiber hat sections and the two carbon fiber woven fabric composite hats. All the results from the sets of experiments will be compared with results from a FEA.

#### 3.2 Experimental Equipment

The equipment needed to conduct the experiments includes an modally tuned impact hammer, cables, shear accelerometers, oscilloscope, hand held calibrator, and signal conditioners. For the cantilever beam experiments a fixture is used to clamp the beams on the constrained end. For the unconstrained experiments a steel frame and string

is used to hang the structures from. The specifications for the equipment used are given in the following figures.


	<b>PCB 352 C22 Piezoelectric Accelerometer</b>	
	<b>Model #</b>	<b>352 C22</b>
	<b>Sensitivity(±15%)</b>	<b>1.0 mV/(m/s<sup>2</sup>)</b>
	<b>Frequency Range</b>	<b>1 to 10 kHz</b>
	<b>Mass</b>	<b>.5 grams</b>
	<b>Broadband Resolution</b>	<b>.04 (m/s<sup>2</sup>) rms</b>

Figure 3: Accelerometer




	<b>PCB 086 C02 Modally Tuned Impact Hammer</b>	
	<b>Model #</b>	<b>086 C02</b>
	<b>Sensitivity(±15%)</b>	<b>11.2mV/N</b>
	<b>Measurement Range</b>	<b>±444N</b>
	<b>Mass</b>	<b>.16 kilograms</b>
	<b>Resonant Frequency</b>	<b>≥22kHz</b>

Figure 4: Impact Hammer



	<b>Dytran Instruments 4103C</b>	
	<b>Model #</b>	<b>4103C</b>
	<b>Sensor Supply Current</b>	<b>2 mA</b>
	<b>Voltage Gain</b>	<b>1</b>
	<b>Compliance Voltage</b>	<b>18 VDC</b>
	<b>Weight</b>	<b>12 oz</b>

Figure 5: Current Source

	<b>PCB 394C06 Handheld Shaker</b>	
	Model #	394C06
	Operating Frequency ( $\pm 1\%$ )	159.2 Hz
	Acceleration Output ( $\pm 3\%$ )	9.81 (m/s <sup>2</sup> ) rms
	Maximum Load	210 grams
	Mass	900 grams

**Figure 6: Handheld Shaker Calibrator**

### 3.3 Experimental Set-up for Cantilever Beam Structures

The first experiment is designed to establish that the FEM is applicable to transient dynamic analysis of fiber-reinforced composite materials. A simple low impact test is performed where no impact or damage occurs to the structure. The experiment consists of a cantilever beam that is clamped into a stationary fixture that applies equal to the constrained end of the beam. A schematic of the test set up is shown in Figure 7.

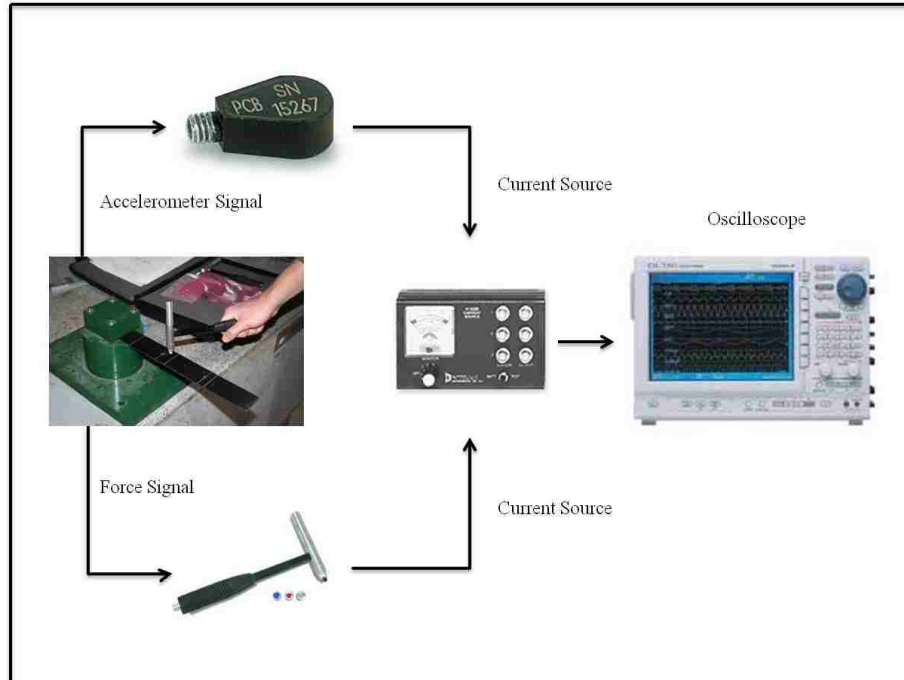


**Figure 7: Experimental Set-up for Cantilever Beam Test**

The structure consists of a rectangular bar used as a cantilever beam. For the aluminum beam the length is .4064m, width .0506m, and height of .0063m and for the unidirectional composite cantilever beam the length is .4064m, width of .0506m, and a height of .003m and for woven fabric composite cantilever beam the length is .4064m, width of .0506m, and a height of .00254m. The dimensions of the aluminum cantilever beam are shown in Figure 8. The dimensions of the unidirectional composite cantilever beam are shown in Figure 9 and the dimensions of the woven fabric composite cantilever beam in Figure 10.

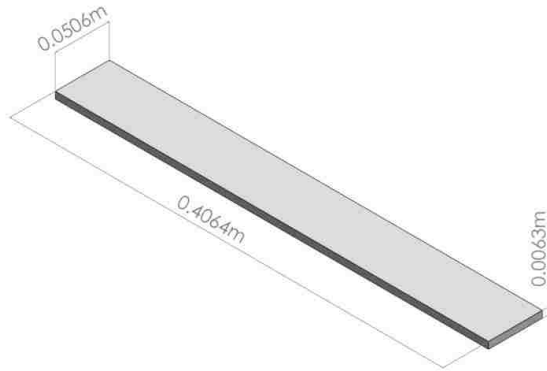


**Figure 8: Aluminum Cantilever Beam**

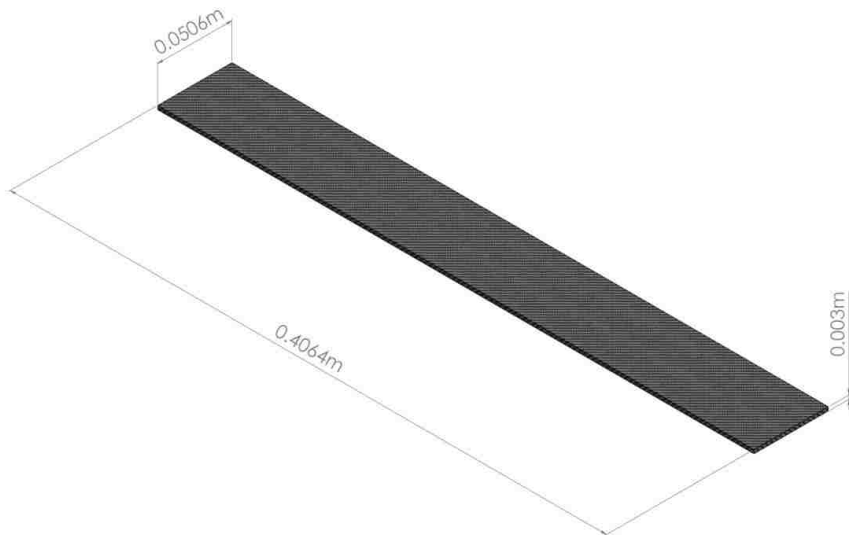


**Figure 9: Unidirectional Composite Cantilever Beam**

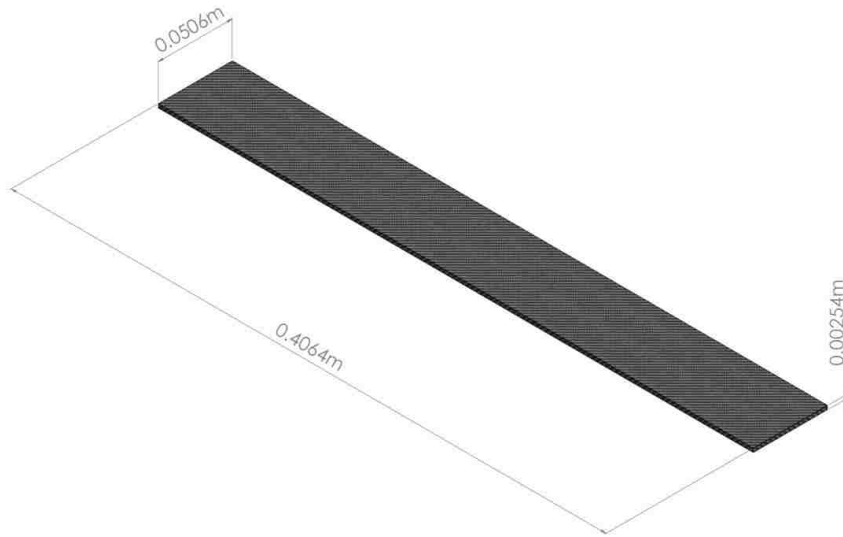


**Figure 10: Woven Fabric Composite Cantilever Beam**

The composite beam thickness is different from the aluminum beam because of the available thickness of individual carbon fiber preforms and the uncertainties of the consolidation during fabrication. The aluminum cantilever beam is used as a control for the experiment to give a criterion for error for the composite cantilever beams. The FEM has already been shown as a valid numerical solution for transient dynamic analysis of isotropic materials as seen in Feghhi, Kumarswamy, and Doppola [3-6]. The experiment on the composite beams will determine if the Finite Element Method is a valid numerical solution of the transient dynamic response to low impact of fiber-reinforced composites. This will be determined by the error analysis. The natural frequencies will be compared by experimental error and the time history will be compared by a Normalized Root Mean Square Difference (NRMSD) criteria. If the error of the results for the composite beams is similar to that of the aluminum beam the FEM will be used for the time history of the

bolted hat structure. The two results that will be analyzed are the natural frequencies and the time history of the response to the low impact. The natural frequencies will be found experimentally, analytically, and numerically using the FEM. The experimental dynamic response will be compared to the results from the FEA.

The procedure for this experiment begins with placing the cantilever beam inside the fixture with care to insure that even pressure is applied to the free end of the cantilever beam. The accelerometer calibrated using a hand held calibrator. The accelerometer is attached to the cantilever beam using petro wax. The accelerometer is placed at a determined location on the cantilever beam and then impacted with the hammer at another determined location. The impact and accelerometer location are shown in Fig 12. The accelerometer and impact hammer are connected to the oscilloscope through the current source and a sampling frequency and range of voltage specified. The cantilever beam is impacted by the modally tuned impact hammer and the data is recorded. In the cantilever beam experiments the hammer is impacted at 30.48 cm from the free end of the beam and the accelerometer is placed 20.32 cm from the free end of the beam. The beam is clamped along a section 6.35 cm long along the entire width of the beam. The set up can be seen in the following figures.

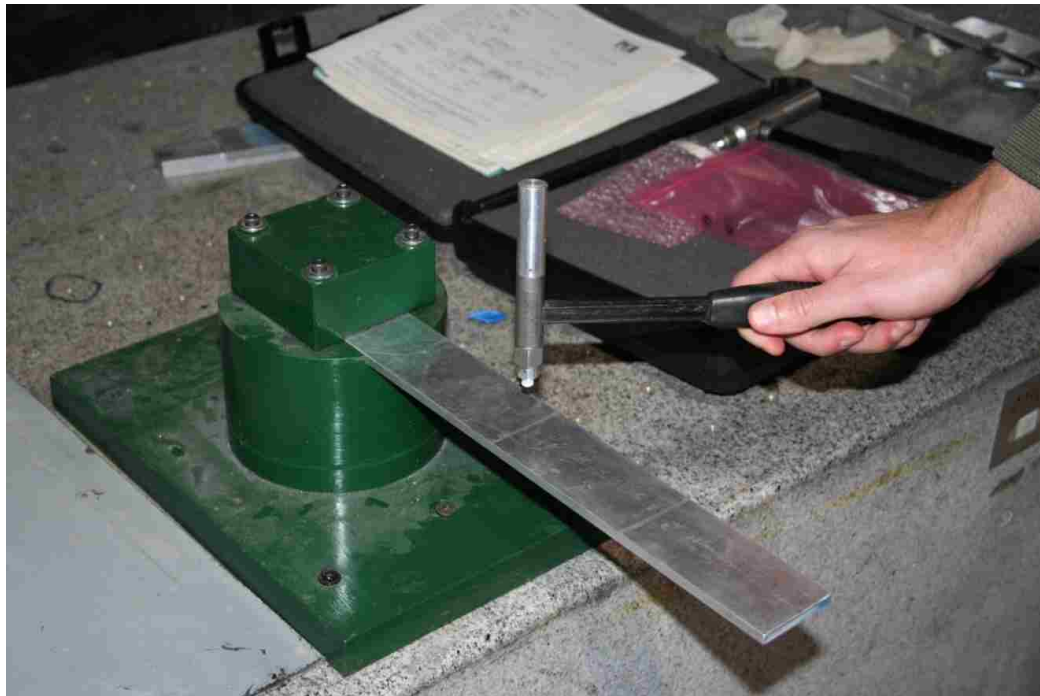


Figure 11: Experimental Cantilever Beam Fixture

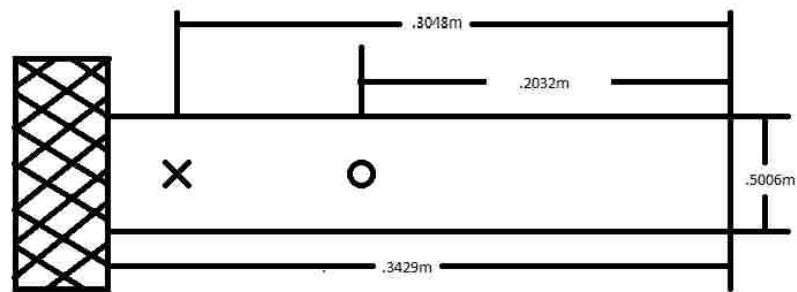


Figure 12: Cantilever Beam Experiment Layout (X marks Hammer Impact and O Marks Accelerometer)

### 3.4 Experimental Set-up of Unconstrained Structures without Joints

The simple structure of hat section is used to determine if the material models used in the FEA are accurate. As before a low impact test is used and the structural response is found. The dimensions of the unidirectional composite hat are given in Figure 13 and the dimensions of the woven fabric composite hat are given in Figure 14. The hat section is suspended from a steel frame and is assumed to be unconstrained in the FEA.

The procedure for the unconstrained structure without joint experiment involves hanging the structure from the steel from using string. The accelerometer is calibrated using a hand held calibrator. The accelerometer is placed on the center of the side wall of the composite hat. The hammer is impacted on the center of the top section of the composite hat. The drawings of the unidirectional composite hat and the woven fabric composite hat are shown in Figure 13 and Figure 14 respectively. The hanging mass fixture and the experimental setup of the composite hat experiment are found in Figures 15 and 16 respectively. The accelerometer and impact hammer are connected to the oscilloscope through the current source and a sampling frequency and range of voltage specified. The hat section is impacted by the modally tuned impact hammer and the data is recorded.



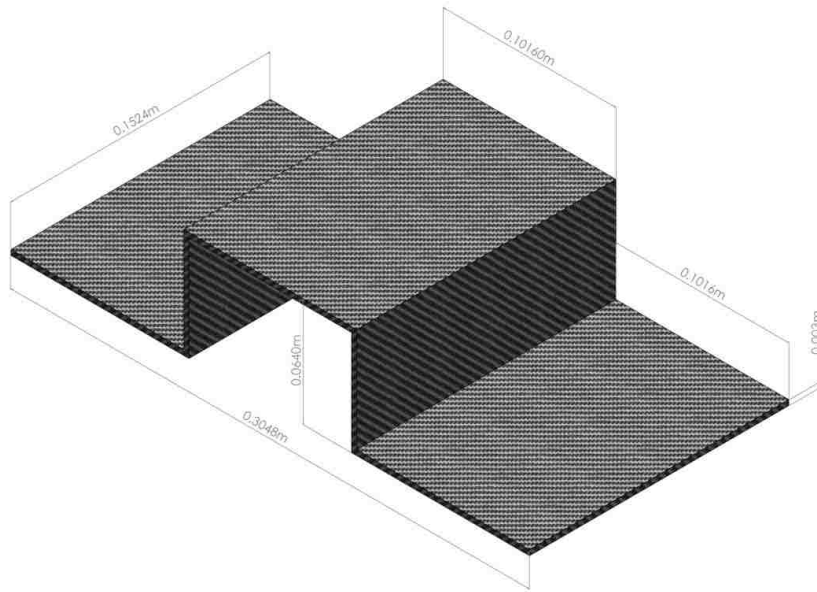


**Figure 13: Unidirectional Composite Hat**

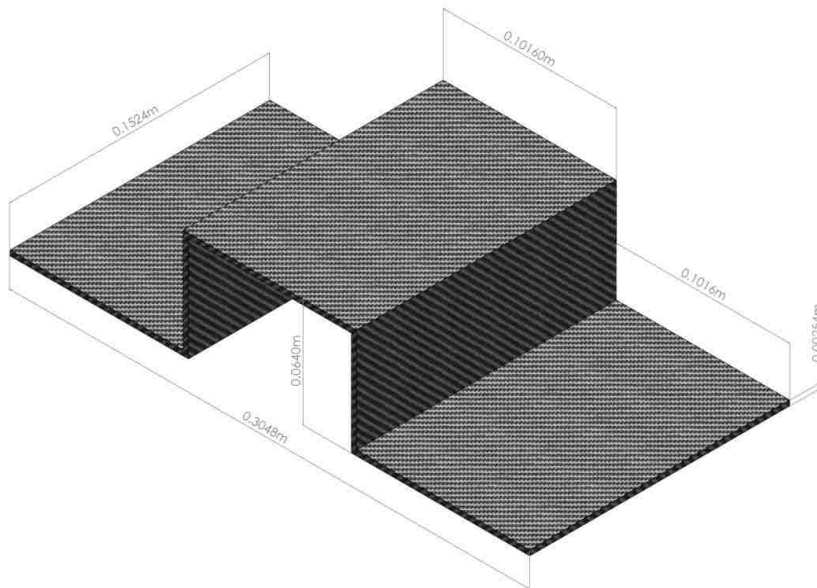


**Figure 14: Woven Fabric Composite Hat**

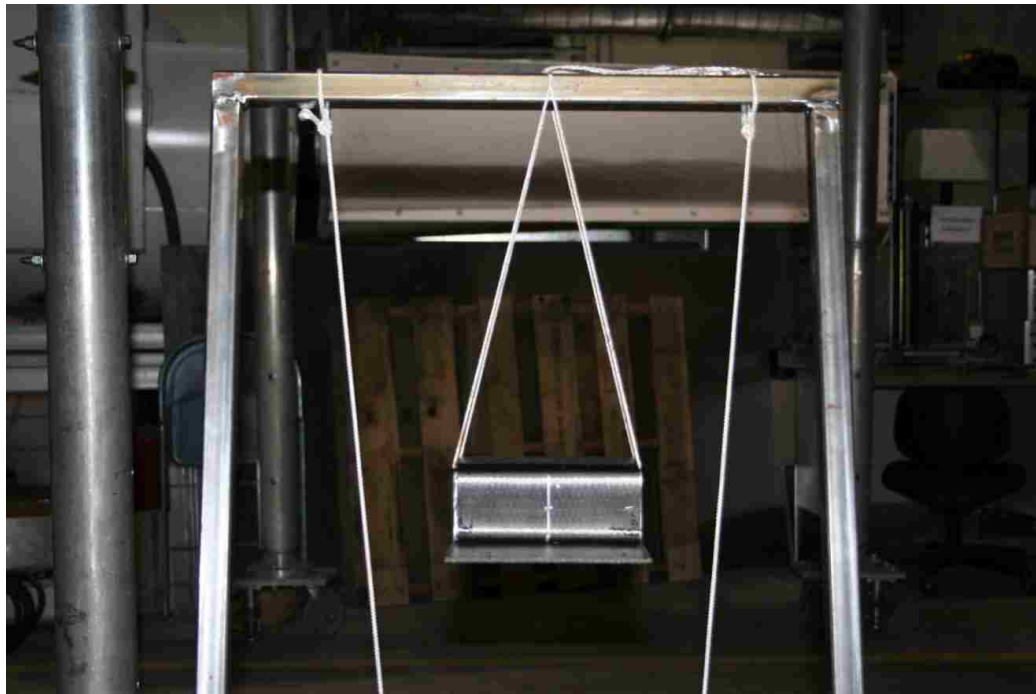


**Figure 15: Hanging Mass Structure for Unconstrained Structure without Joints Experiment**

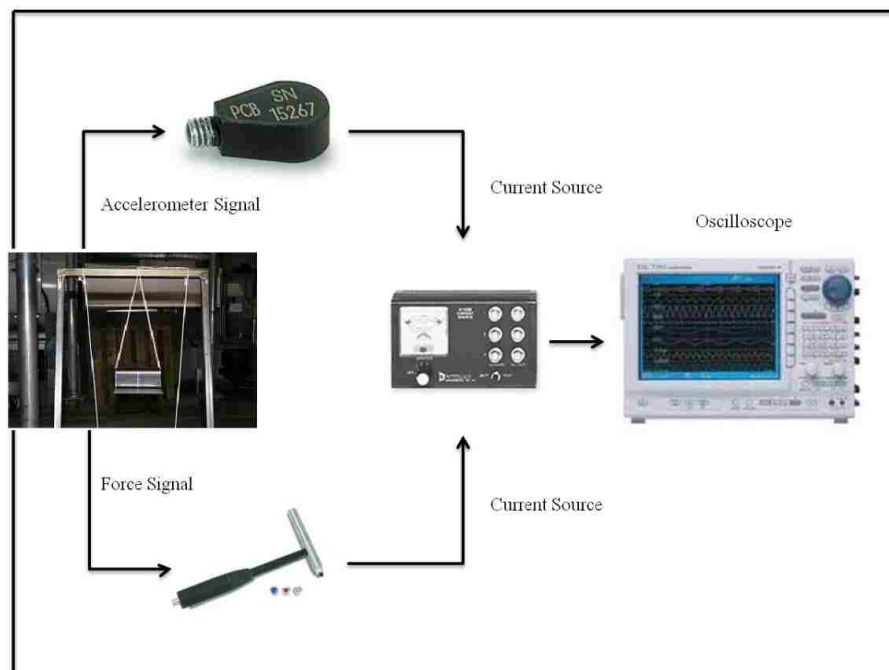


**Figure 16: Experimental Set-up for Unconstrained Structure without Joints Experiment**

### 3.5 Experimental Set-up of Unconstrained Bolted Structures

The bolted hat structure experiment is used to determine the shock transmission across a bolted connection using composite sections. The bolted structure consists of two hat sections bolted together with class 8.8 grade 5 M10 bolts with 1.0 mm fine threads and 30mm length, M10 by 1.0mm pitch nuts, and washer. Three washers will be used to evenly distribute the stress from the torque on the bolts to the composite hats. This is necessary as composites layers can be crushed by the applied stress from the torque of the bolts the three washers evenly distributed the stress and insure that the hat sections meet evenly. A washer is placed under the head of the bolt in between the two hat sections and on top of the nut. The bolted hat assembly can be seen in Figure 17. Figure 18 shows the bolted hat assembly hanging from the support frame and Figure 19 shows the experimental set-up of the bolted hat structure experiment. There will be two different bolted hat sections tested, one using unidirectional carbon fiber hat sections and the other using woven fabric carbon fiber hat sections. Two accelerometers are used to record the acceleration caused by the impact of the impact hammer. The location of the accelerometers and the impact of the hammer can be seen in Figure 20.

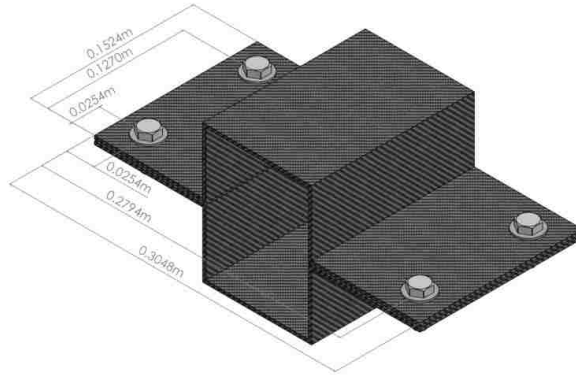


**Figure 17: Bolted Hat Structure**



**Figure 18: Hanging Mass Structure for Unconstrained Bolted Hat Structure Experiment**

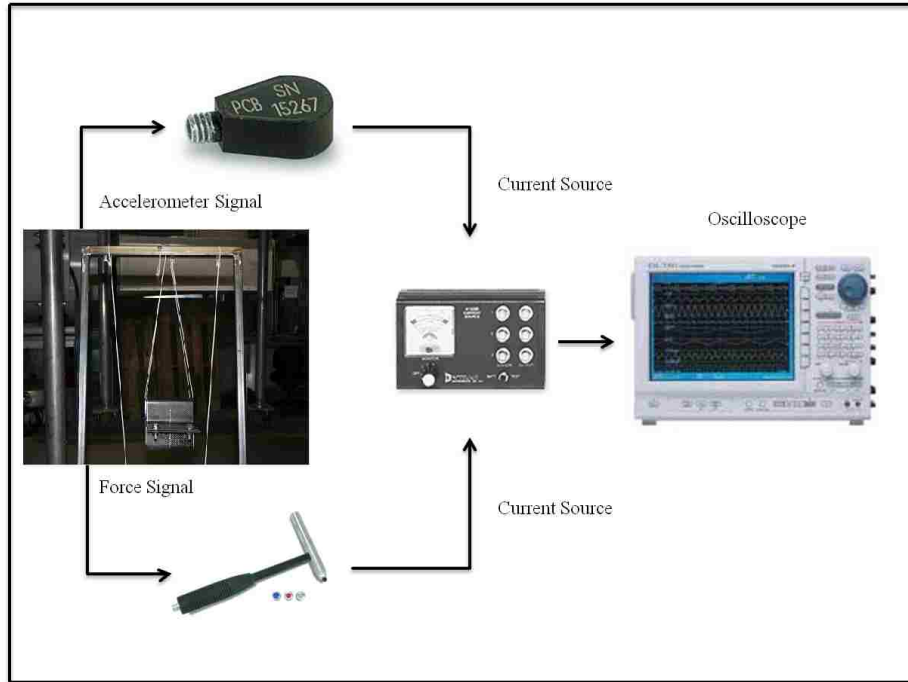


**Figure 19: Experimental Set-up for Unconstrained Bolted Hat Structure Experiment**

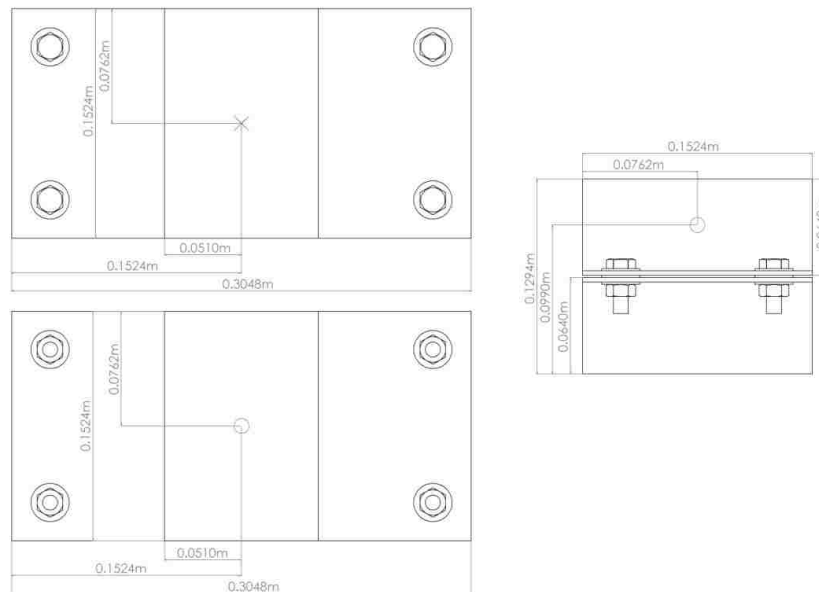


**Figure 20: Location of Accelerometers (O) and Impact (X) on Unconstrained Bolted Hat Structure**

The experiment begins by calibrating the accelerometers that will be used. Both accelerometers used in the experiment are calibrated using the hand held calibrator. The hat structure is then assembled and the bolts tightened to 5.3 N-m. The hat structure is suspended by string to the steel frame. The accelerometers are attached to the bolted hat section using petro wax. Accelerometer 1 is placed on the center of the side wall of the top hat and Accelerometer 2 is placed on the center of the top section of the bottom hat. The hammer is impacted at the center of the top section of the top hat. The accelerometers and impact hammer are connected to the oscilloscope through the current source and a sampling frequency and range of voltage specified. The bolted hat section is impacted by the modally tuned impact hammer and the data is recorded. The data is filtered and the natural frequencies of the hat section determined using a computer algorithm.

## CHAPTER 4

### ANALYSIS OF COMPOSITE CANTILEVER BEAM

#### 4.1 Background

To understand the shock transmission in a simple structure the cantilever beam experiment is performed. The cantilever beam experiment is performed without joints in order to evaluate the shock propagation in carbon fiber reinforced composites. A numerical solution is ideal for solving the nonlinear dynamic response of a structure to shock impact. The FEM is a commonly used numerical solution for such problems. The modal analysis of the cantilever beams was done using an implicit solver. The solution of the shock transmission requires an explicit analysis due to the wave propagation from impact. ALTAIR Hypermesh was used as a preprocessor to create the geometry and mesh. The Non-Linear FE code LS-DYNA v971, henceforward referred to as LS-DYNA, was used as the solver for both the implicit and explicit analysis. To interpret the results LS Pre-Post v4, henceforward referred to as LS Pre-Post, and MATLAB were used as a post processor. The cantilever beam experiment is designed to give a simple test of the effectiveness of the FEA of shock transmission in fiber reinforced composites. The test consists of three samples, aluminum, unidirectional carbon fiber/epoxy composite, and a woven fabric carbon fiber/epoxy composite. The simple geometry of the cantilever beam is ideal as an initial test specimen. The rectangular beam allows for better geometrical tolerances of the composite sections. Complex shapes lead to greater inaccuracies in terms of the geometrical tolerances. The inaccuracies compound the error in the FEA leading to poorer results. The aluminum specimen is used as a control subject to test that the FEA is a method for this type of loading, geometry, and boundary conditions. The

results of the experiment and the FEA are compared using a Normalized Root Mean Square algorithm.

#### 4.2 Experimental Calibration of Equipment

The equipment used in the proceeding experiments must be calibrated to insure that the results are accurate. Calibration of equipment also builds confidence in the validity of results. The accelerometers used and the impact hammer are calibrated before they are used in the experiments. The accelerometers are calibrated using the PCB 3946 Handheld calibrator. The calibrator creates a constant 1 g acceleration. The accelerometers sensitivity can then be obtained by observing the mV output of the accelerometer during the application of the constant 1 g acceleration from the calibrator. The impact hammer is calibrated by impacting a freely suspended mass with an attached reference accelerometer. The sensitivity of the hammer is then found by dividing the peak output of the hammer by the mass of the freely suspended specimen times the peak acceleration. This will give the impact hammer sensitivity in mV/lb or mV/N.

#### 4.3 Repeatability and Consistency Test

The impact response of the cantilever beam is a transient phenomenon and can therefore be either random or deterministic. “If an experiment producing specific data of interest can be repeated many times with identical results (within the limits of experimental error), then the data can generally be considered deterministic. Otherwise the data is random.” [21]. If the impact response is random it is impossible to simulate the result.



A simple test is performed to insure that the experiment is not random. For the three cantilever beam experiments, several trials are conducted and the force of the impact and the acceleration of the response are recorded. The hammer impacts in which the force signals are the most similar are chosen to compare the signals. MATLAB is used to perform a FFT on the time history response. The time history response and the frequency response can be used to determine if the signal is random or deterministic. For the aluminum cantilever beam a force peak of 200N is chosen, for the unidirectional beam a force peak of 100N is chosen, and for the woven fabric beam a force peak of 90N is chosen. The figures below make it clear that all three of the cantilever beam specimens have similar responses in both the time and frequency domains. The force impact curves are not identical as it is not possible to exactly repeat a physical action, however the force curves are acceptable in the range of experimental error. The response show that the experiment is deterministic and therefore a numerical result can be made.

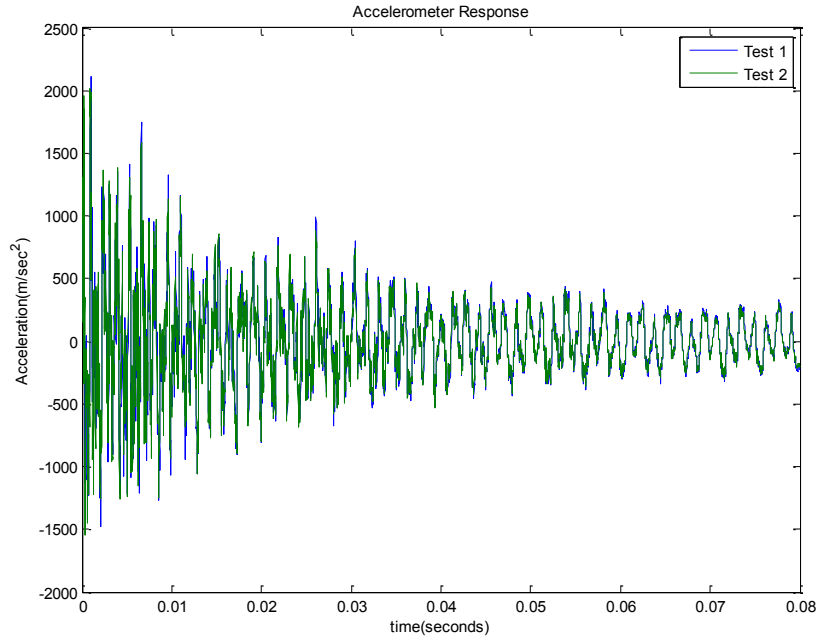


**Figure 21: Time History Response of Aluminum Cantilever Beam Repeatability Test**

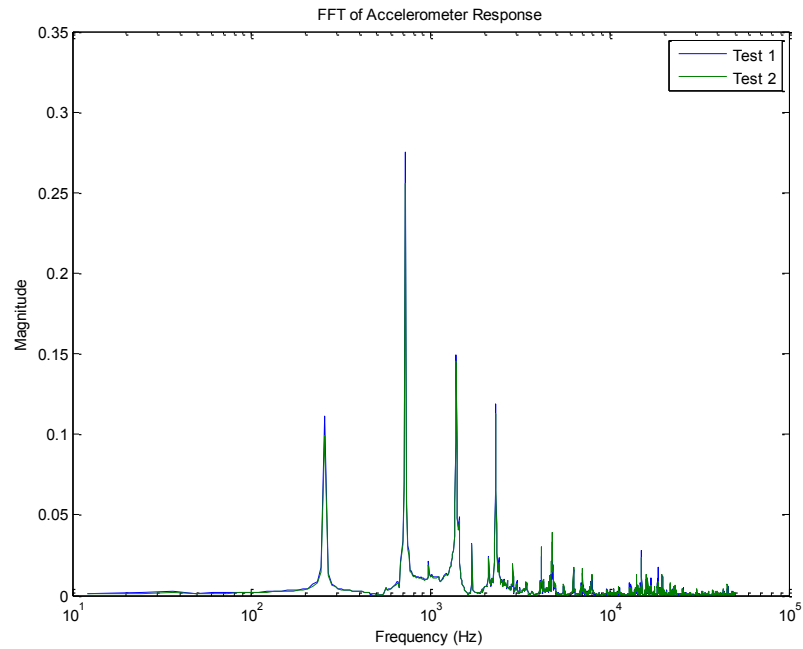


**Figure 22: Frequency Response of Aluminum Cantilever Beam Repeatability Test**

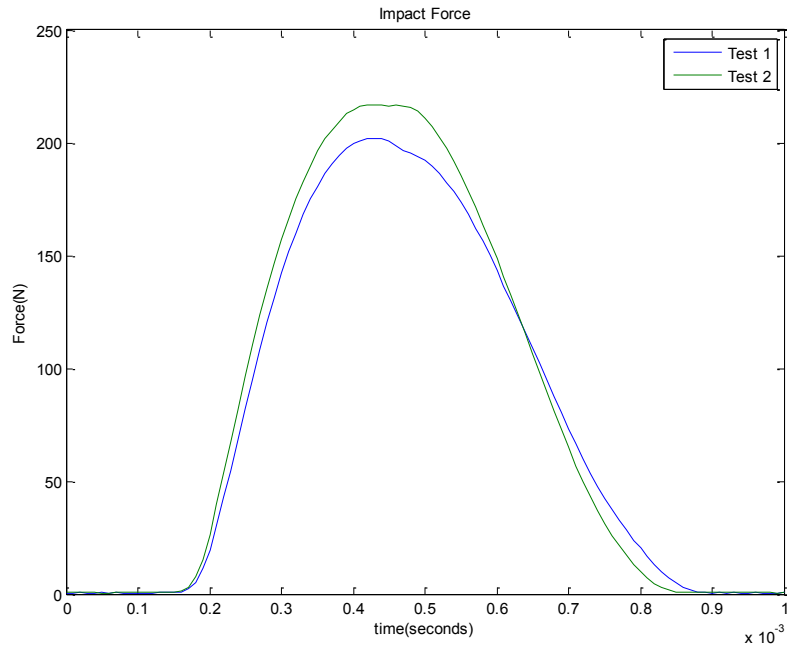


**Figure 23: Impact Force of Aluminum Cantilever Beam Repeatability Test**

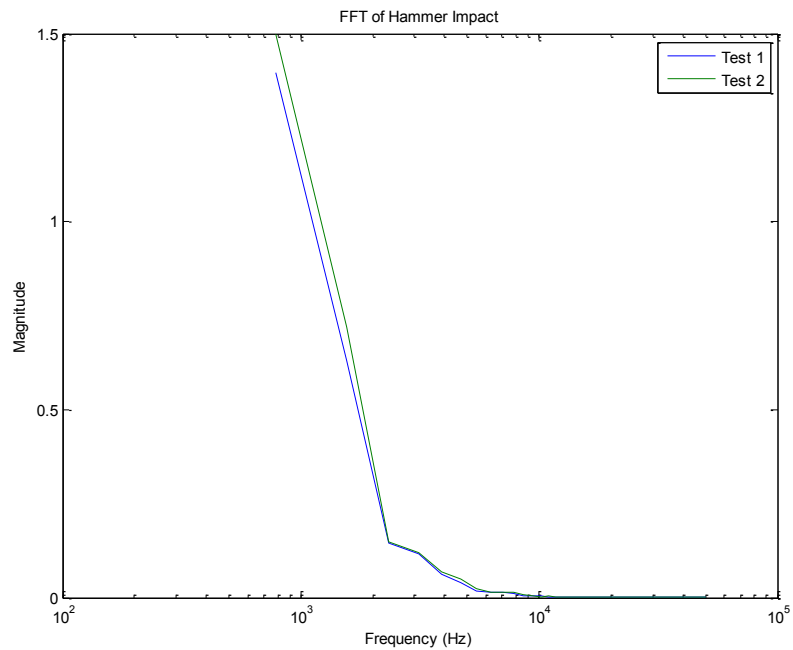


**Figure 24: Frequency Response of Impact Force of Aluminum Cantilever Beam Repeatability Test**

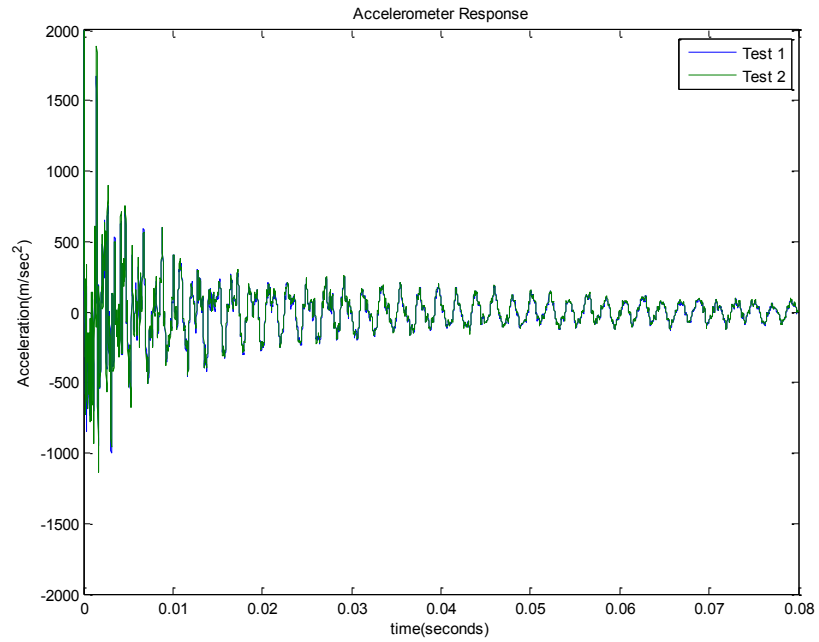


**Figure 25: Time History Response Unidirectional Composite Cantilever Beam Repeatability Test**

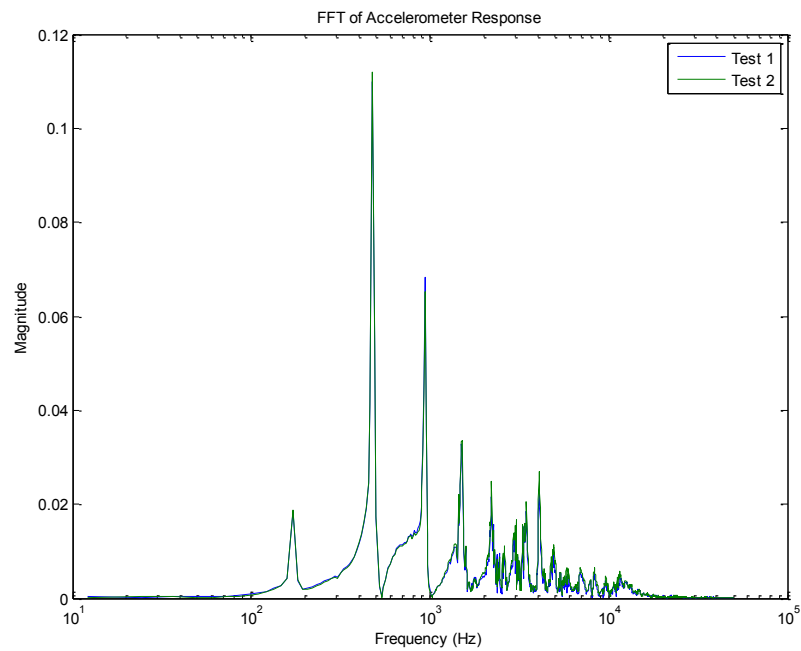


**Figure 26: Frequency Response of Unidirectional Composite Cantilever Beam Repeatability Test**

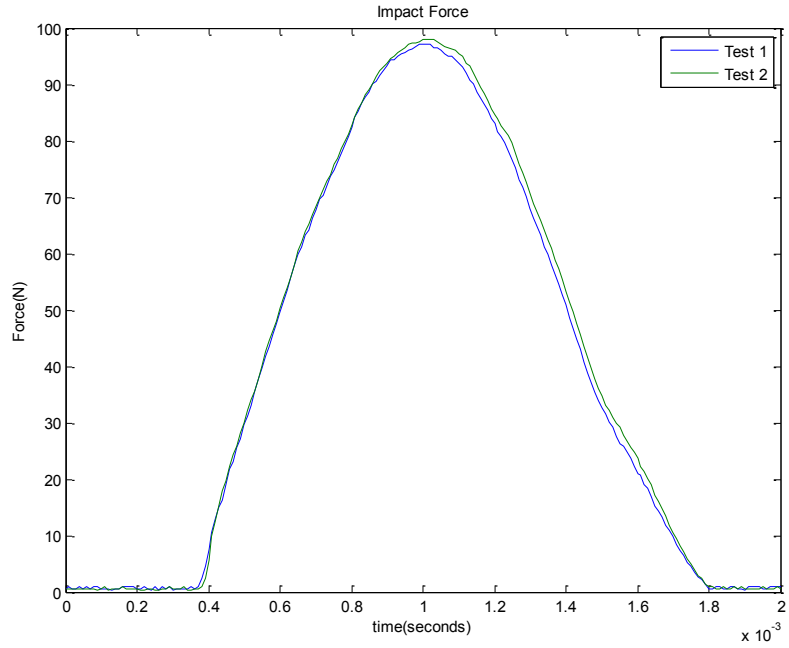


**Figure 27: Impact Force of Unidirectional Composite Cantilever Beam Repeatability Test**

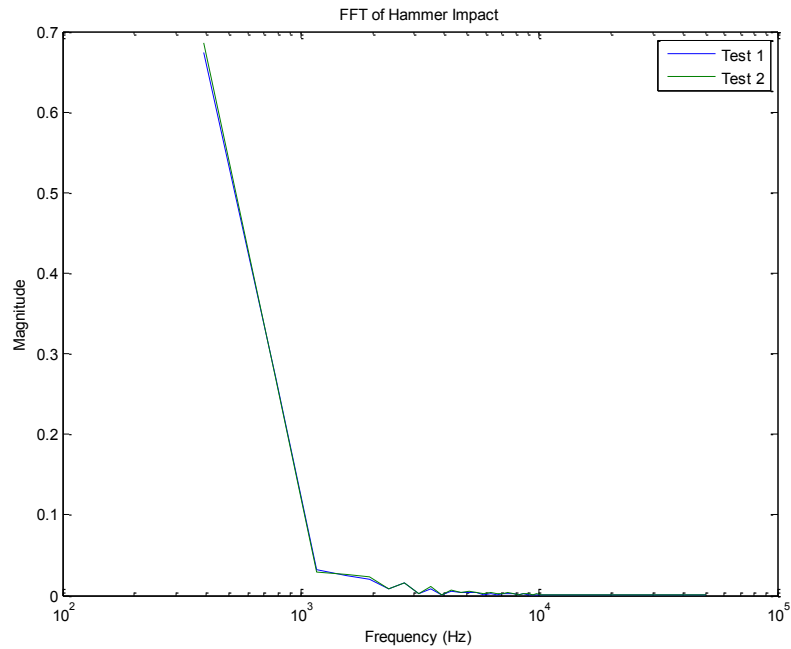


**Figure 28: Frequency Response of Impact Force of Unidirectional Composite Cantilever Beam Repeatability Test**

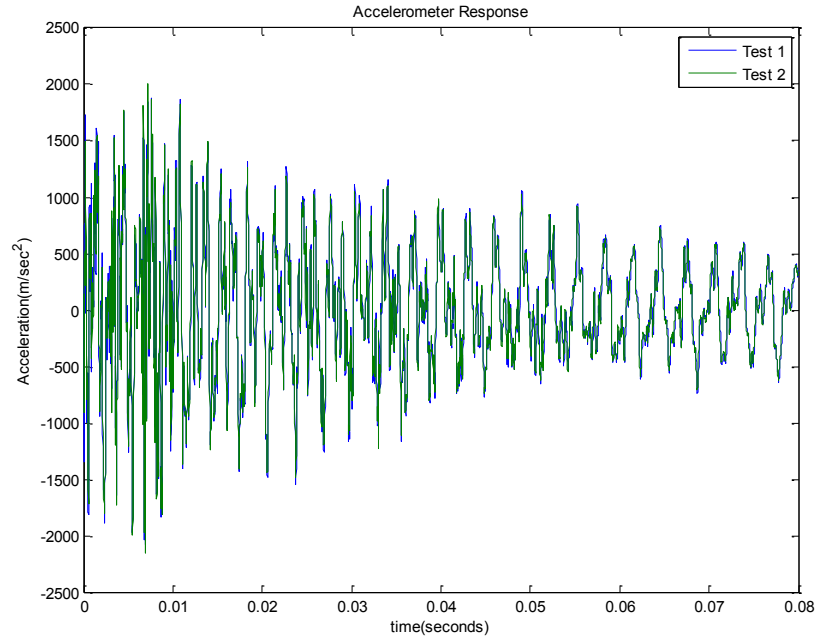


**Figure 29: Time History Response of Woven Fabric Cantilever Beam Repeatability Test**

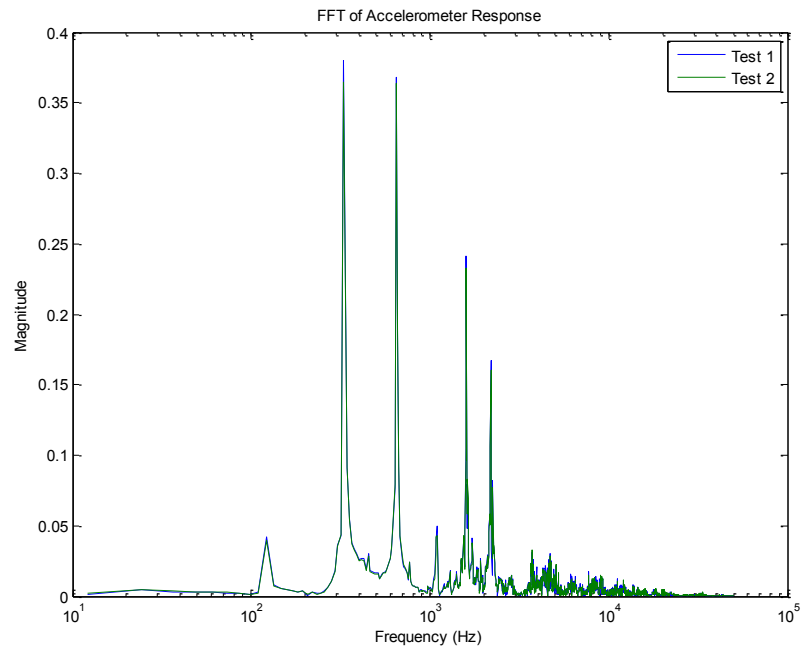


**Figure 30: Frequency Response of Woven Fabric Composite Cantilever Beam Repeatability Test**

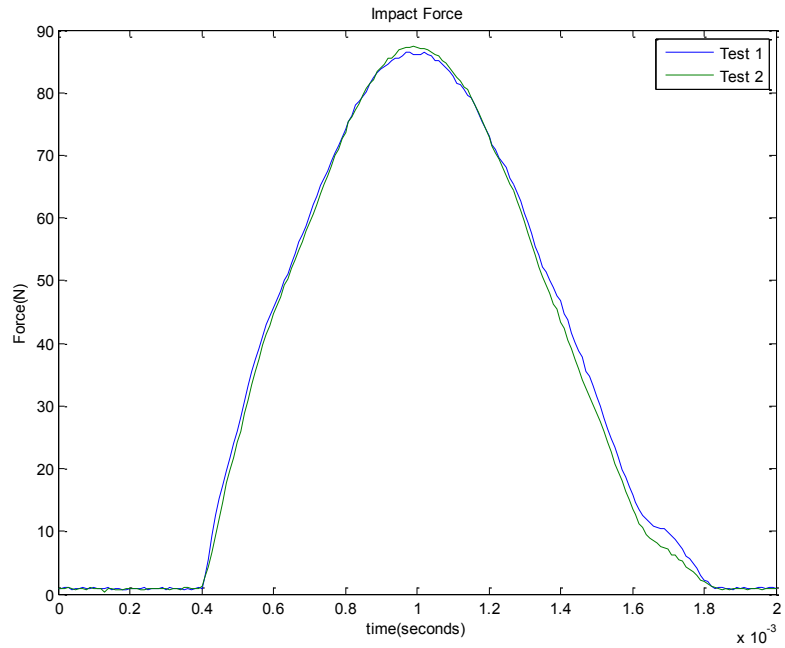


**Figure 31: Impact Force of Woven Fabric Composite Cantilever Beam Repeatability Test**

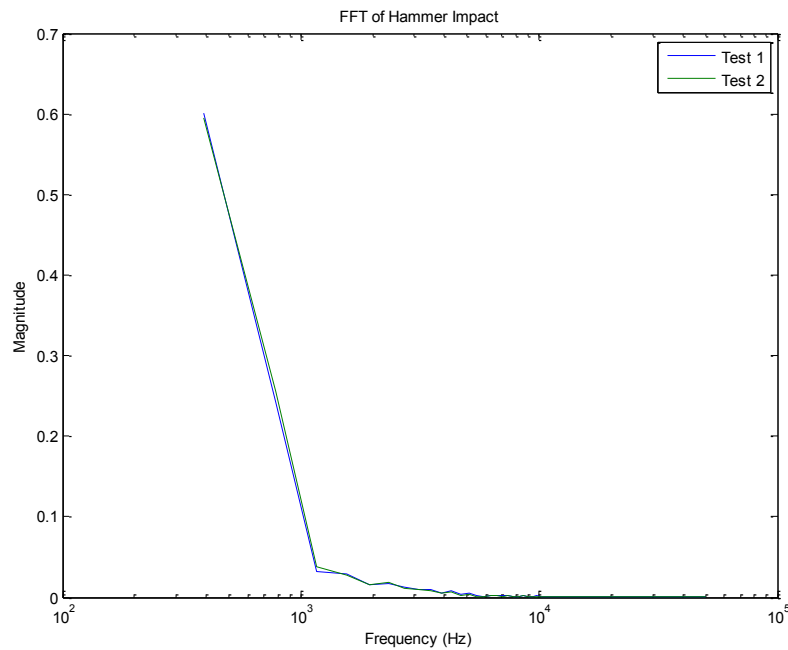


**Figure 32: Frequency Response of Impact force of Woven Fabric Composite Repeatability Test**

#### 4.4 Experimental, Analytical, and Finite Element Analysis of Cantilever Beam Natural Frequencies

The cantilever beam study contains three different investigations. The experimental section includes the results from the experimental data. The analytical section is the analytical solution of the natural frequency response of the cantilever beams. The analytical solution of the cantilever beam gives the fundamental natural frequency of the beam. The finite element section includes the implicit analysis to determine the natural frequency response of the cantilever beams and an explicit analysis to give the acceleration of the beam at the point where the accelerometer is placed. The results from the experiment are then compared to the FEA results to determine the accuracy of the FEA. The experimental acceleration data and the resulting natural frequencies are compared to the simulation results of the FEA and the natural frequencies obtained from the implicit solution. The analytical fundamental natural frequency is also compared to that found from the FEA. The experimental results of the cantilever beam experiment include the measured force input of the hammer, the acceleration of the cantilever beam at the point where the accelerometer is placed, and the modal analysis of the beam including the natural frequencies.

The data collected from the experiments are multiplied by their respective sensitivity and then filtered to remove high frequency noise. This is done for all three of the experimental samples the aluminum, unidirectional, and woven fabric composite beam. The data for the experiments was recorded at 100,000 samples/second and filtered at 10,000 Hz as that is the limit of the accelerometers. The experiments were conducted several times and the data recorded. The force inputs chosen were those that were the



closest in similarity. The following figures provided the force input curve, the time history response, and the frequency response of the three cantilever beams. The time history response and the frequency have both the filtered and the unfiltered data plotted.

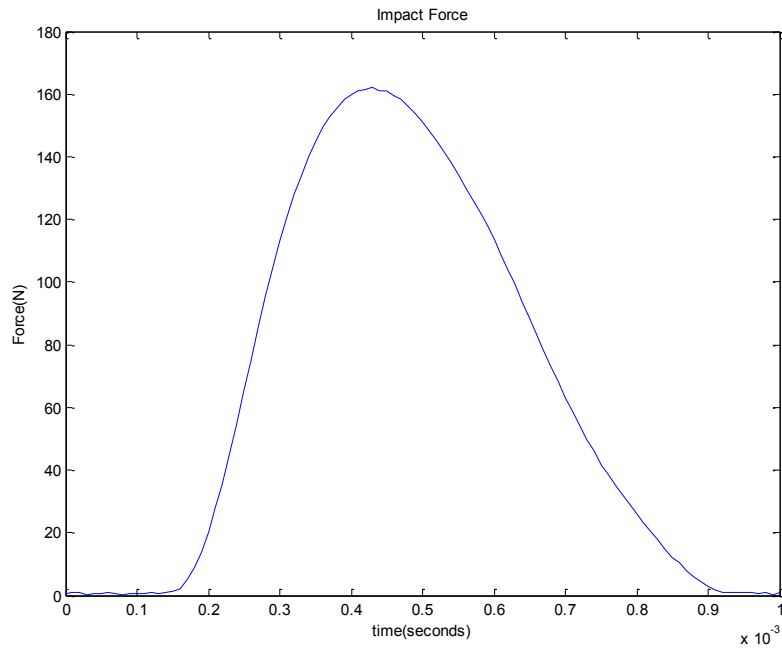


**Figure 33: Impact Force for Aluminum Cantilever Beam Analysis**

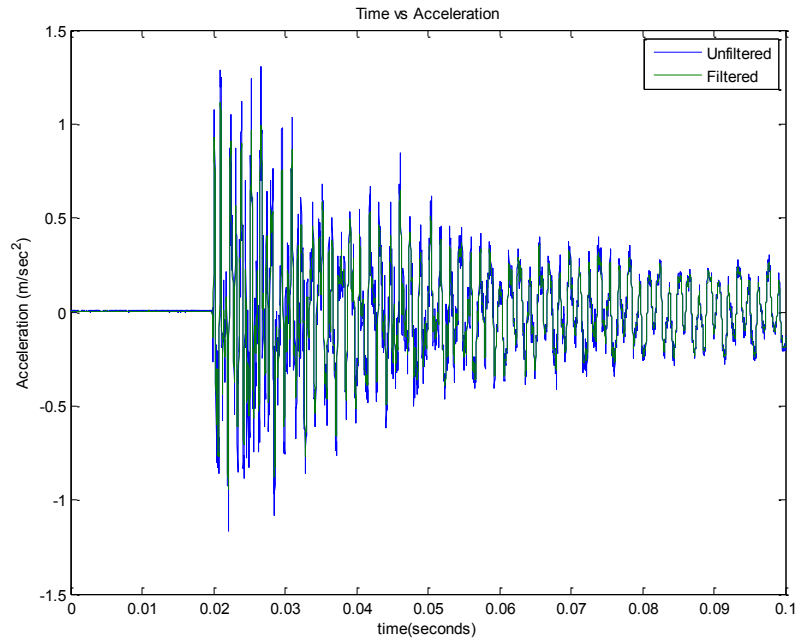


**Figure 34: Time History Response of Aluminum Cantilever Beam**

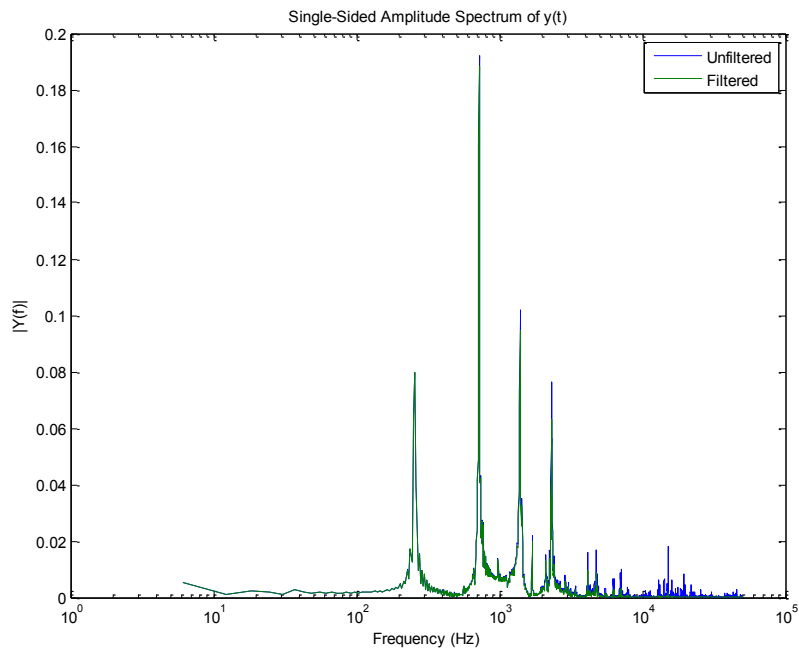


**Figure 35: Frequency Response of Aluminum Cantilever Beam**

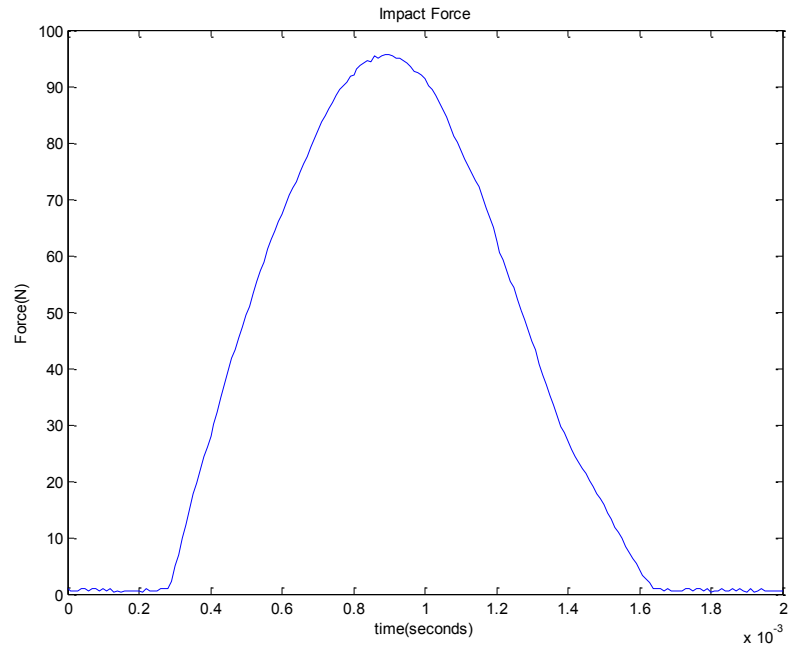


**Figure 36: Impact Force for Unidirectional Composite Cantilever Beam**

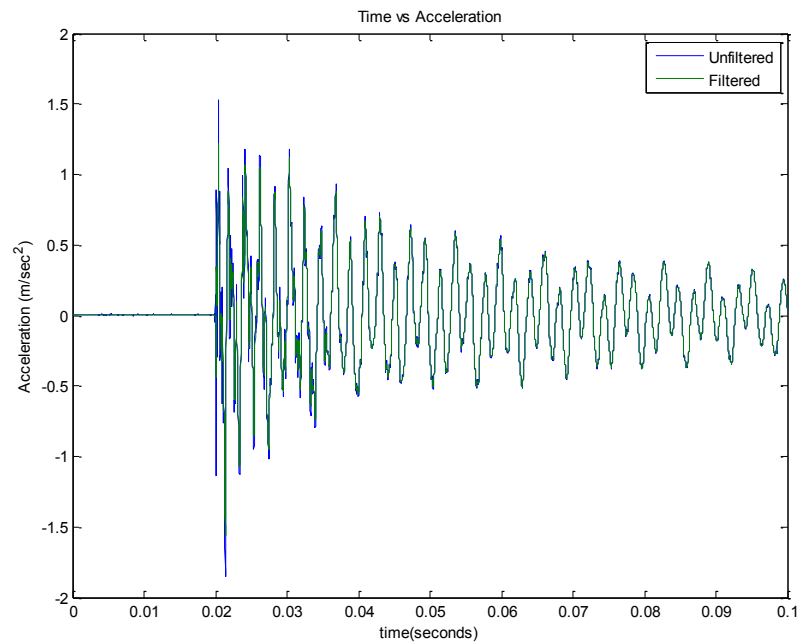


**Figure 37: Time History Response of Unidirectional Composite Cantilever Beam**

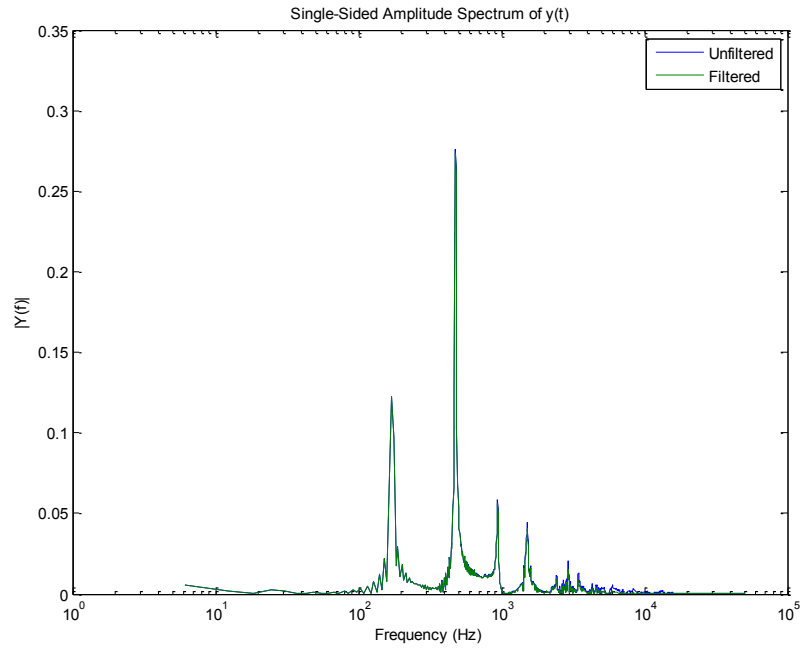


**Figure 38: Frequency Response of Unidirectional Composite Cantilever Beam**

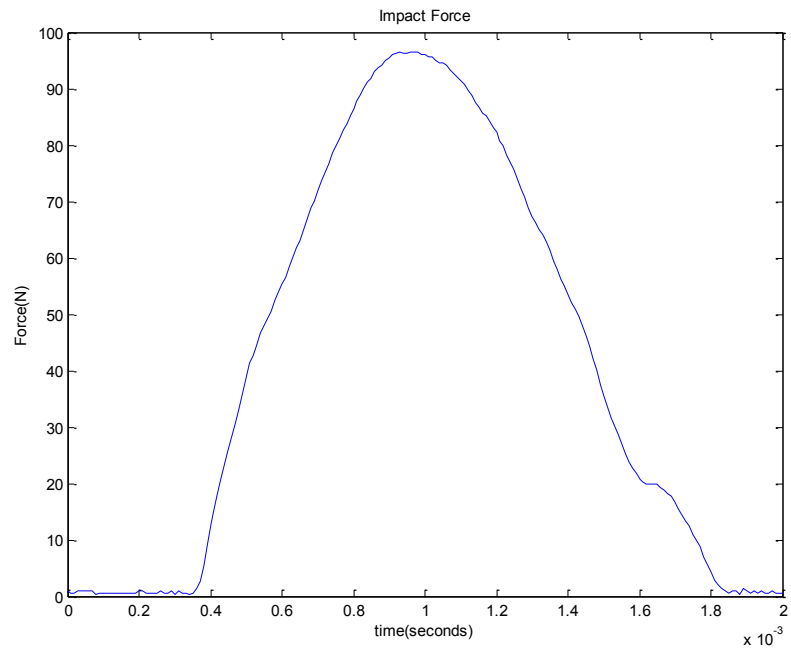


**Figure 39: Impact Force of Woven Fabric Composite Cantilever Beam**

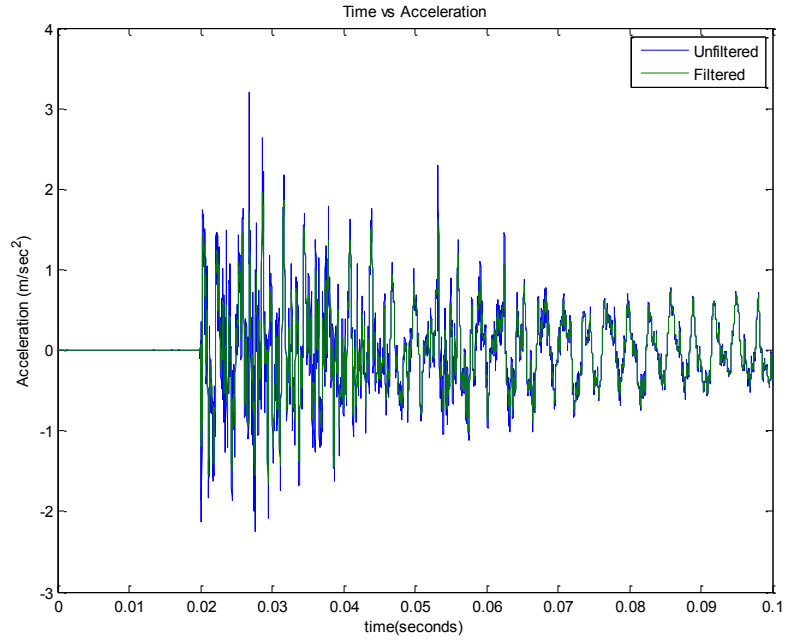


**Figure 40: Time History Response of Woven Fabric Composite Cantilever Beam**

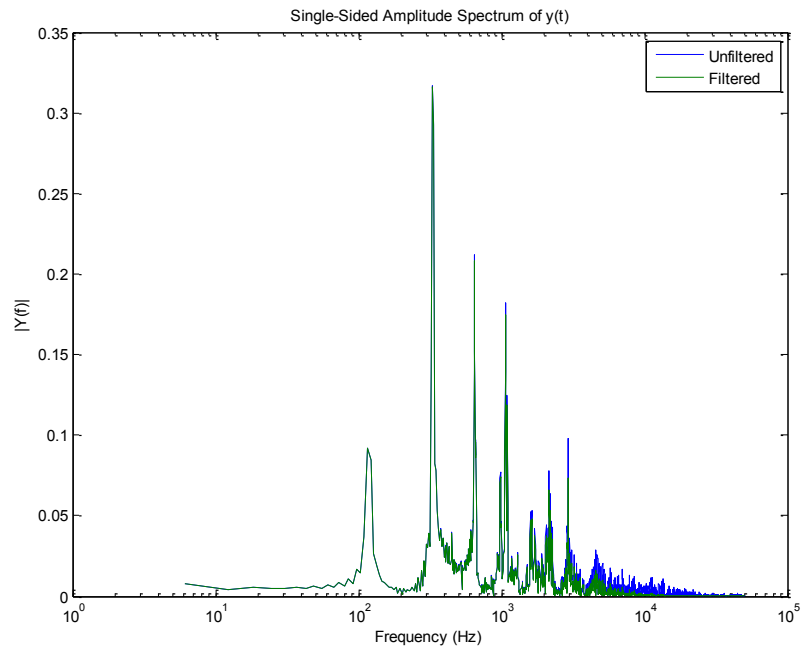


**Figure 41: Frequency Response of Woven Fabric Composite Cantilever Beam**

The fundamental natural frequency of the cantilever beam can be solved analytically for the three different cantilever beams. The two composite beams require an approximation of the elastic bending modulus. The bending modulus of a composite can be approximated by the following equation [2].

$$(EI)_B = \sum (E_{11})_j I_j$$

The fundamental natural frequency begins with the equation of motion for the forced lateral vibration of a non uniform beam.

$$\frac{\partial^2}{\partial x^2} \left[ E_B I(x) \frac{\partial^2 w}{\partial x^2}(x, t) \right] + \rho A(x) \frac{\partial^2 w}{\partial x^2}(x, t) = f(x, t)$$

Where E is the elastic modulus in bending, I(x) is the moment of inertia, w is the lateral displacement,  $\rho$  is the mass density and A is the cross sectional area of the beam. This equation can be simplified for a uniform beam in free vibration [3].

$$\left[ c^2 \frac{\partial^4 w}{\partial x^4}(x, t) \right] + \frac{\partial^2 w}{\partial x^2}(x, t) = 0$$

Where the variable c is defined as

$$c = \sqrt{\frac{E_B I}{\rho A}}$$

The fourth order PDE can be solved using separation of variables method and resulting ordinary differential equations can be solved with the given boundary conditions ending with the solution to the natural frequency of the beam.

$$\omega = \beta^2 \sqrt{\frac{E_B I}{\rho A}} = (\beta l)^2 \sqrt{\frac{E_B I}{\rho A l^4}}$$

The resulting fundamental natural frequencies for the three cantilever beam specimens are given in table 7.

**Table 7: Fundamental Frequency of Cantilever Beams**

Material	$E_B$ (GPa)	$\omega$ (Hz)
Aluminum	70	197
Unidirectional	94.78	143
Woven Fabric	47.12	101

**Table 8: Comparison of Analytical and Experimental Natural Frequencies of Cantilever Beams**

Material	Experimental	Analytical	Error
Aluminum	256	277	%7.58
Unidirectional	171	198	%13.6
Woven Fabric	122	137	%10.64

The Finite Element Analysis of the natural frequencies of the cantilever beams includes a mesh optimization. Mesh optimization is conducted in order to find the mesh density that allows for the most accurate simulation without being overly computationally demanding. The mesh optimization will be performed through a natural frequency analysis of the cantilever beams. An implicit FEA is performed comparing the natural frequencies of the beams resulting from the experiment and FEA. The mesh optimization includes both shell and solid elements to determine which element type is the best for transient dynamic analysis. All the models used in the mesh optimization are meshed in ALTAIR Hypermesh, processed using LS-DYNA, and results are analyzed using LS-DYNA Pre-Post. The Shell elements are best for simulations with thin specimens and models using shell elements are less computationally demanding than solid element

models due to fewer nodes and elements used. Models with solid elements offer better accuracy in terms of shock response, but require increased computational time due to the increased number of elements necessary to model the geometry. The shell element models are separated into three different mesh densities from fine to coarse. The solid element models are separated into 2, 4, and 8 elements along the thickness of the beam. A modal analysis is conducted in order to test the effectiveness of the various mesh densities. A modal analysis gives both the natural frequencies and the mode shapes of the cantilever beam. The modal analysis will serve as a good starting point for the FEA as it gives a good representation of the accuracy of the numerical model. The modal analysis is also important in the composite FEA as it determines whether or not the material models used for the composite materials are valid.



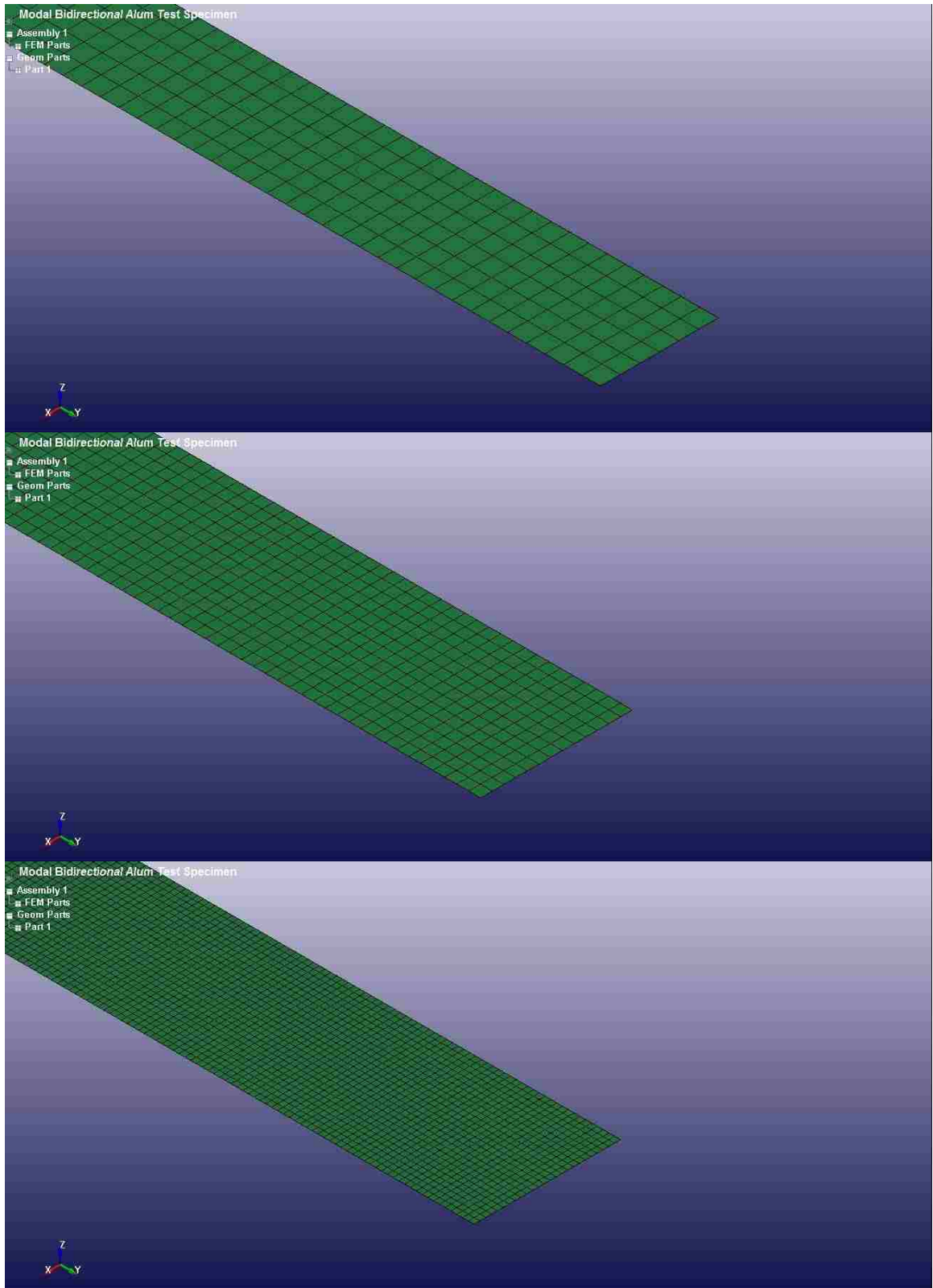


**Figure 42: Cantilever Beam Meshed with Shell Elements (Corse, Medium, Fine)**

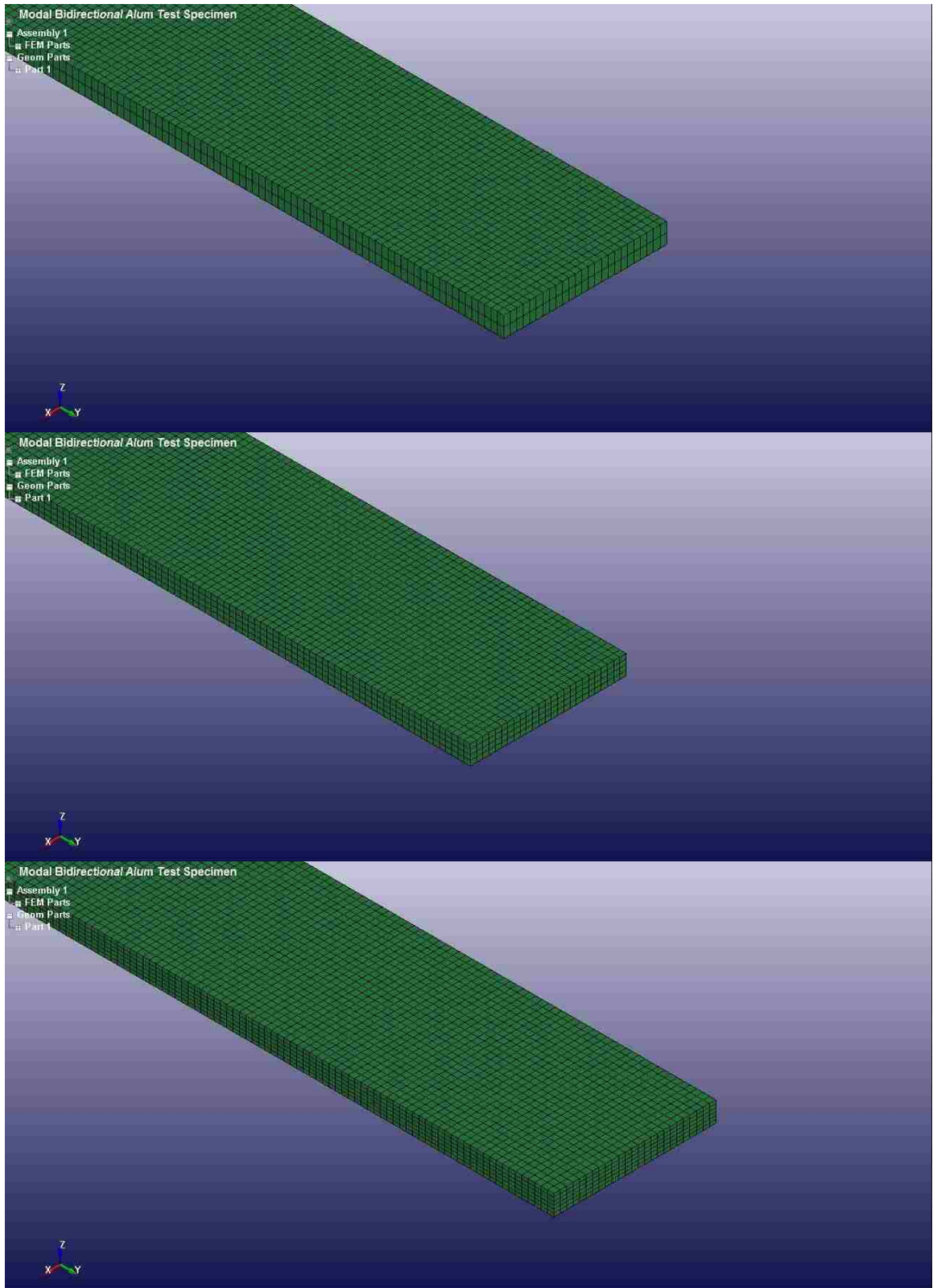


**Figure 43: Cantilever Beam with Solid Mesh 2, 4, and 6 Elements along the Thickness**

The experimental part of the cantilever beam analysis includes an FFT of the time history in MATLAB. The FFT gives the natural frequencies of the three cantilever beam specimens used in the experimental analysis. The natural frequencies of the FEA, the analytical solution, and the experiment are compared to determine which mesh is best for the time history transient dynamic analysis. The mesh that is the best compromise of shortest computational time with the least error compared to the experimental frequencies will be chosen for the time history transient dynamic FEA analysis. A simple initial test of the accuracy of the material models is a mass test. A mass test compares the mass of the specimen to that calculated by the FEM.

**Table 9: Mass Test for Cantilever Beams**

Cantilever Beam Material	Cantilever Beam Mass (Kg)	Finite Element Mass (Kg)	Error
Aluminum	.346	.3497	% 1.1
Unidirectional	.06868	.06869	% .015
Woven Fabric	.067	.0713	% 6.42

**Table 10: Total Number of Elements and Nodes for Mesh Optimization**

FE Model	Total Nodes	Total Elements
Shell Corse	364	306
Shell Medium	1442	1326
Shell Fine	5304	5075
Solid 2	15912	10150
Solid 4	26520	20300
Solid 6	37128	30450

**Table 11: Natural Frequencies of Aluminum Cantilever Beam**

Frequency		Shell Coarse	Shell Medium	Shell Fine	Solid 2	Solid 4	Solid 6
<b>277</b>	256.3	275	275	275	242	268	272
<b>720.2</b>		770	769	771	678	748	760
<b>1392</b>		1500	1508	1511	1328	1464	1488
<b>1607</b>		1649	1686	1695	1482	1629	1654
<b>2307</b>		2497	2493	2496	2193	2416	2456

**Table 12: Natural Frequencies of Unidirectional Composite Cantilever Beam**

Frequency		Shell Coarse	Shell Medium	Shell Fine	Solid 2	Solid 4	Solid 6
<b>198</b>	171	186	186	186	163	181	184
<b>476</b>		504	508	510	454	504	511
<b>940</b>		1013	1012	1014	886	982	998
<b>1514</b>		1665	1663	1665	1457	1611	1638
<b>2430</b>		2474	2465	2439	2430	2469	2492

**Table 13: Natural Frequencies of Woven Fabric Composite Cantilever Beam**

Frequency		Shell Coarse	Shell Medium	Shell Fine	Solid 2	Solid 4	Solid 6
<b>137</b>	122	134	136	136	119	132	134
<b>330</b>		357	364	367	333	360	363
<b>647</b>		657	672	677	651	662	668
<b>1074</b>		1036	1063	1070	1073	1045	1056
<b>1624</b>		1512	1553	1564	1597	1523	1541

**Table 14: Aluminum Cantilever Beam Natural Frequency Error of FEA**

Frequency	Aluminum Experimental	Aluminum FEA	Error
1	277	268	3.25%
2	720.2	748	3.9%
3	1392	1464	5.2%
4	1607	1629	1.4%
5	2307	2416	4.7%

**Table 15: Unidirectional Composite Cantilever Beam Natural Frequency Error of FEA**

Frequency	Unidirectional Experimental	Unidirectional FEA	Error
1	198	181	8.6%
2	476	504	5.9%
3	940	982	4.5%
4	1514	1611	6.4%
5	2430	2469	1.6%

**Table 16: Woven Fabric Composite Cantilever Beam Natural Frequency Error of FEA**

Frequency	Woven Fabric Experimental	Woven Fabric FEA	Error
1	137	132	3.65%
2	330	360	9.1%
3	647	662	2.3%
4	1074	1045	2.7%
5	1624	1523	6.2%

To determine the best mesh to be used for the FEA the aluminum cantilever beam is used. The aluminum beam is chosen due to the properties of aluminum. Aluminum is an isotropic material and its material and mechanical properties are well understood and defined. Due to the nature of composite materials both the material and mechanical properties vary according to the manner in which it is produced. It follows that the material and mechanical properties found are not as reliable as of aluminum. It was determined from the mesh optimization of the natural frequency analysis of the cantilever beam experiments that a solid mesh with 4 elements across the thickness of the beam would be best for the time history transient dynamic analysis. The natural frequency analysis indicates that solid elements are preferential to those of the shell elements, even considering the increased computational time. The solid mesh density chosen was that of 4 elements along the thickness direction of the mesh.

#### 4.5 Mode Shapes of Cantilever Beams

The mode shapes and natural frequencies are important parts in understanding the dynamic response of any structure. The mode shapes for the aluminum cantilever beam, unidirectional composite cantilever beam, and the woven fabric cantilever beam will be shown for the first five natural frequencies for the aluminum cantilever beam and unidirectional composite cantilever beam. The first four natural frequencies are shown for

the woven fabric composite cantilever beam. The aluminum cantilever beam is shown in Appendix A, the unidirectional composite cantilever beam in Appendix B, and the woven fabric in Appendix C

#### 4.6 Transient Analysis of Cantilever Beam

The transient analysis of the cantilever beams is performed to better understand how to solve transient dynamic responses to impact of composite materials using the Finite Element Method. The aluminum cantilever beam is used as a control in this analysis as isotropic materials, like metals, have been used in previous studies on shock response analysis, where the FEM was used as a numerical solution to the problem. The composite cantilever beams are compared to the aluminum beam to determine if the FEM is an appropriate numerical solution method for shock response analysis of composite materials.

The FEA of the cantilever beam is divided into three sections pre-processing, processing, and post-processing. Altair Hypermesh is used as the preprocessor, LS-DYNA for processing, and LS-PrePost for post processing for all the models in the cantilever beam analysis. As determined in the natural frequency analysis the beams are meshed with solid elements and 4 elements across the thickness of the beam. The three cantilever beams have the same number of elements and nodes, 20,300 elements and 26,520 nodes. The cantilever beams are rigidly constrained, where they are clamped in the vise during the experiments. There are 3770 nodes rigidly constrained in all directions.

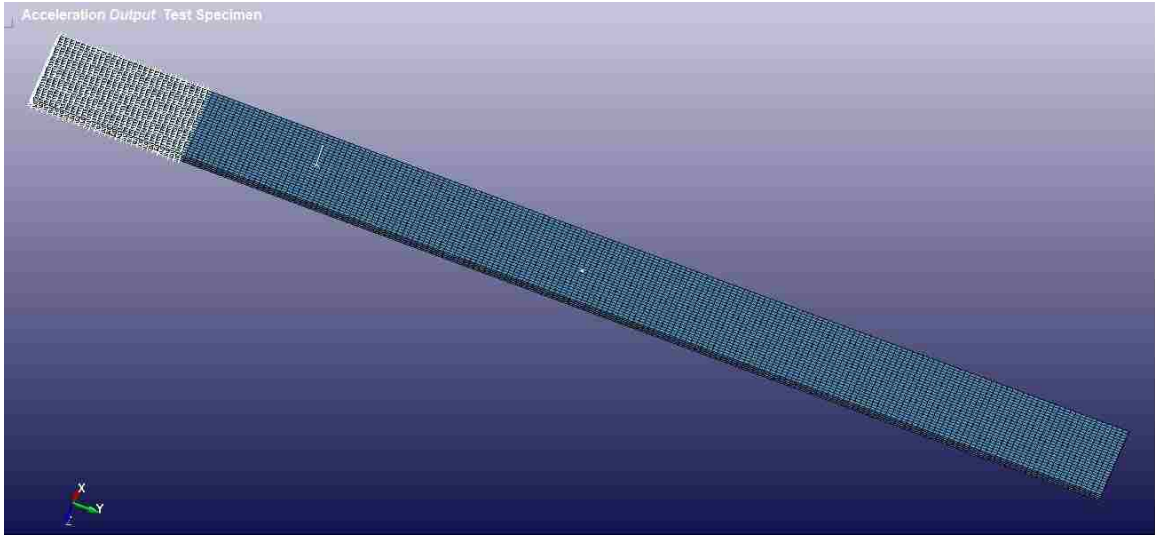


**Figure 44: Finite Element Model of Cantilever Beam Experiment Showing Constraints, Impact Force, and Accelerometer Placement**

The material card used for the aluminum beam is \*MAT\_001/ \*MAT\_ELASTIC.

\*MAT\_001 can be used in this analysis as all deformation is kept with the elastic limit.

The material card for aluminum is defined as follows [22].

\*MAT\_ELASTIC

\$ Material Card for Aluminum Cantilever Beam

\$	MID	RO	E	PR
	1	2700.06	8.000E+10	0.33

The material cards used for the composite beams is \*MAT\_002/

\*MAT\_ORTHOTROPIC\_ELASTIC. This material card is chosen for the composite beams due to the configuration of the lamina in the composite. The fibers are arranged in every lamina of the composite in the same direction. This allows the composite to be modeled as a single structure with orthotropic material properties negating the need to define individual lamina properties in the model. The material card for the unidirectional

carbon fiber reinforced cantilever beam and the woven fabric carbon fiber reinforced cantilever beam are defined as follows [22].

\*MAT\_ORTHOTROPIC\_ELASTIC

\$ Material Card for Unidirectional Carbon Fiber Reinforced Cantilever Beam

\$	MID	RO	EA	EB	EC	PRBA	PRCA	PRCB
	1	1310.09	4.780E+10	.7540E+10	.7540E+10	0.0246	0.0246	0.4356
\$	GAB	GBC	GCA	AOPT				
	0.2770E+100	.2625E+100	.2770E+10	2				
\$		A1	A2	A3				
		0.0	1.0	0.0				
\$		D1	D2	D3				
		0.1	0.0	0.0				

\*MAT\_ORTHOTROPIC\_ELASTIC

\$ Material Card for Unidirectional Carbon Fiber Reinforced Cantilever Beam

\$	MID	RO	EA	EB	EC	PRBA	PRCA	PRCB
	1	1360	4.7120E+10	4.7120E+10	.6607E+10	0.0470	0.0266	0.0266
\$	GAB	GBC	GCA	AOPT				
	.25800E+10	.2394E+10	.2490E+10	2				
\$		A1	A2	A3				
		0.0	1.0	0.0				
\$		D1	D2	D3				
		0.1	0.0	0.0				

MID- Material ID

RO- Mass Density of Material

EA- Modulus of Elasticity in direction of vector A



EB- Modulus of Elasticity in direction of vector B

EC- Modulus of Elasticity in direction of vector C

PRBA- Poisson's Ration in direction of vector BXA

PRCA- Poisson's Ration in direction of vector CXA

PRCB- Poisson's Ration in direction of vector CXB

GAB- Shear modulus in direction of vector AXB

GBC- Shear modulus in direction of vector BXC

GCA- Shear modulus in direction of vector CXA

AOPT- Option for defining vectors A, B, and C (Option 2 defines vector A and a vector D to which the normal of A and D are vector C)

A1- X-coordinate of head of vector A

A2- Y-coordinate of head of vector A

A3- Z-coordinate of head of vector A

D1- X-coordinate of head of vector D

D2- Y-coordinate of head of vector D

D3- Z-coordinate of head of vector D

The FEA termination time is 20 milliseconds and the data plotted every 50 microseconds. The experimental data was recorded for 80 milliseconds. A shorter run time for the FEA was preferred due to the decreased computational time. The termination time of 20 milliseconds was enough to determine the accuracy of the FEA. The results of the FEA were filtered at the same frequency as the experimental data and the time history and frequency response compared. In order to compare the time history data a Normalized Root Mean Square Error routine was used. The NRMSD function is used to compare to two time history responses. The NRMSD function is defined in the following equation.

$$RMSD = \sqrt{\frac{\sum_{i=1}^n (x_i - a_i)^2}{n}}$$

$$NRMSD = \frac{RMSD}{(x, a)_{max} - (x, a)_{min}}$$

Where x is the experimental acceleration, a is the FEA acceleration, and n is the number of points.

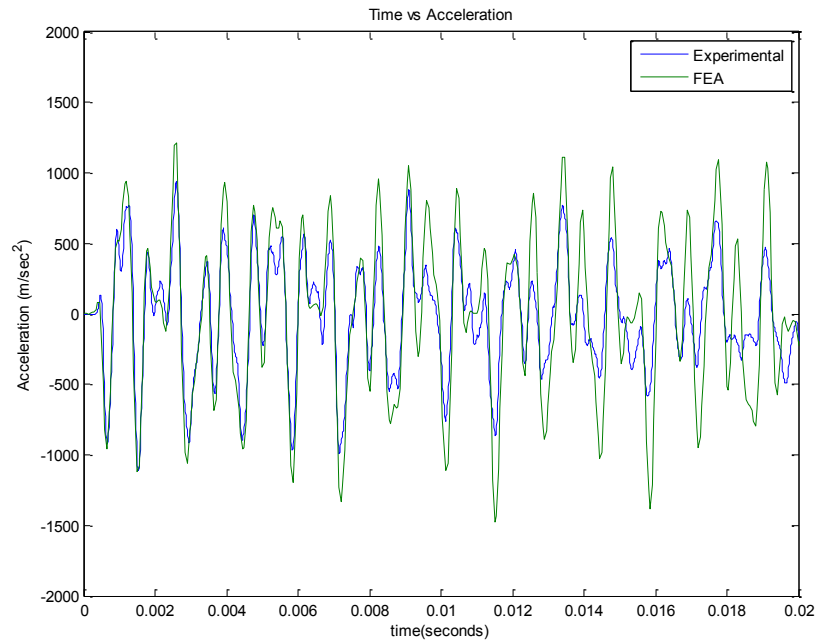


**Figure 45: Time History Plot of Aluminum Cantilever Beam Experimental and FEA**

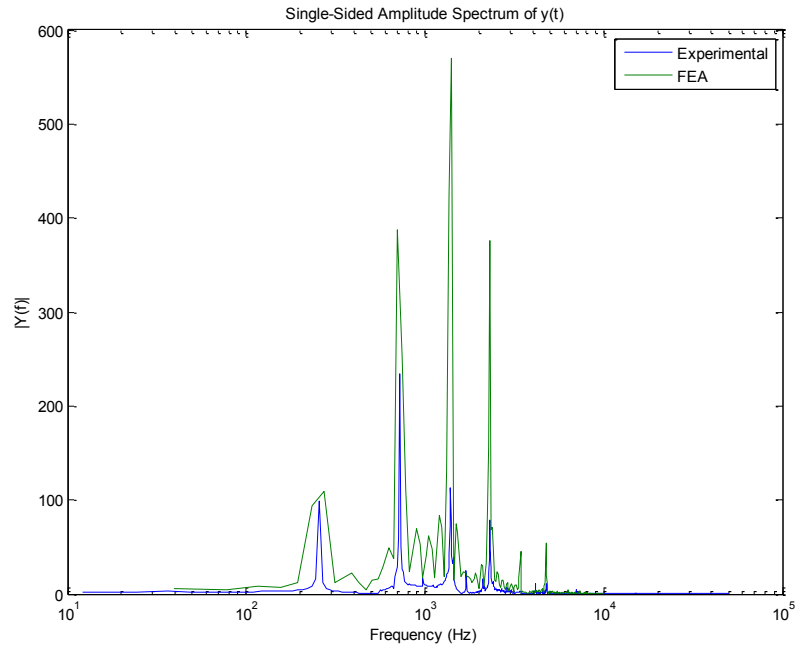


**Figure 46: Frequency Domain of Aluminum Cantilever Beam Experimental and FEA**

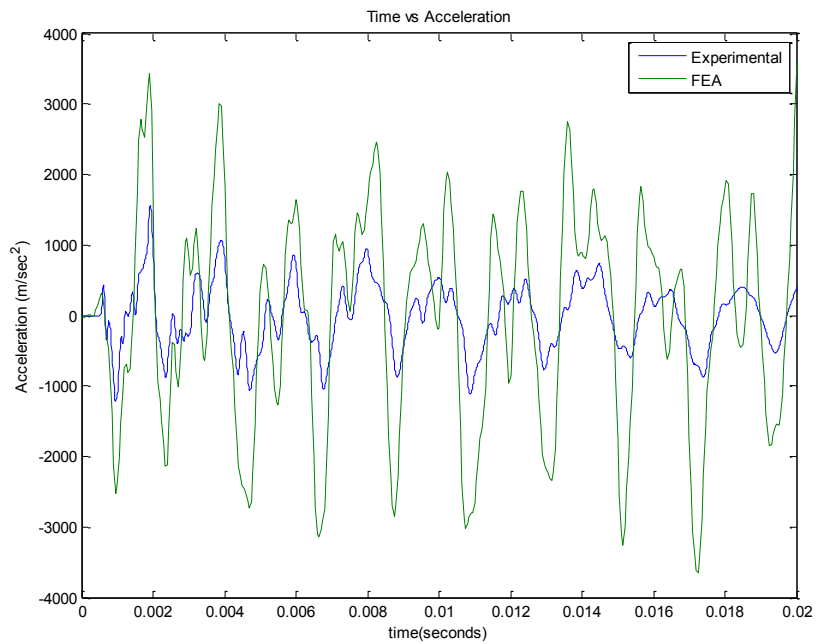


**Figure 47: Time History Plot of Unidirectional Composite Cantilever Beam Experimental and FEA**

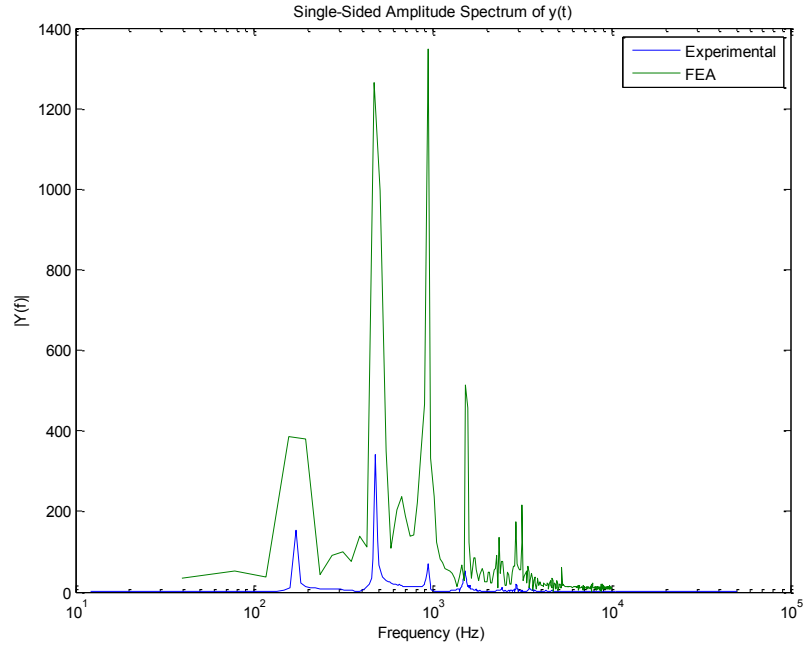


**Figure 48: Frequency Domain of Unidirectional Composite Cantilever Beam Experimental and FEA**

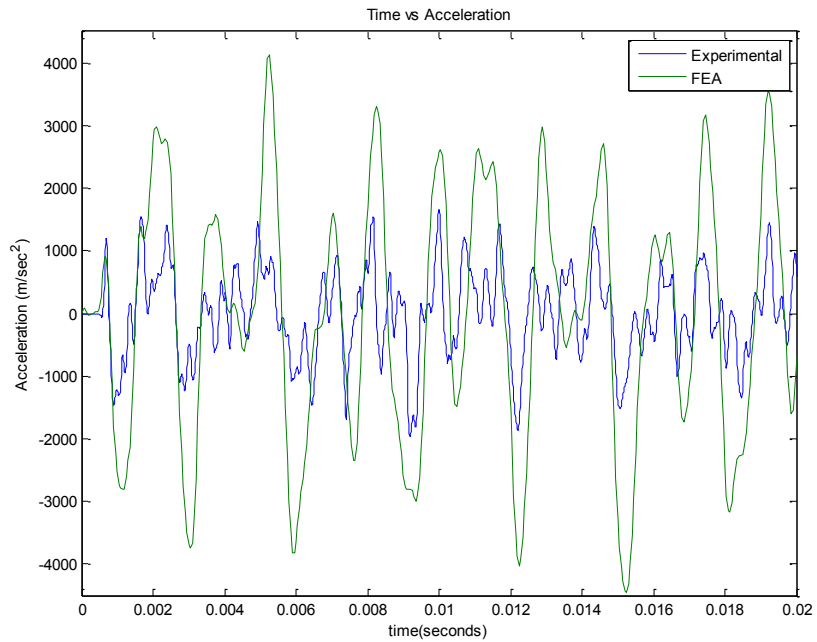


**Figure 49: Time History Plot of Woven Fabric Composite Cantilever Beam Experimental and FEA**

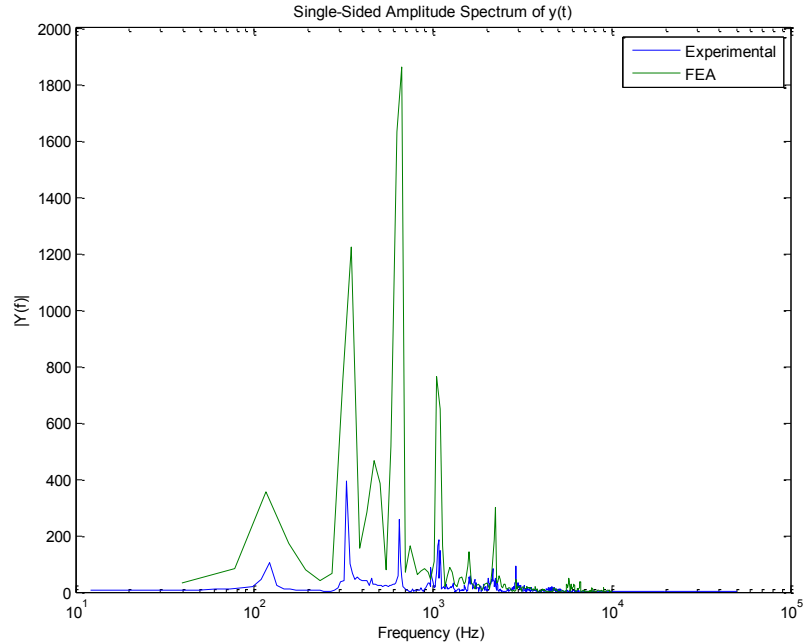


**Figure 50: Frequency Domain of Woven Fabric Composite Cantilever Beam Experimental and FEA**

The results of the FEA show that all of the models have higher magnitude natural frequencies and the time history response has higher magnitude peaks. The FEA shows that in all models damping is needed to better model the time history response. The composite cantilever beams need more damping than that of the aluminum beam due to the higher magnitude of peaks in the time history response in comparison to the experimental time history response. The NRMSD shows that the composite beams have a large difference in amplitude compared to that of the aluminum beam.

**Table 17: NRMSD of Experimental and FEA Cantilever Beam Time History**

Cantilever Beam	NRMSD
Aluminum	0.140
Unidirectional	0.430
Woven Fabric	0.445

The Cantilever Beam analysis shows that in order to get accuracy of the composite FEA equivalent to that of the aluminum cantilever beam damping must be included. There are several techniques that can be used to introduce damping into the finite element model. Damping is necessary as the material models in LS-DYNA do not support any kind of material damping. To damp the response of the FEA the damping card \*DAMPING\_FREQUENCY\_RANGE is used. This feature provides approximately constant damping (i.e. frequency independent) over a range of frequencies. This method of damping reduces the dynamic stiffness of the model. Therefore it is necessary to adjust the mechanical and material properties. The reduction in dynamic stiffness depends on the damping coefficient and the range of frequencies damped [22].

```
*DAMPING_FREQUENCY_RANGE
$ CDAMP FLOW FHIGH PSID
CDAMP- Damping in fraction of critical
FLOW- Lowest frequency in range of interest
FHIGH- Highest frequency in range of interest
PSID- Part Set ID
```

This method of damping was chosen as it gives control to what frequencies can be damped. In order to obtain the correct damping coefficient and to adjust the stiffness of the model to account for the reduced dynamic stiffness multiple simulations must be run. This method does not allow for the values to be determined analytically they must be determined empirically. The magnitudes of the frequency analysis can be used as a judge to the amount of damping necessary. The damping and adjusted dynamic stiffness was found satisfactory when the NRMSD was similar to that of the aluminum cantilever beam

model. The following damping cards were arrived at for the unidirectional composite cantilever beam and the woven fabric cantilever beam.

To determine the damping factor in the simulation the half-bandwidth method is used in the frequency domain. This method works from the concept that the shape of the frequency response is controlled by the amount of damping in the system. Damping factor is calculated from the two frequencies near the fundamental frequency, whose magnitude is equal to  $Rd/\sqrt{2}$ . The damping factor can then be determined from the following equation [3].

$$\xi = \frac{(f_2 - f_1)}{(f_2 + f_1)}$$

**Table 18: Damping Factor for Composite Cantilever Beams**

Cantilever Beam	Damping Factor
Unidirectional Composite	0.030
Woven Fabric Composite	0.045

\*DAMPING\_FREQUENCY\_RANGE

\$ Unidirectional Cantilever Beam Damping

.03 100 3000

\*DAMPING\_FREQUENCY\_RANGE

\$ Woven Fabric Cantilever Beam Damping

.045 100 2500

The material model has to be changed in order to reflect the reduction in dynamic stiffness caused by the damping card added. The difference needed to offset the reduction in dynamic stiffness must also be found empirically. The LS-DYNA keyword manual gives a rough estimate of the needed increase in stiffness depending on the frequency

range and the coefficient of damping. The original material card for the model with no damping and the updated material card for the model with damping is given in the following cards [22].

**Table 19: Stiffness Reduction from \*DAMPING\_FREQUENCY\_RANGE**

Frequency Error at $F_{low}$ Damping Ratio	$F_{high}/F_{low}$			
		3 to 30	30 to 300	300 to 3000
.01		3%	4.5%	6%
.02		6%	9%	12%
.04		12%	18%	24%

\*MAT\_ORTHOTROPIC\_ELASTIC

\$ Unidirectional Composite Material Card No Damping

```

$ MID   RO      EA      EB      EC   PRBA  PRCA  PRCB
      1  1310 9.4780E+10 .7540E+10 .7540E+10 0.0246 0.0246 0.4356

$   GAB      GBC      GCA AOPT
.2770E+10 .2625E+10 .2770E+10    2

$           A1   A2   A3
           0.0   1.0   0.0

$           D1   D2   D3
           0.1   0.0   0.0

```



\*MAT\_ORTHOTROPIC\_ELASTIC

\$ Unidirectional Composite Material Card with Damping

\$ MID	RO	EA	EB	EC	PRBA	PRCA	PRCB
1	1310	1.0317E+11	.8078E+10	.8078E+10	0.0239	0.0239	0.4289
\$	GAB	GBC	GCA	AOPT			
	.2996E+10	.2827E+10	.2996E+10	2			
\$		A1	A2	A3			
		0.0	1.0	0.0			
\$		D1	D2	D3			
		0.1	0.0	0.0			

\*MAT\_ORTHOTROPIC\_ELASTIC

\$ Woven Fabric Composite Material Card No Damping

\$ MID	RO	EA	EB	EC	PRBA	PRCA	PRCB
1	1360	4.7120E+10	4.7120E+10	.6607E+10	0.0470	0.0266	0.0266
\$	GAB	GBC	GCA	AOPT			
	.258E+10	.2394E+10	.2490E+10	2			
\$		A1	A2	A3			
		0.0	1.0	0.0			
\$		D1	D2	D3			
		0.1	0.0	0.0			

\*MAT\_ORTHOTROPIC\_ELASTIC

\$ Woven Fabric Composite Material Card with Damping

\$ MID	RO	EA	EB	EC	PRBA	PRCA	PRCB
1	1360	5.6460E+10	5.6460E+10	.7540E+10	0.0442	0.0246	0.0246

\$ GAB	GBC	GCA	AOPT
2.180E+10	.2755E+10	.2755E+10	2

\$	A1	A2	A3
	0.0	1.0	0.0

\$	D1	D2	D3
	0.1	0.0	0.0

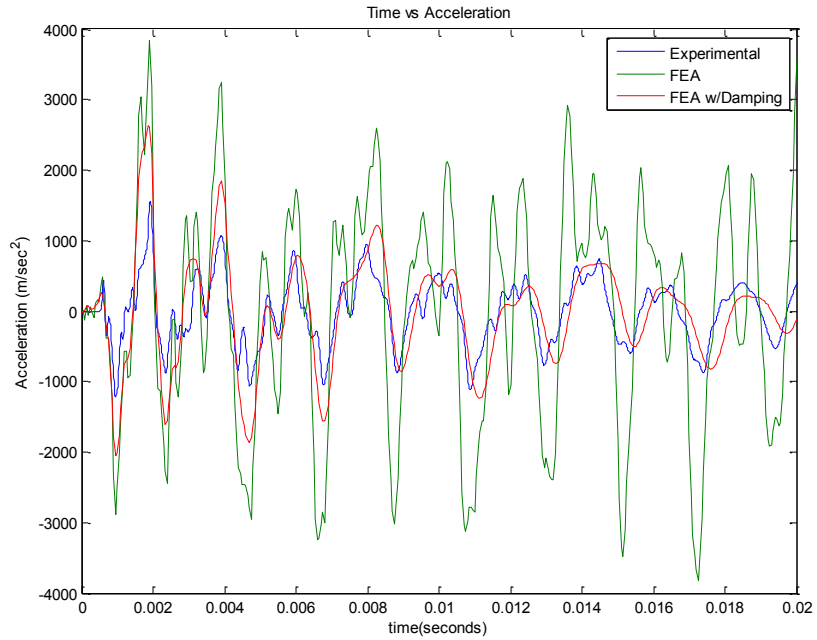
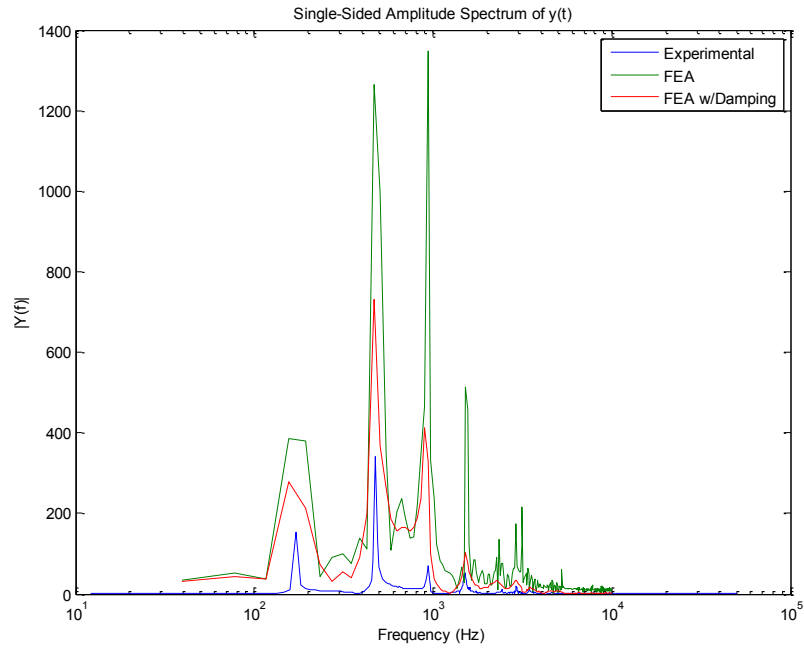
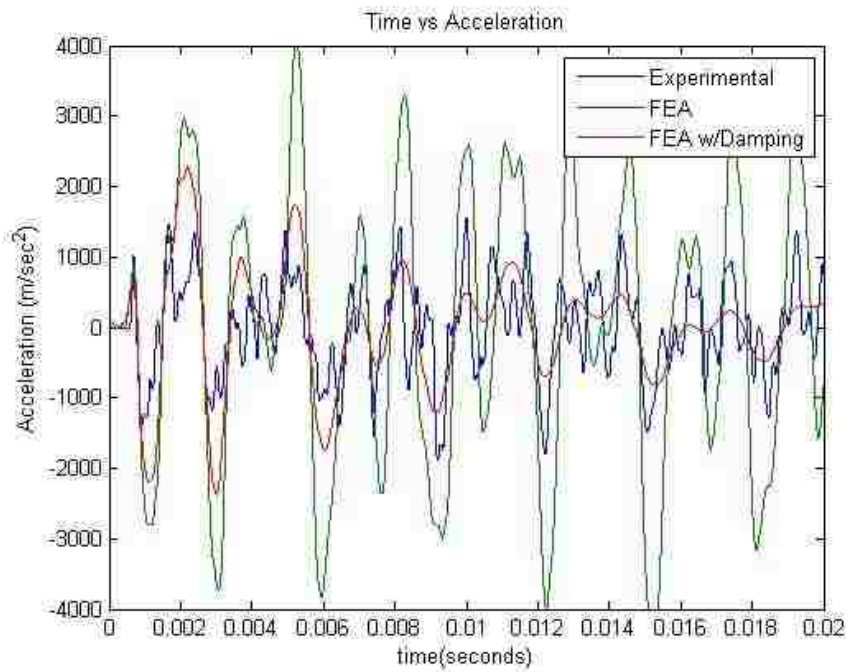


Figure 51: Time History Plot of Unidirectional Composite Cantilever Beam FEA with Damping



**Figure 52: Frequency Domain of Unidirectional Composite Cantilever Beam FEA with Damping**



**Figure 53: Time History Plot of Woven Fabric Composite Cantilever Beam FEA with Damping**

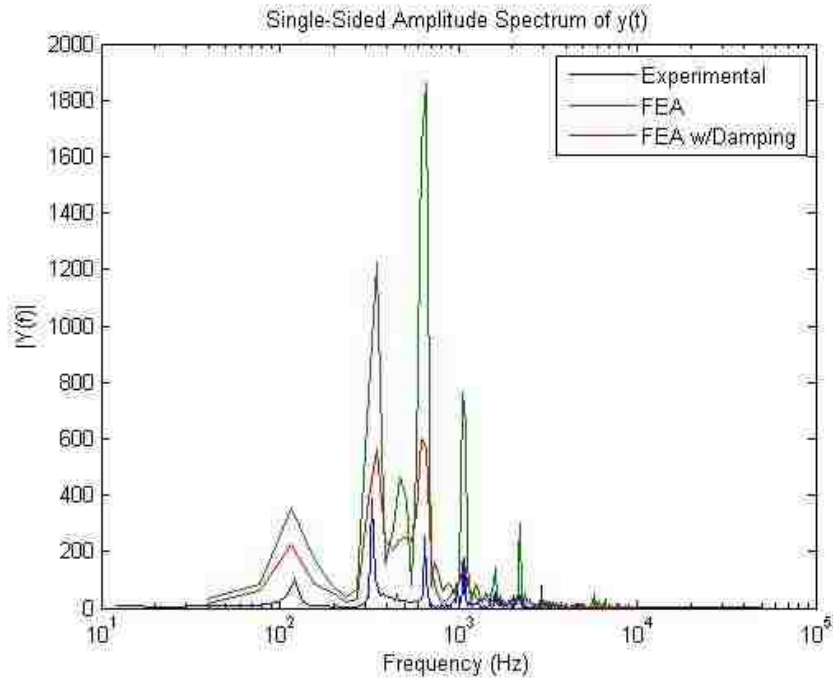


**Figure 54: Frequency Domain of Woven Fabric Composite Cantilever Beam FEA with Damping**

**Table 20: NRMSD of Experimental and FEA with Damping Cantilever Beam Time History**

Cantilever Beam	NRMSD
Aluminum	0.140
Unidirectional	0.140
Woven Fabric	0.125

The simulations of the composite cantilever beams were at or near the accuracy of the simulations of the cantilever beams when damping was added to the composite cantilever beam FEA. It is understood that due to the nature of the composite more damping is necessary in the composite simulations than that of the aluminum. It must be noted as well that the increased need for damping in the composite simulations may be due in part to several experimental attributes. The difference of thickness of the composite cantilever beams in comparison to the aluminum cantilever beam could cause excess vibration in the FEA for the composite cantilever beams. The composite cantilever

beams were clamped slightly different than the aluminum cantilever beam as a spacer was needed for the composite cantilever beams. The mesh density may also be a factor as the mesh for the elements in the aluminum cantilever beam were longer along the thickness of the beam than that of the composite cantilever beam elements. The conclusion of the cantilever beam analysis is that composite materials can be accurately modeled using the FEM.

## CHAPTER 5

### ANALYSIS OF BOLTED HAT STRUCTURE

#### 5.1 Background

The bolted hat section analysis is used to test the shock response of bolted joints. There are two carbon fiber fabrics used in the creation of the hat sections. The two hat sections will be a unidirectional carbon fiber composite and a woven fabric carbon fiber composite. As in the cantilever beam experiments these simple composites are used as they allow for easier determination of material and mechanical properties and allow for the use of a simpler material model in the FEA. Almost all composite laminates used for industrial applications will be constructed from multiple layers of unidirectional and/or woven fabric layers in different orientations. The bolted hat section analysis is separated into two different studies the natural frequency analysis of the simple hat section with no joints and the time history analysis of the bolted hat section. The natural frequency analysis will be performed using an implicit solver in LS-DYNA. The time history analysis will be performed using an explicit solve in LS-DYNA. For all experiments the equipment is calibrated and a repeatability test performed as in the cantilever beam experiment. The study begins with the natural frequency analysis of the composite hat section. The natural frequency analysis will determine if the material and mechanical properties of the composite hats are valid. The natural frequency analysis will be performed on both the experimental and the FEA. For the experimental results MATLAB will be used to perform an FFT and to filter the data. The data will be filtered at 10,000hz. The natural frequencies of the hat section will be determined. The FEA will be conducted with Altair Hypermesh used as a preprocessor to build the geometry and

meshing, LS-DYNA as a processor, and LS-PrePost and MatLab as a post processor. The results of the FEA will be filtered at 10,000 hz and an FFT performed. The natural frequencies of the experimental and FEA will be compared to determine the accuracy of the model. The second part of the study is the time history analysis of the bolted hat section. The experimental data will be filtered at 10,000 hz using MATLAB and compared to the FEA results using a NRMSD algorithm. The FEA will be conducted with Altair Hypermesh used as a preprocessor, LS-DYNA as a processor, and LS-PrePost as a post processor.

## 5.2 Natural Frequency Analysis of Hat Section

The natural frequency analysis of the single hat section is performed to better understand and validate the material and mechanical properties used in the FEA of the bolted hat structure. The experimental portion is conducted by hanging the hat section from a support structure. The data is recorded at 100,000 samples a second and processed using MATLAB. The FEA begins by meshing the geometry of the hat section. The mesh was chosen with the characteristics that were found to be the best from the cantilever beam optimization, with the exception that 2 elements along the thickness direction were chosen. The decrease in the number of elements was needed to decrease the computational time. As before a simple mass test is conducted to compare the physical hat section to that of the modeled one.

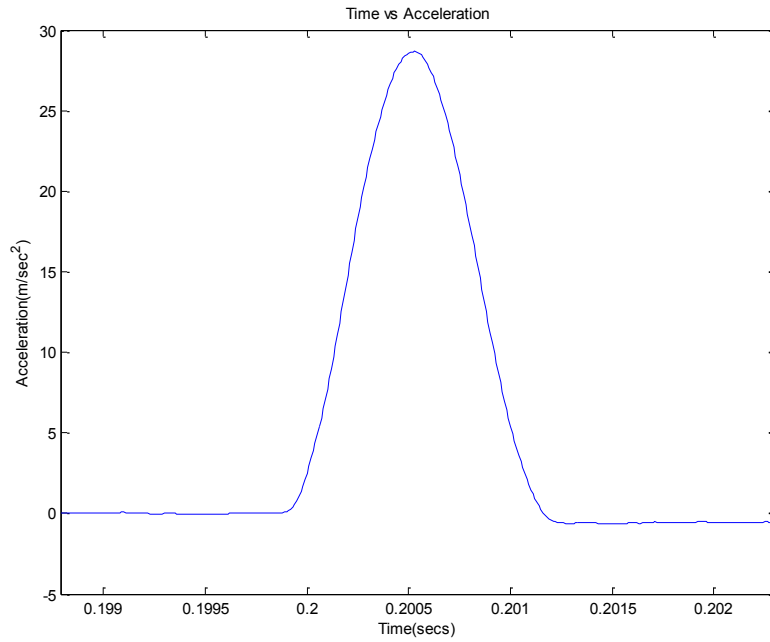


**Figure 55: Force Impact Curve Unidirectional Hat**

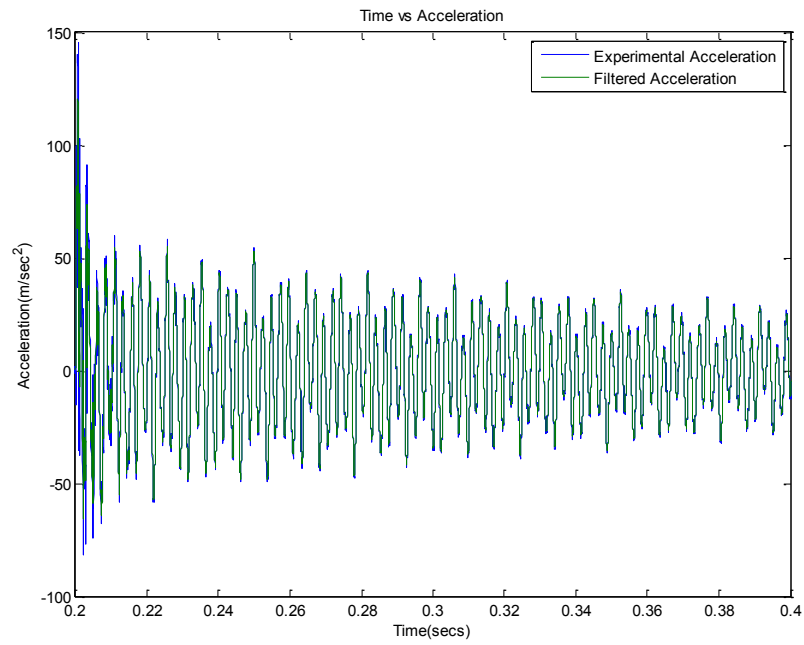


**Figure 56: Time History Plot of Unidirectional Hat Experimental Unfiltered and Filtered**



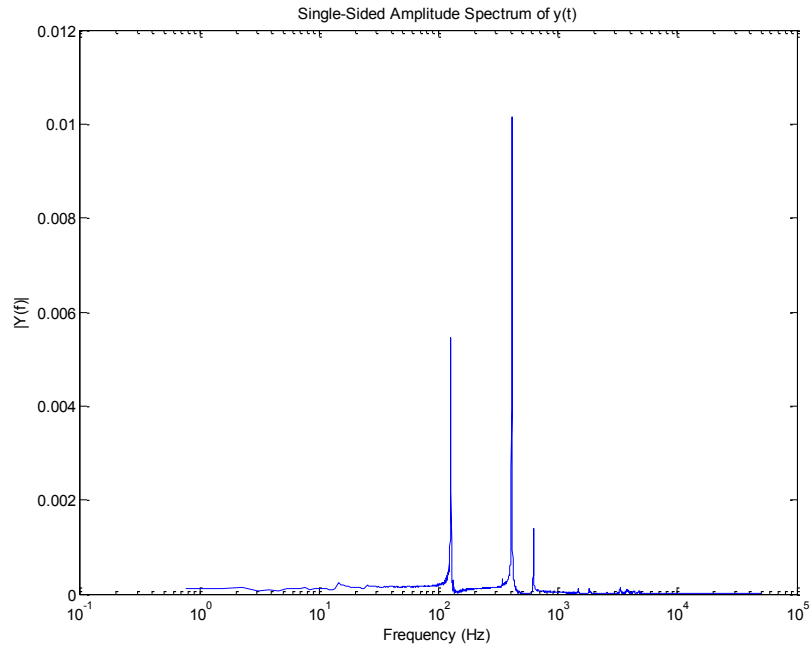


**Figure 57: Frequency Domain of Unidirectional Composite Hat**

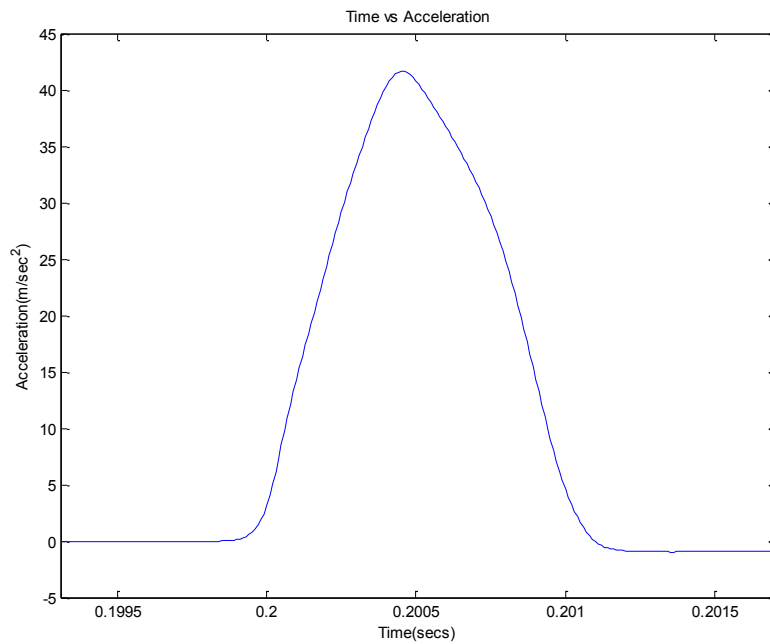


**Figure 58: Impact Force Curve of Woven Fabric Hat**

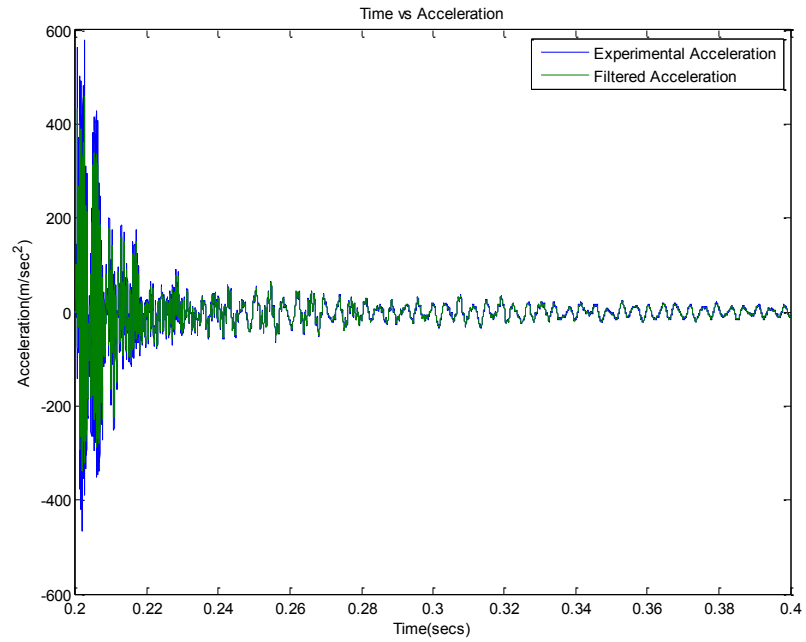


**Figure 59: Time History Plot of Woven Fabric Composite Hat Experimental Unfiltered and Filtered**

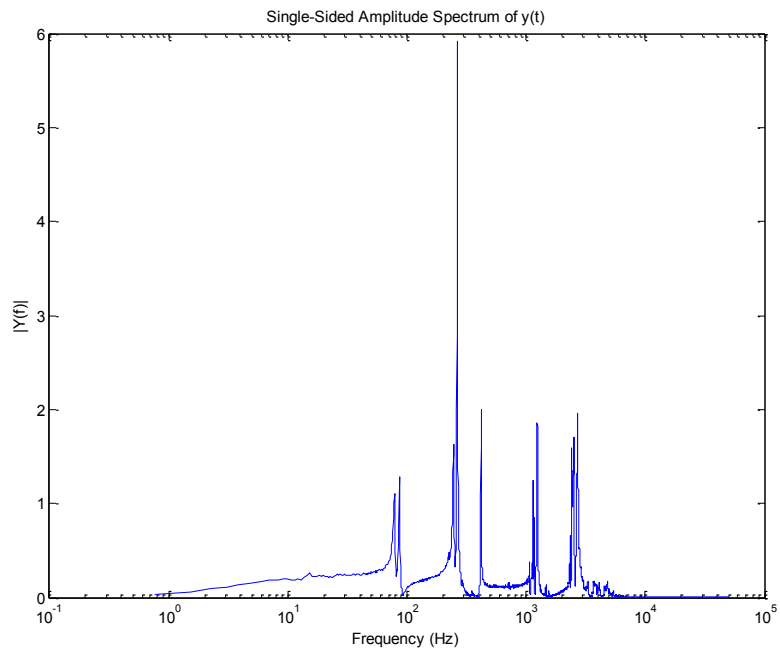


**Figure 60: Frequency Domain Plot of Woven Fabric Composite Hat**

**Table 21: Mass Test of Hat**

Hat Section Material	Hat Section Mass (Kg)	Finite Element Mass (Kg)	Error
Unidirectional	0.256	0.240	% 6.25
Woven Fabric	0.265	0.216	% 18.5

The large error in the woven fabric hat section is due to geometrical errors. The woven fabric hat section was cut incorrectly leading to different geometry than those of the unidirectional and the woven fabric lamina is smaller than the unidirectional. These geometrical errors are addressed in the time history analysis. The mass analysis with the new geometry for the woven fabric hat section is given.

**Table 22: Mass Test of Improved Hat**

Hat Section Material	Hat Section Mass (Kg)	Finite Element Mass (Kg)	Error
Unidirectional	.256	.240	% 6.25
Woven Fabric	.224	.216	% 3.6

The original geometry of the woven fabric hat section is used for the natural frequency analysis. The difference in mass will affect the natural frequency analysis, but not to an extent that another model and simulation need to be created. Due to the nature of composites the model of the hat section had to be altered so that the material model could reflect physical realities, for example the fiber direction of the composite. In the simulated model of the hat section the fiber direction is defined globally this necessitates the use of multiple parts to create the single hat section. Two material models were created for the single hat section to simulate the orientation of the fiber. This will be further discussed in the time history analysis.

**Table 23: Nodes and Elements of Finite Element Model of Hat**

Material	Nodes	Elements
Unidirectional Hat	43911	28600
Woven Fabric Hat	43911	28600

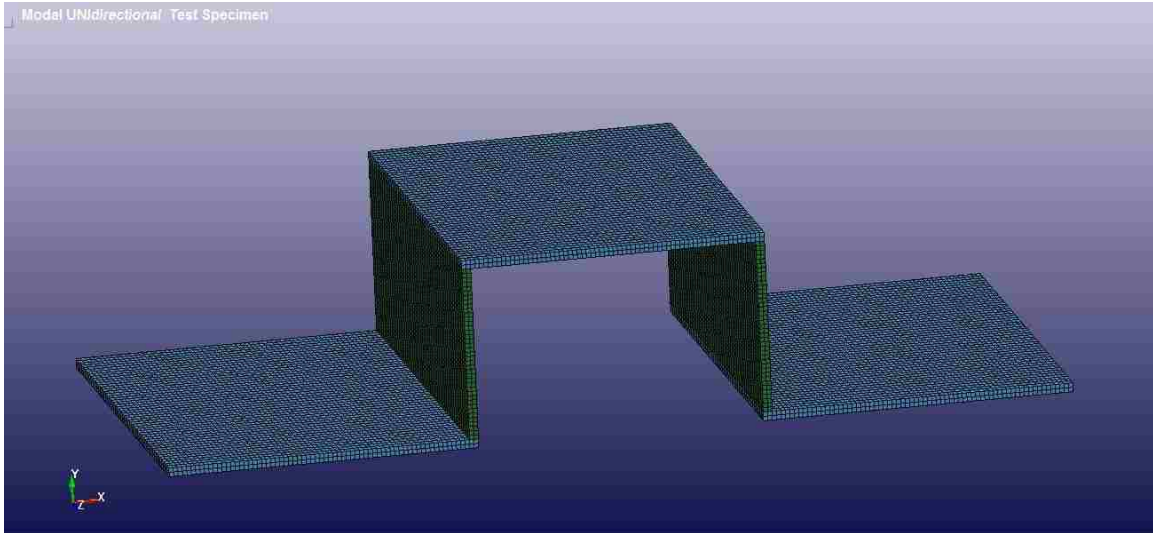


**Figure 61: Finite Element Model of Hat**

**Table 24: Natural Frequencies of Unidirectional and Woven Fabric Hat**

Frequency	Unidirectional Experimental	Unidirectional FEA	Error	Woven Fabric Experimental	Woven Fabric FEA	Error
1	127	124	1.9%	86.21	97	12.3%
2	410	384	6.4%	264	265	.4%
3	623	616	1.3%	418.1	493	17.9%
4				1149	1318	14.7%
5				1241	1423	14.7%

The natural frequency analysis shows that the large difference of mass of the physical woven fabric composite hat and the simulated woven fabric composite hat may cause large errors in the natural frequencies. The unidirectional composite hat had only 3 peaks in the experimental FFT, therefore only these 3 natural frequencies can be

compared to the natural frequencies from the FEA. The natural frequencies resulting from the FEA of the unidirectional composite hat are in good agreement with those of the experiment. The model of the composite hat is therefore used in the unidirectional composite bolted hat structure. The geometry of the woven fabric composite hat was changed to account for the geometrical differences in the woven fabric composite bolted hat structure.

### 5.3 Mode Shapes of Hat Section

The mode shapes for the hat section are important factors in understanding the dynamic response of the bolted hat structure. The mode shapes for the first three natural frequencies are shown for the unidirectional composite hat and the first five natural frequencies for the woven fabric composite hat. The unidirectional composite hat mode shapes are shown in Appendix D and the woven fabric composite hat mode shapes are shown in Appendix E.

### 5.4 Preload on Bolt

A fully tightened bolt is necessary to prevent joint failure. A fully tightened bolt is able to prevent failure from forces which in a loosely tightened bolt would fail. It is necessary to accurately determine what preload on the bolt in order to properly simulate the shock propagation across it. Preload of a bolt is caused by the nut tightening of the bolt that stretches the bolt causing tension in the bolt. The preload on the bolt can be found from the torque applied to the torque. The torque can consistently be placed on the bolts through the use of a torque wrench. The torque value was determined by increasing the torque on the bolt until deformation was caused in the composite. It was discovered that 5.3 N-m was adequate enough to clamp the hat sections together, but low enough to

prevent deformation in the composite hat sections. The preload can then be determined from the torque and applied to the finite element model.

$$T = K * F * D$$

T= Torque

K= Constant

F= Bolt Preload

D= Bolt Nominal Diameter

For the bolt it is known that the K is .19064 and D is .01 m and T is 5.3 Nm. The resulting preload is 2.78kN.

To add the bolt preload to the finite element model a pre-stress is defined in the section of the bolt where the tension would be. There are several methods that can be used to add the bolt preload in LS-DYNA. The method used in this model is \*INITIAL\_STRESS\_SECTION. A section of the bolt is defined that corresponds to the area where the stress is. The stress in the area of the bolt can be found from the bolt preload. The addition of this stress into the model requires that dynamic relaxation is added to the model to adjust for the displacements and deformation caused by the stress in the bolt. The stress calculated for the bolt preload is 35 Mpa. The resulting stress in the model is shown in the following figures.



**Figure 62: Bolt Preload**

### 5.5 Time History Analysis of Composite Bolted Hat Structure

The time history analysis of the composite hat structure is conducted to better understand shock transmission across bolted joints in composite materials. As in previous analysis the bolted hat section is composed of two parts the experimental numerical and the FEA. The experimental analysis is described thoroughly in the experimental procedures section. The experiment involves hanging the composite bolted hat structure from the steel frame and conducting the experiment as previously described. The experimental data is post processed with MATLAB. The data of the experiment is filtered at 10,000 hz and a FFT performed to obtain the frequency spectrum. The FEA will be performed as in the other analysis. Altair Hypermesh is used as a preprocessor to build the geometry and mesh the model, LS-DYNA was used as the processor, and LS-PrePost and MATLAB used for post processing. The time history of the experimental data is compared to the results of the FEA using the NRMSD algorithm.

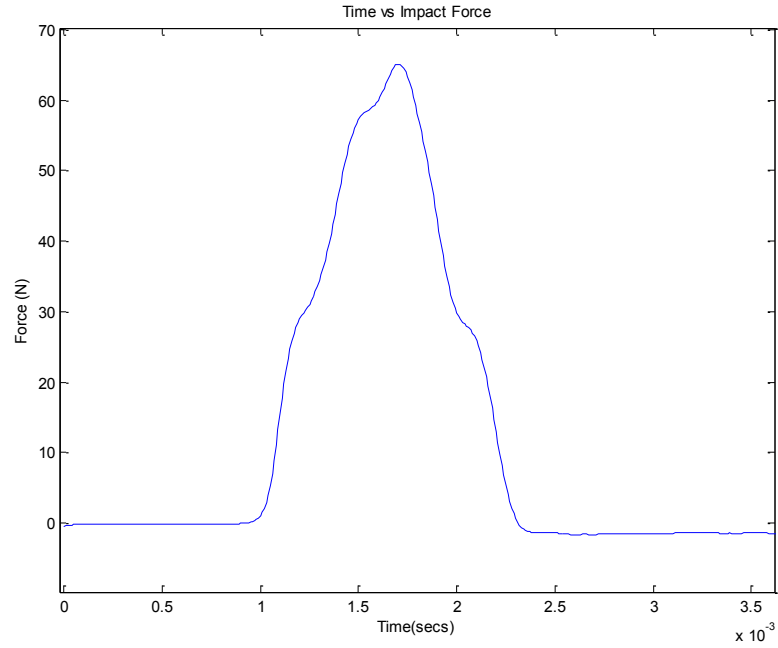


**Figure 63: Impact Force Curve for Unidirectional Composite Bolted Hat Structure**

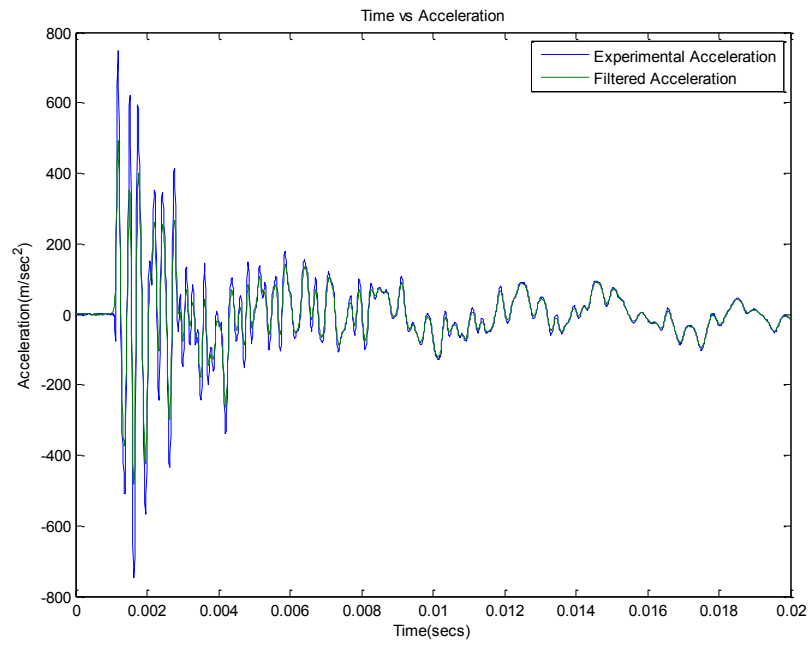


**Figure 64: Time History of Accelerometer 1 Unidirectional Composite Bolted Hat Structure Experimental Unfiltered and Filtered**



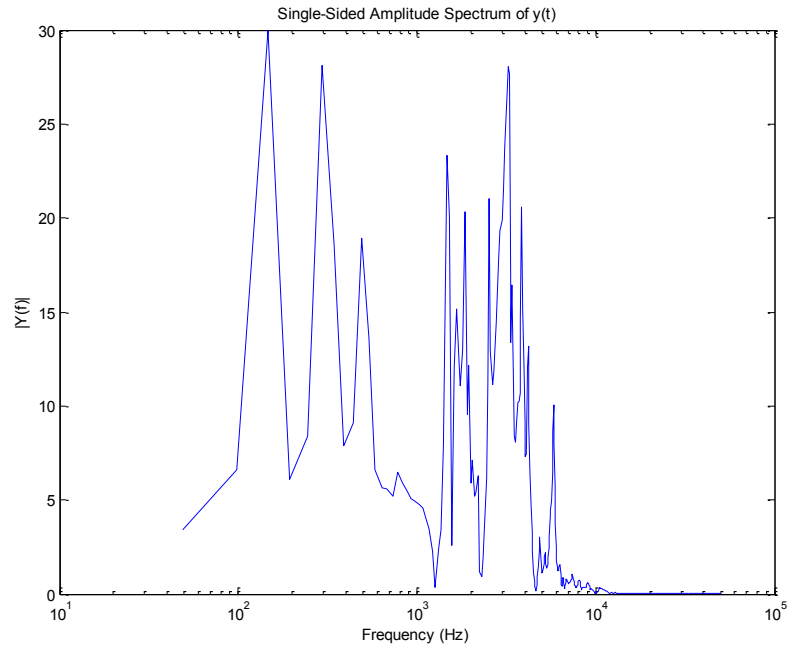


**Figure 65: Frequency Domain of Accelerometer 1 Unidirectional Composite Bolted Hat Structure**

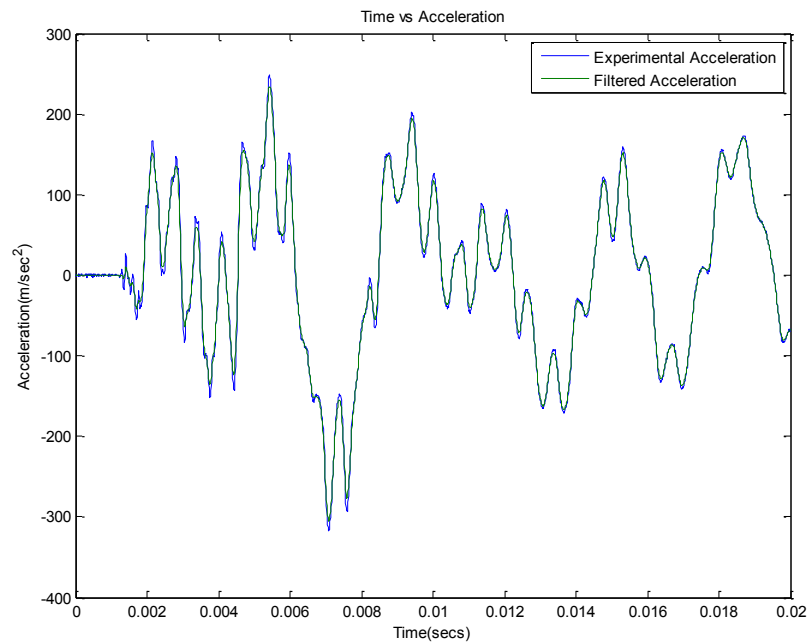


**Figure 66: Time History of Accelerometer 1 Unidirectional Composite Bolted Hat Structure Experimental Unfiltered and Filtered**

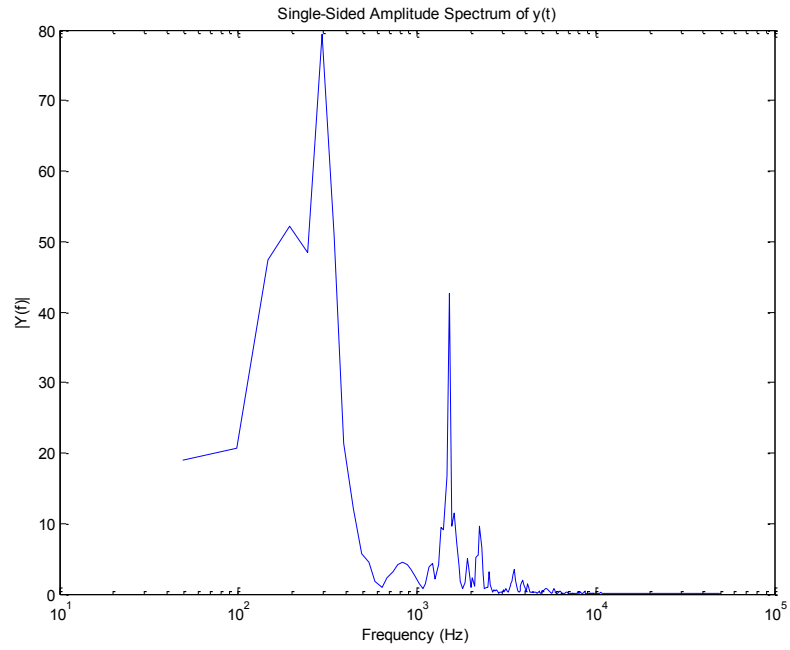


**Figure 67: Frequency Domain of Accelerometer 2 Unidirectional Composite Bolted Hat Structure**

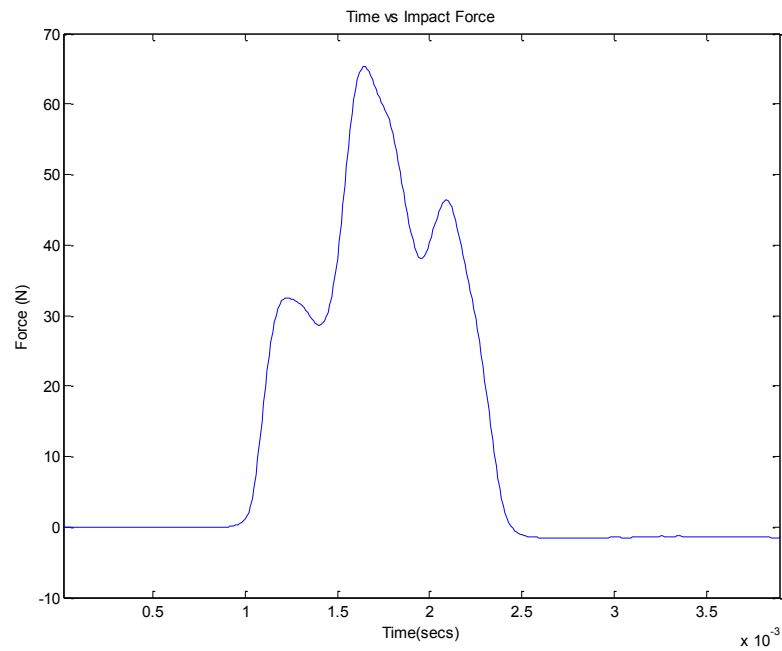


**Figure 68: Impact Force Curve for Woven Fabric Composite Bolted Hat Structure**

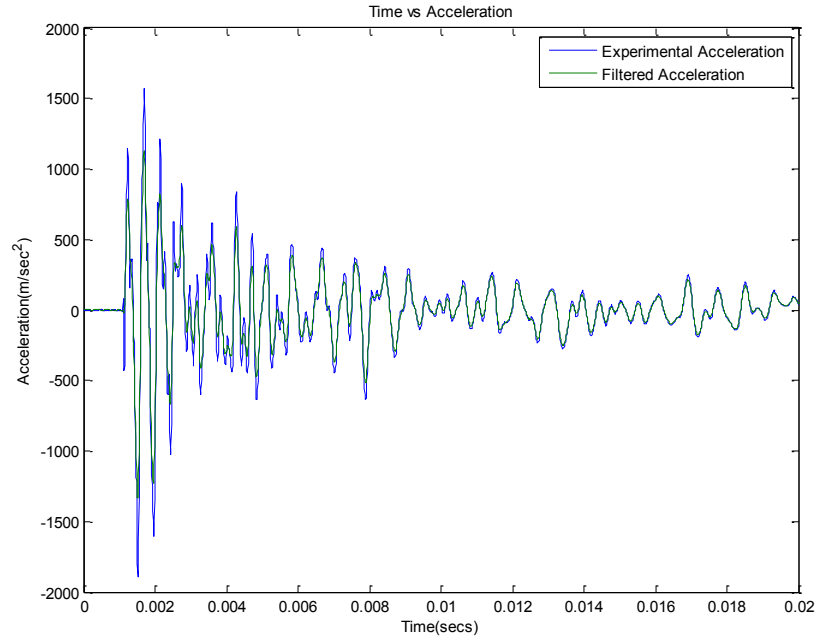


**Figure 69: Time History of Accelerometer 1 Woven Fabric Composite Bolted Hat Structure Experimental Unfiltered and Filtered**

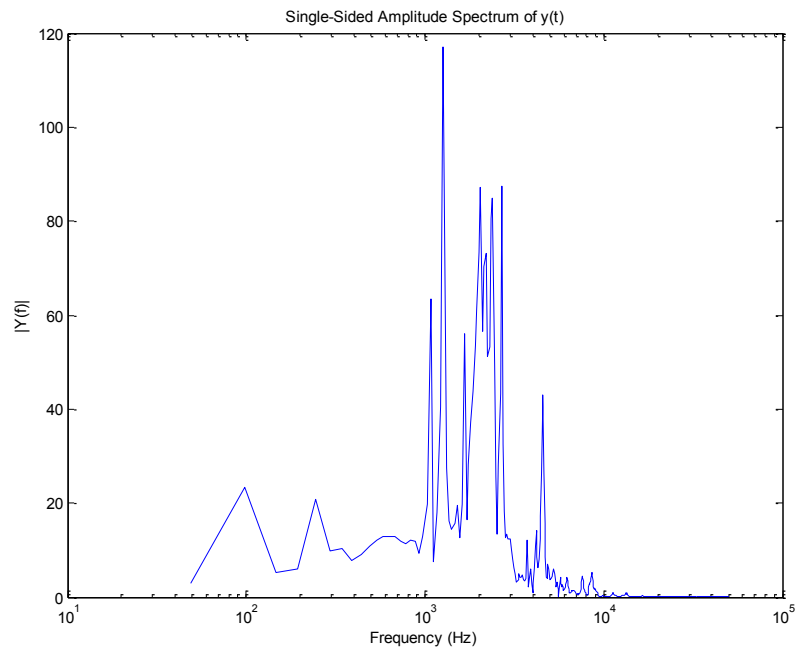


**Figure 70: Frequency Domain of Accelerometer 1 Woven Fabric Composite Bolted Hat Structure**

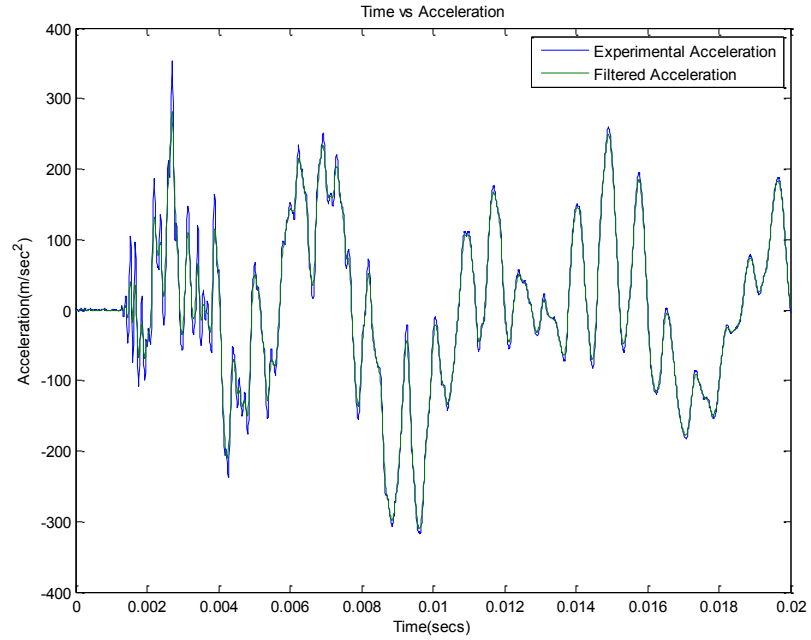


**Figure 71: Time History of Accelerometer 2 Woven Fabric Composite Bolted Hat Structure Experimental Unfiltered and Filtered**

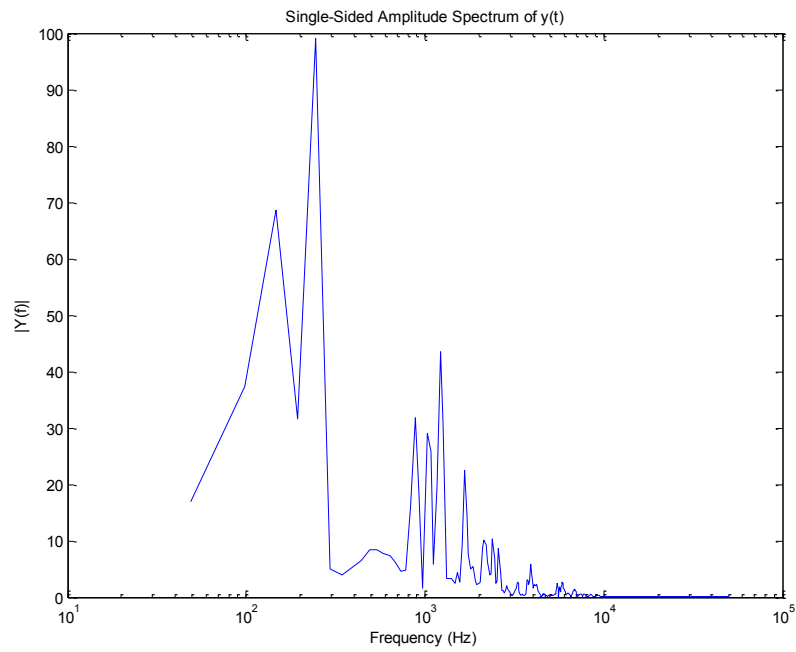


**Figure 72: Frequency Domain of Accelerometer 2 Woven Fabric Composite Bolted Hat Structure**

The FEA of the composite bolted hat structure is more complex and has more elements than that of the cantilever beam and hat section. The increased complexity causes exponential increases in computational time. To make the computational time manageable the processing was performed on a server with up to 46 processors. A \*CONTROL\_MPP\_DECOMPOSITION\_AUTOMATIC card is added to simulation to allow for the file to run with multiple processors. The woven fabric composite hat section had significant differences in the mass and geometry in the finite element model, therefore two models were used. The first model is for the unidirectional composite bolted hat structure and the second for the woven fabric composite bolted hat structure. To properly model the material and mechanical properties of the composite hats multiple material cards and parts had to be made. The material cards of the composites define a material coordinate that is based on the global coordinate system. The material coordinate system defines the axis of the fiber direction, it is therefore necessary to create a material card for every change in fiber direction. The unidirectional composite hat has two material and part cards and the woven fabric composite hat, due to its geometry, has four material and part cards. For the unidirectional composite hats, and for the bottom woven fabric composite hat, the fiber direction runs in the x direction for the horizontal sections of the hats and in the y direction in the vertical sections of the hats. The woven fabric composite hat section is composed of two hats of different geometry. The bottom hat has the same fiber running in the same direction as the unidirectional composite hats. The top hat of the woven fabric composite bolted structure has the vertical members at an angle, since the angle of the vertical members of the hat are 90 degrees offset they each require their own material and part card.

\*MAT\_ORTHOTROPIC\_ELASTIC

\$ Unidirectional Material Properties for the horizontal section of the hats

1 1310.09.4780E+100.7540E+100.7540E+10 0.0246 0.0246 0.4356  
0.2770E+100.2625E+100.2770E+10 2  
1.0 0.0 0.0  
0.0 0.0 1.0

\*MAT\_ORTHOTROPIC\_ELASTIC

\$ Unidirectional Material Properties for the vertical section of the hats

3 1310.09.4780E+100.7540E+100.7540E+10 0.0246 0.0246 0.4356  
0.2770E+100.2625E+100.2770E+10 2  
0.0 1.0 0.0  
0.0 0.0 1.0

\*MAT\_ORTHOTROPIC\_ELASTIC

\$ Woven Fabric material properties of horizontal sections of hats

1 1360.05.6460E+105.6460E+100.7540E+10 0.0442 0.0246 0.0246  
2.1800E+100.2755E+100.2755E+10 2  
1.0 0.0 0.0  
0.0 0.0 1.0

\*MAT\_ORTHOTROPIC\_ELASTIC

\$ Woven Fabric material properties of vertical section of bottom hat

3 1360.05.6460E+105.6460E+100.7540E+10 0.0442 0.0246 0.0246  
2.1800E+100.2755E+100.2755E+10 2  
0.0 1.0 0.0  
0.0 0.0 1.0

\*MAT\_ORTHOTROPIC\_ELASTIC

\$ Woven Fabric material properties of left vertical section of top hat

```
4 1360.05.6460E+105.6460E+100.7540E+10 0.0442 0.0246 0.0246
2.1800E+100.2755E+100.2755E+10 2
-4.57 62.456 0.0
0.0 0.0 1.0
```

\*MAT\_ORTHOTROPIC\_ELASTIC

\$ Woven Fabric material properties of right vertical section of top hat

```
5 1360.05.6460E+105.6460E+100.7540E+10 0.0442 0.0246 0.0246
2.1800E+100.2755E+100.2755E+10 2
4.57 62.456 0.0
0.0 0.0 1.0
```

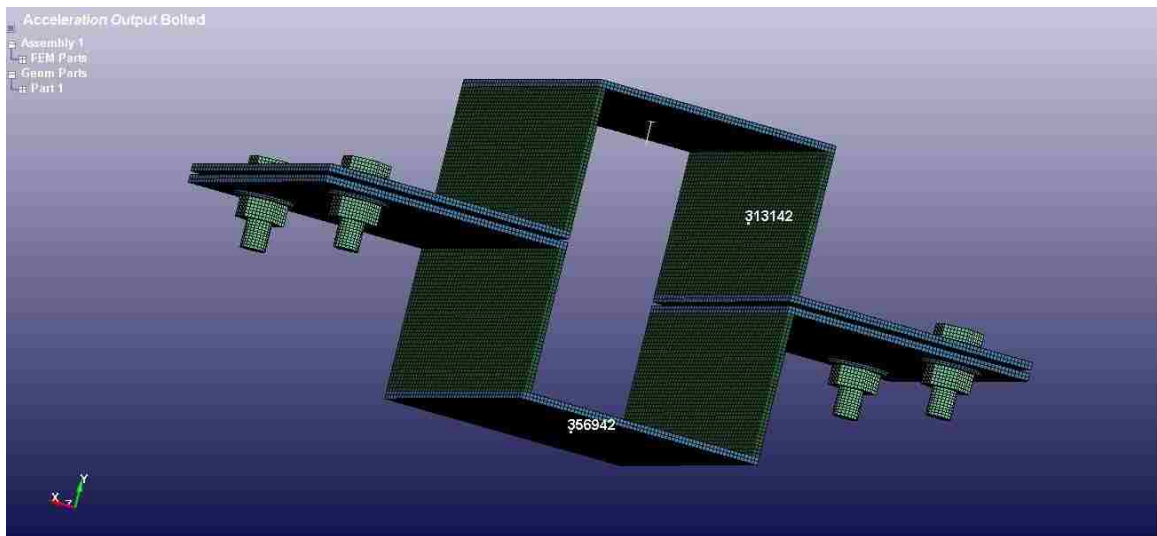
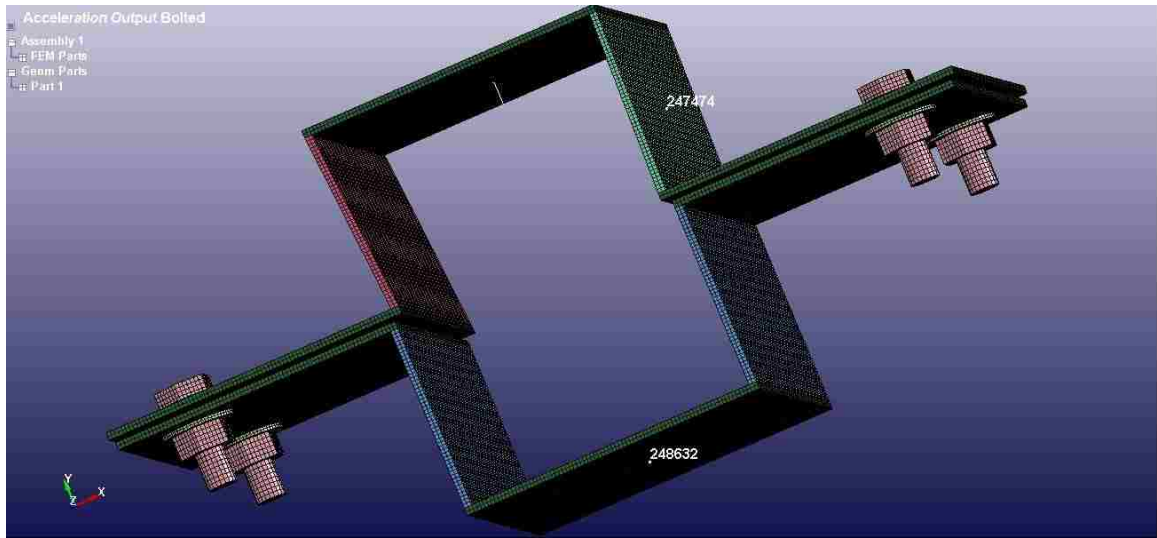


Figure 73: Finite Element Model of Unidirectional Composite Bolted Hat Structure Showing Impact, Accelerometer 1, and Accelerometer 2 Location ↑, 313142, and 356942 respectively.



**Figure 74: Finite Element Model of Woven Fabric Composite Bolted Hat Structure Showing Impact, Accelerometer1, and Accelerometer 2 Location ↑, 247474, and 248632 respectively.**

**Table 25: Nodes and Elements of Unidirectional Finite Element Model and Woven Fabric Finite Element Model**

Material	Nodes	Elements
Unidirectional Bolted Hat Section	110949	76102
Woven Fabric Bolted Hat Section	147392	99825

The introduction of the initial stress into the model to model the bolt preload causes an initial vibration in the structure that must be damped out before the impact analysis can begin. A simple \*DAMPING\_PART\_MASS card is added to the first 10 milliseconds of the simulation to get rid of the unwanted vibrations. The time history analysis is ran for another 20 milliseconds for comparison of the experimental data. Both the models are run for 30 milliseconds and data recorded at 50 microseconds intervals. The bolted hat section was modeled with no constraints. Finite element models of the bolted hat section with constraints produced poor results for the accelerometer located on the bottom hat of the hat section.



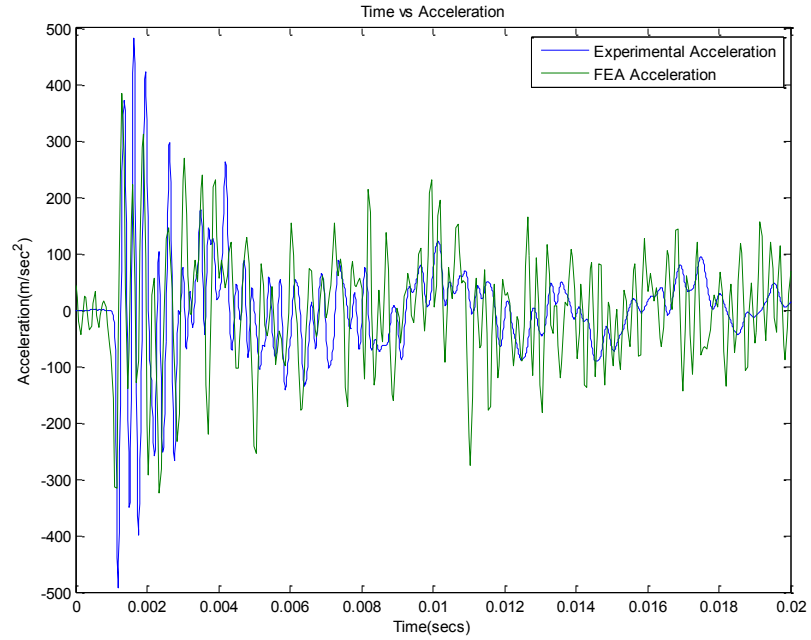


**Figure 75: Time History Plot of Accelerometer 1 Unidirectional Composite Bolted Hat Structure**

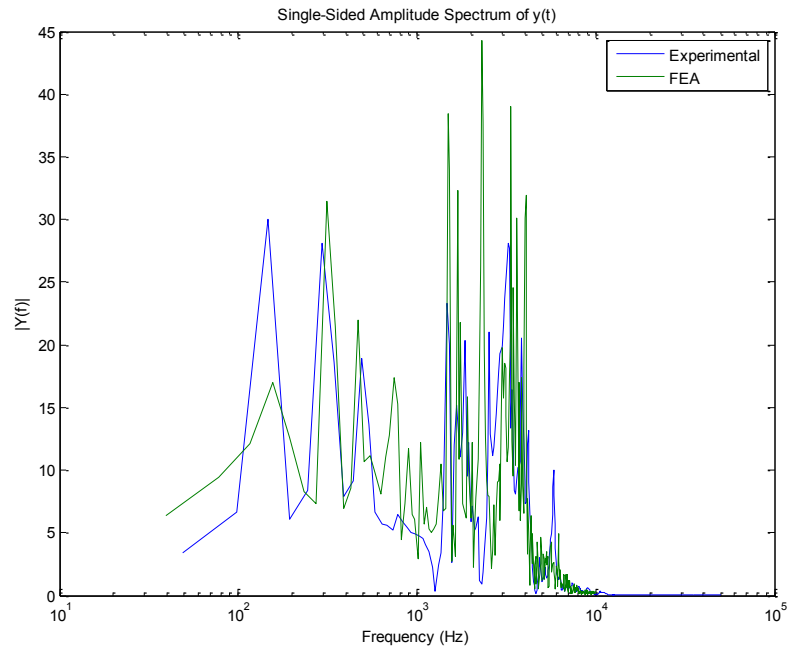


**Figure 76: Frequency Domain of Accelerometer 1 Unidirectional Composite Bolted Hat Structure**

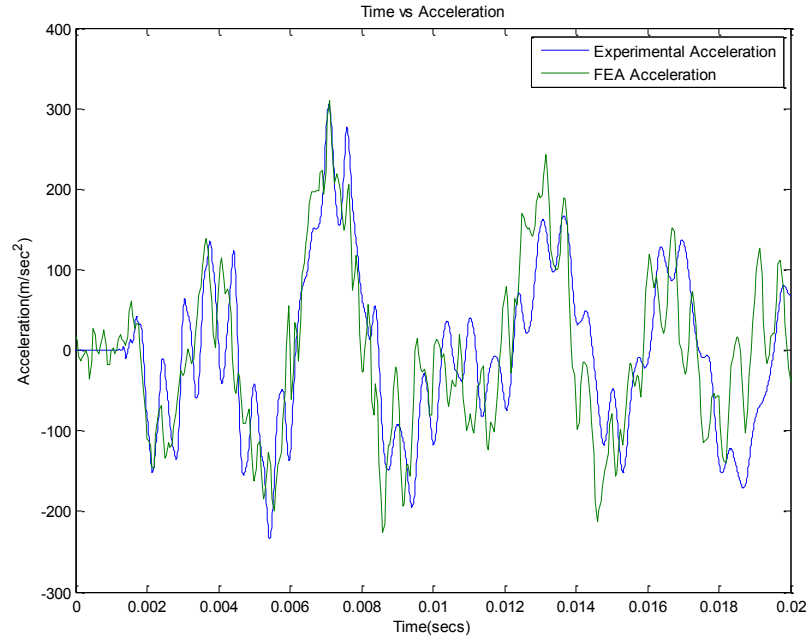


**Figure 77: Time History Plot of Accelerometer 2 Unidirectional Composite Bolted Hat Structure**

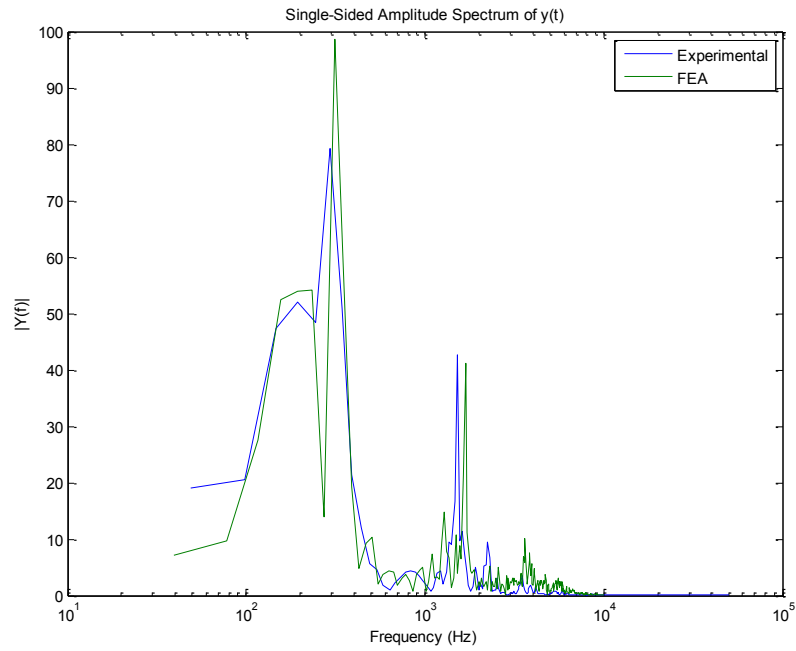


**Figure 78: Frequency Domain of Accelerometer 2 Unidirectional Composite Bolted Hat Structure**

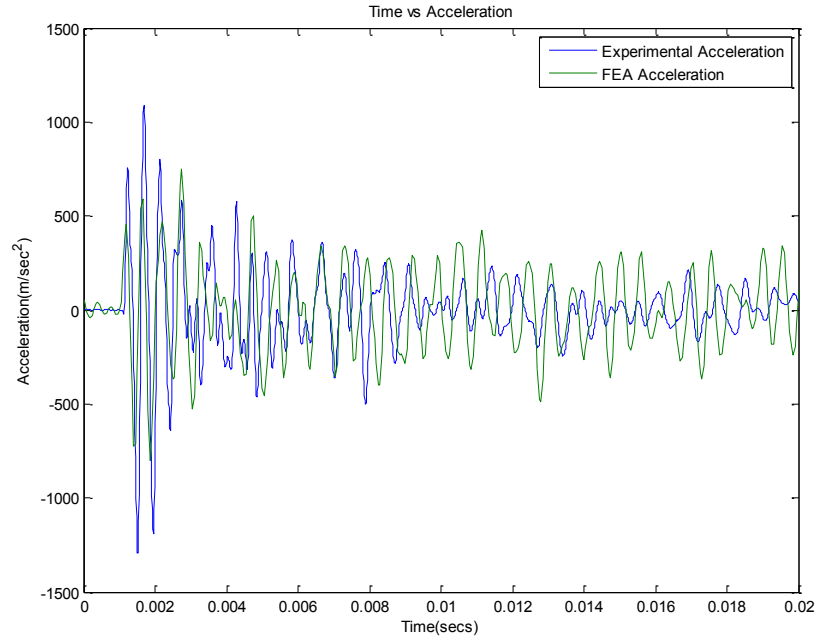


**Figure 79: Time History Plot of Accelerometer 1 Woven Fabric Composite Bolted Hat Structure**

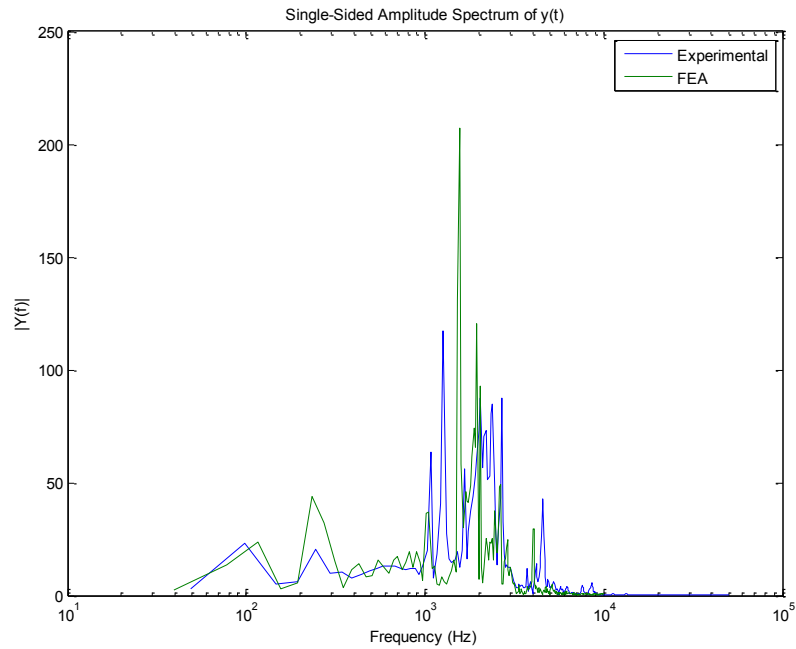


**Figure 80: Frequency Domain of Accelerometer 1 Woven Fabric Composite Bolted Hat Structure**

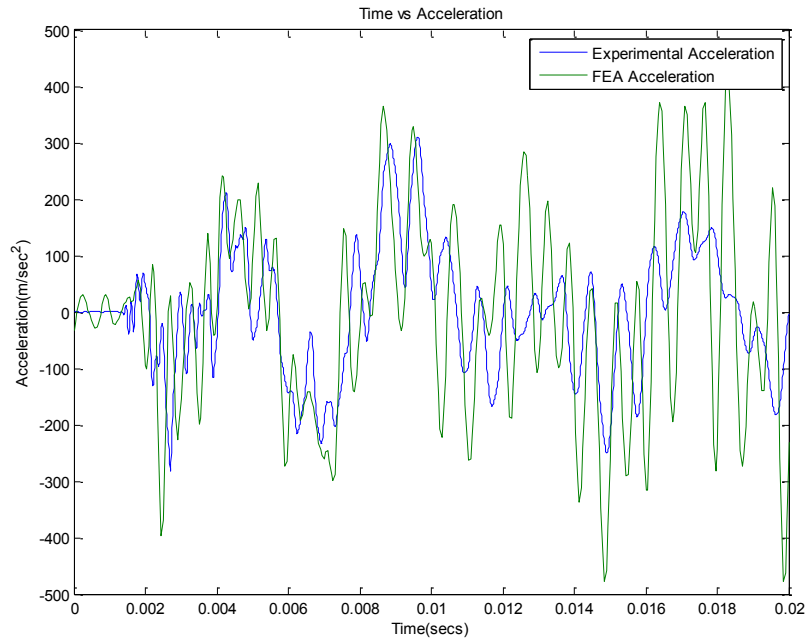


**Figure 81: Time History Plot of Accelerometer 2 Woven Fabric Composite Bolted Hat Structure**

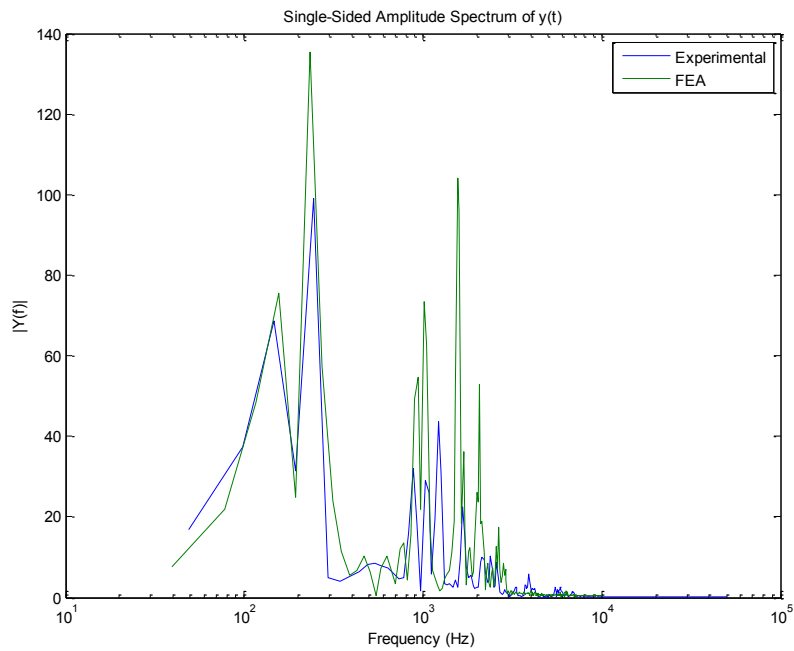


**Figure 82: Frequency Domain Plot of Accelerometer 2 Woven Fabric Composite Bolted Hat Structure Experimental and FEA**

**Table 26: NRMSD of Time History of Accelerometer 1 and Accelerometer 2 Unidirectional Composite Bolted Hat Structure and Woven Fabric Composite Bolted Hat Structure**

	Unidirectional Accelerometer 1	Unidirectional Accelerometer 2	Woven Fabric Accelerometer 1	Woven Fabric Accelerometer 2
NRMSD	0.128	0.136	0.113	0.258

The woven fabric Hat section has improved results for the first 10 milliseconds. The NRMSD of the time history of Accelerometer 2 for the woven fabric composite bolted hat section is .189.

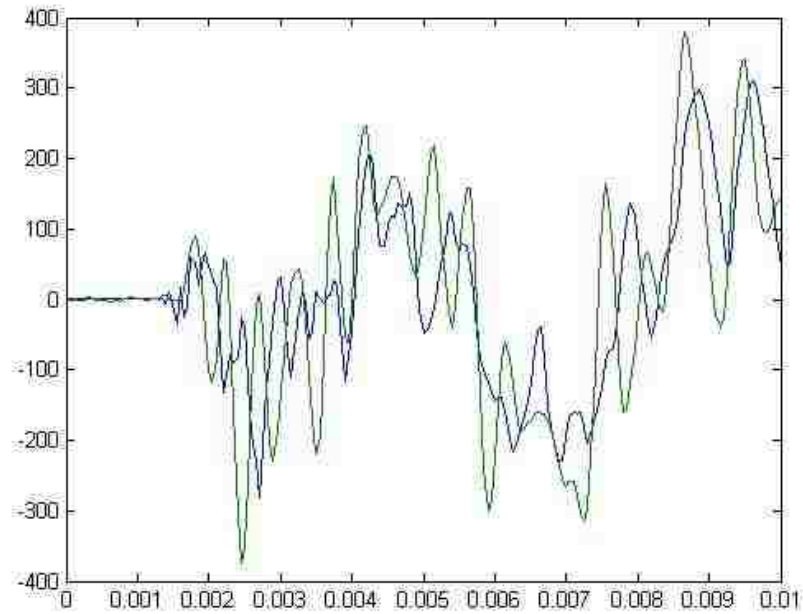


**Figure 83: Time History Plot of Accelerometer 2 Woven Fabric Composite Bolted Hat Structure for 10 milliseconds**

The results of the finite element analysis for both composite bolted hat sections have high frequency noise not seen in the experimental results. The finite element results also have lower initial accelerations peaks for the accelerometer found on the top hat for

the first 3 milliseconds. Do to the lower initial acceleration peaks no damping was added to the composite bolted hat section finite element models. The NRMSD of the unidirectional composite hat section is below that of the all the cantilever beam analysis. The woven fabric has a very low NRMSD for accelerometer 1, but accelerometer 2 has a NRMSD over that of the cantilever beams with damping. The woven fabric composite bolted hat section model accelerometer 2 could be improved using damping as in the cantilever beam analysis, but damping was not added due to the lower initial acceleration peaks for the finite element results of accelerometer 1. Accelerometer 2 finite element results for the woven fabric composite bolted hat are very close to the experimental for the first 10 milliseconds but the finite element result diverge from the experimental results after 10 milliseconds. The frequency plots show that accelerometer 2 for the woven fabric bolted hat section has higher magnitude peaks than the experimental, especially in the range of 1,000 hz to 10,000 hz and at 244 hz.

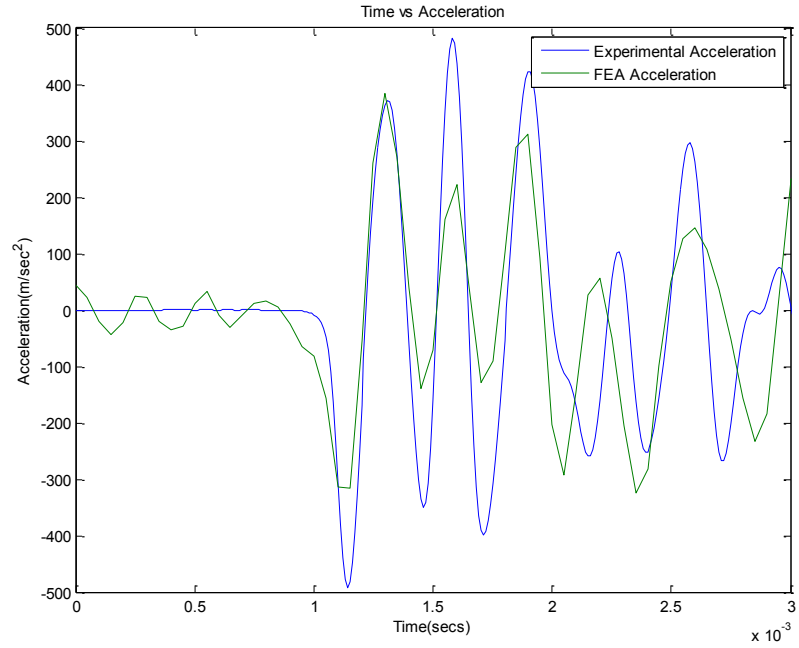


**Figure 84: Plot of Accelerometer 1 Unidirectional Composite Bolted Hat Structure Initial Peaks**

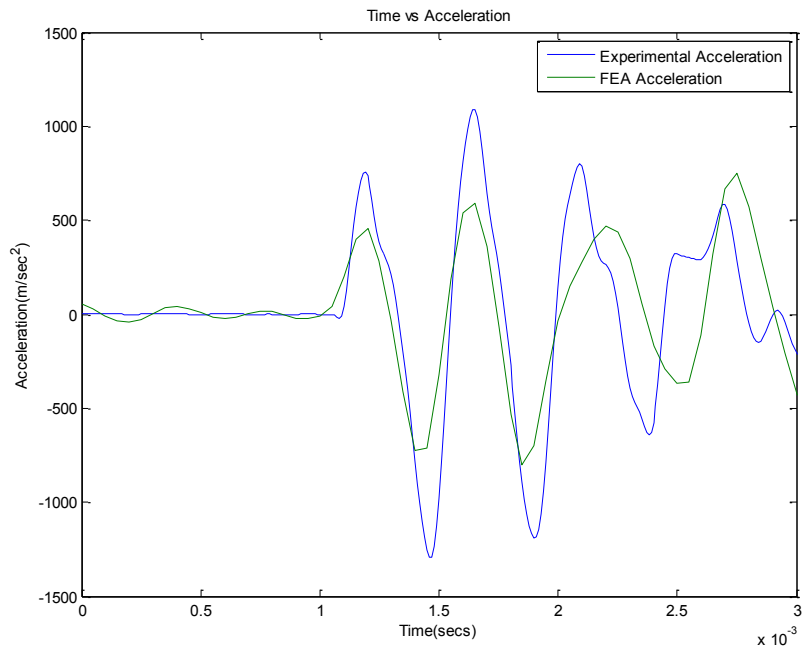


**Figure 85: Plot of Accelerometer 1 Woven Fabric Composite Bolted Hat Structure Initial Peaks**

## 5.6 Summary of Results

The composite bolt hat structure is more complex than the cantilever beam, but with proper modeling the bolt hat structure finite element model has similar NRMSD than the cantilever beam. An increase of magnitude of natural frequencies above 1,000 Hz were seen in the finite element model that did not exist in the experimental analysis. This increase magnitude in the high frequencies could be caused by the contact at the bolted joint. The differences in the stiffness of the two materials at the contact, the steel and the composite, may cause increase magnitudes in the finite element model. Damping in the finite element model would help to decrease the magnitude of frequency peaks in the range of frequencies greater than 1000 hz. It was chosen not to add damping to the bolted hat section model as the initial acceleration peaks were already lower in the finite element model compared to the experimental data. The unidirectional and woven fabric composite hat structure showed good agreement for accelerometer 1 time history, however the woven fabric composite hat structure showed large error in the time history for accelerometer 2. Damping in the frequency range of 1,000 to 10,000 hz may have produced better results for accelerometer 2 in the woven fabric composite bolted hat structure finite element model.



## CHAPTER 6

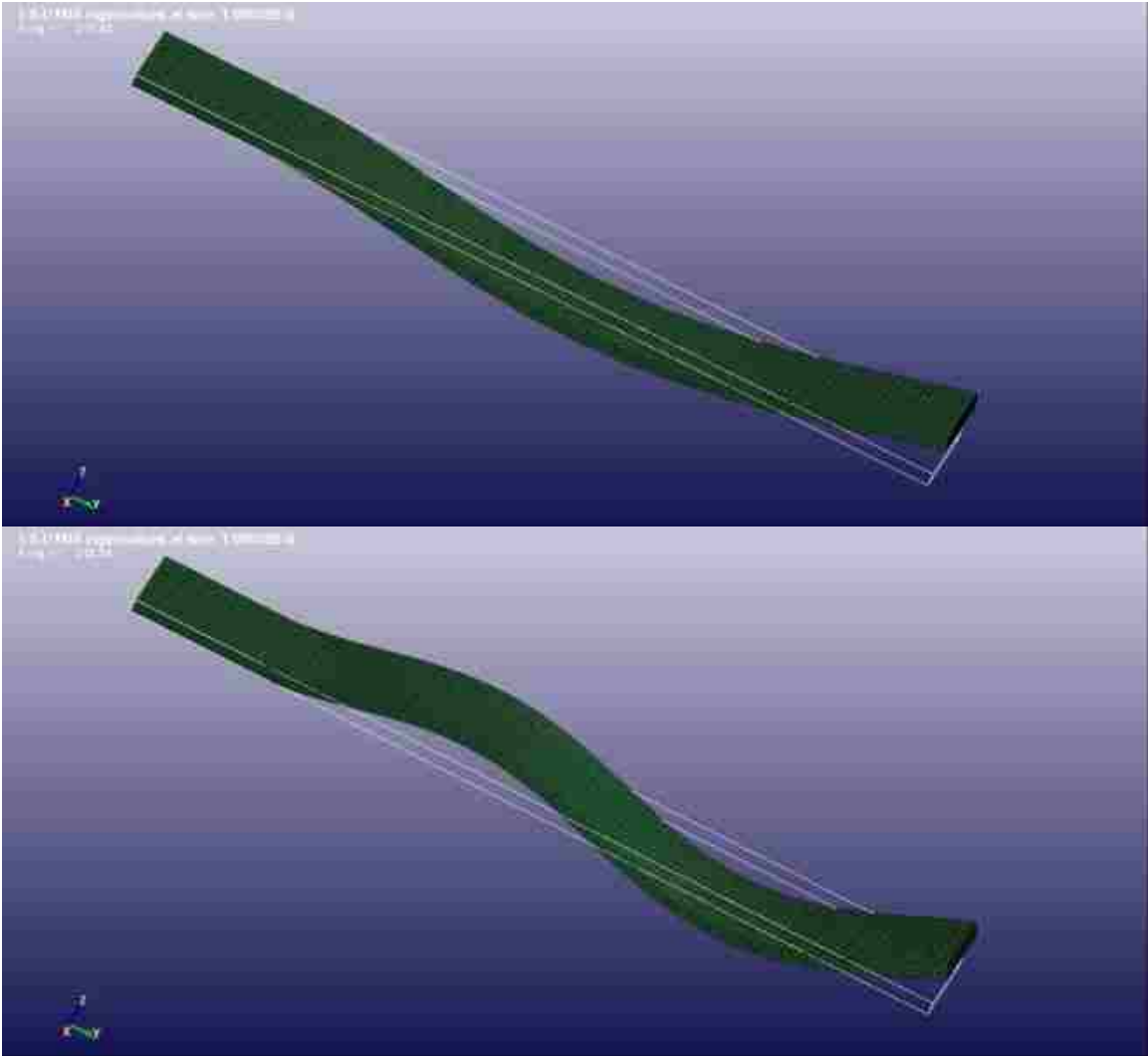
### CONCLUSIONS AND FUTURE WORK

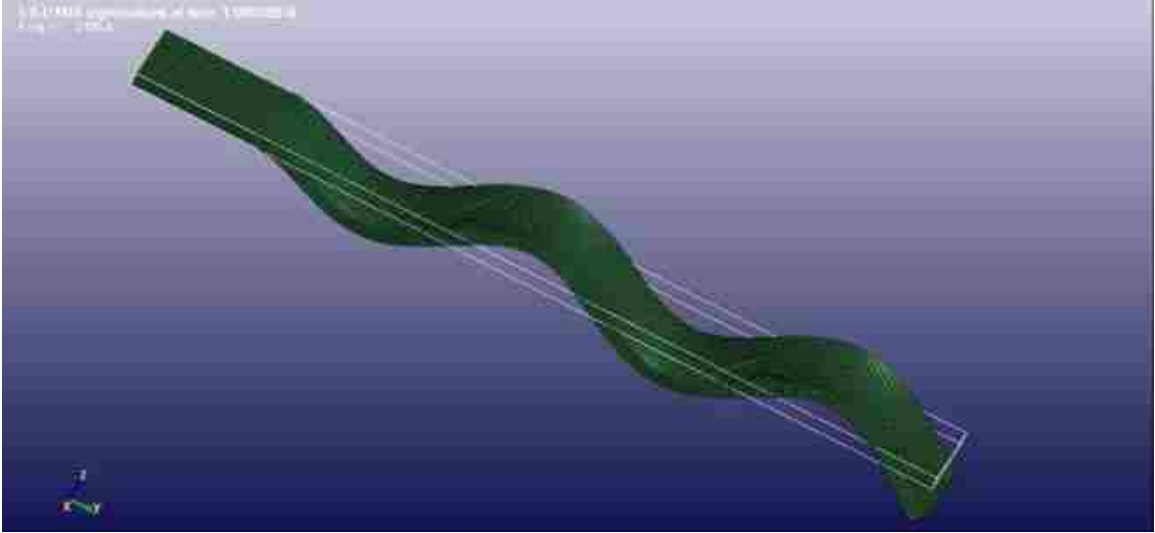
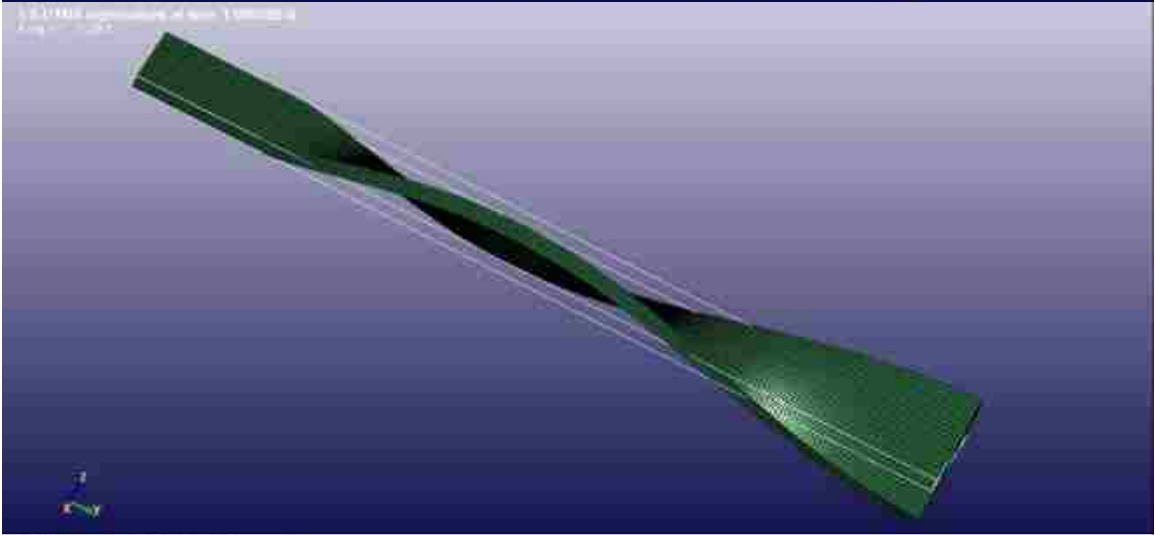
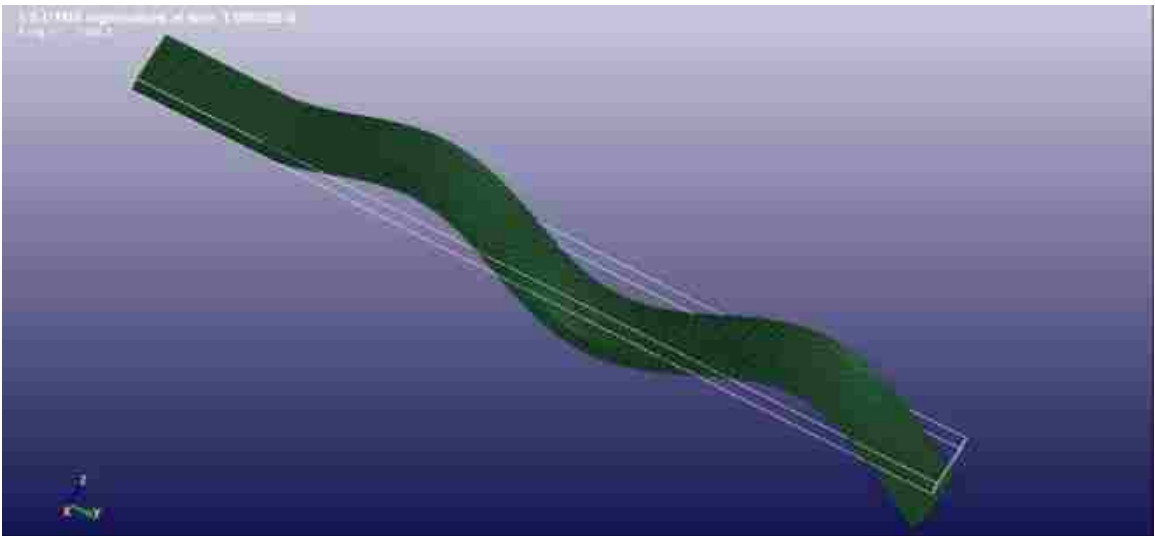
This study began with a literature review into shock analysis on composites. Several papers outlined the special considerations that are necessary in shock analysis on composites. Composites are not isotropic materials and to properly simulate them in an FEA the fiber volume fraction has to be accurately determined. The composite fiber volume fraction could be accurately determined after the density of the finished composites was found using the density submersion test. It was found that the density submersion test produced more repeatable results than the method by which the density is obtained by measuring the volume and dividing it by the mass of the specimen. With the fiber volume fraction determined the cantilever beam analysis was performed. The experimental portion of the cantilever beam analysis showed that the composite beams had more damping than that of the aluminum beam. A mesh optimization was performed to find the best mesh. It was determined that a solid mesh with 4 elements across the thickness met the criteria the best. The natural frequency analysis of the cantilever beam showed that the material and mechanical properties were accurately defined. The FEA of the cantilever beam time history showed that a NRMSD of the composite cantilever beams could be as low as the aluminum cantilever beam if damping was added to the finite element simulation. The natural frequency of the composite hat section showed that the woven fabric composite hat had to be remodeled. Two separated models were created for the composite bolted hat section. The woven fabric composite hat section finite element model had to be altered to account for the differences of geometry and mass of the woven fabric composite hat section in contrast to the unidirectional composite hat

section. The time history FEA for the bolted hat section had NRMSD below that of the cantilever beam for all data recorded with the exception of woven fabric composite bolted hat accelerometer 2, which had a NRMSD in excess of .2. Several factors could account for the increase of error in the woven fabric including the difference of stiffness at the contact of the bolted joint. Large differences in stiffness of contact material can cause error in the FEA. The woven fabric composite bolted hat section has a greater difference of stiffness of contact materials than the unidirectional. The woven fabric composite bolted hat section results could possibly be improved if more accurate contact parameters are investigated to increase simulation accuracy of the interactions of the contact between the bolt and hat section. It is concluded that the shock response of composite materials can be accurately modeled if the material properties can be accurately determined and attention paid to the specific characteristics of composite materials.

The continuation of this study could begin with an improved method of simulating the contact of materials implemented in the FEA. The study could also be altered to investigate other composite materials and fiber orientations. Adhesive joints and other joint types could also be investigated. A more advanced investigation into plastic deformation of composites is needed to better understand composite failure under shock loading. Improved methods of composite construction are also needed for reliable and accurate measurements of fiber volume fraction.

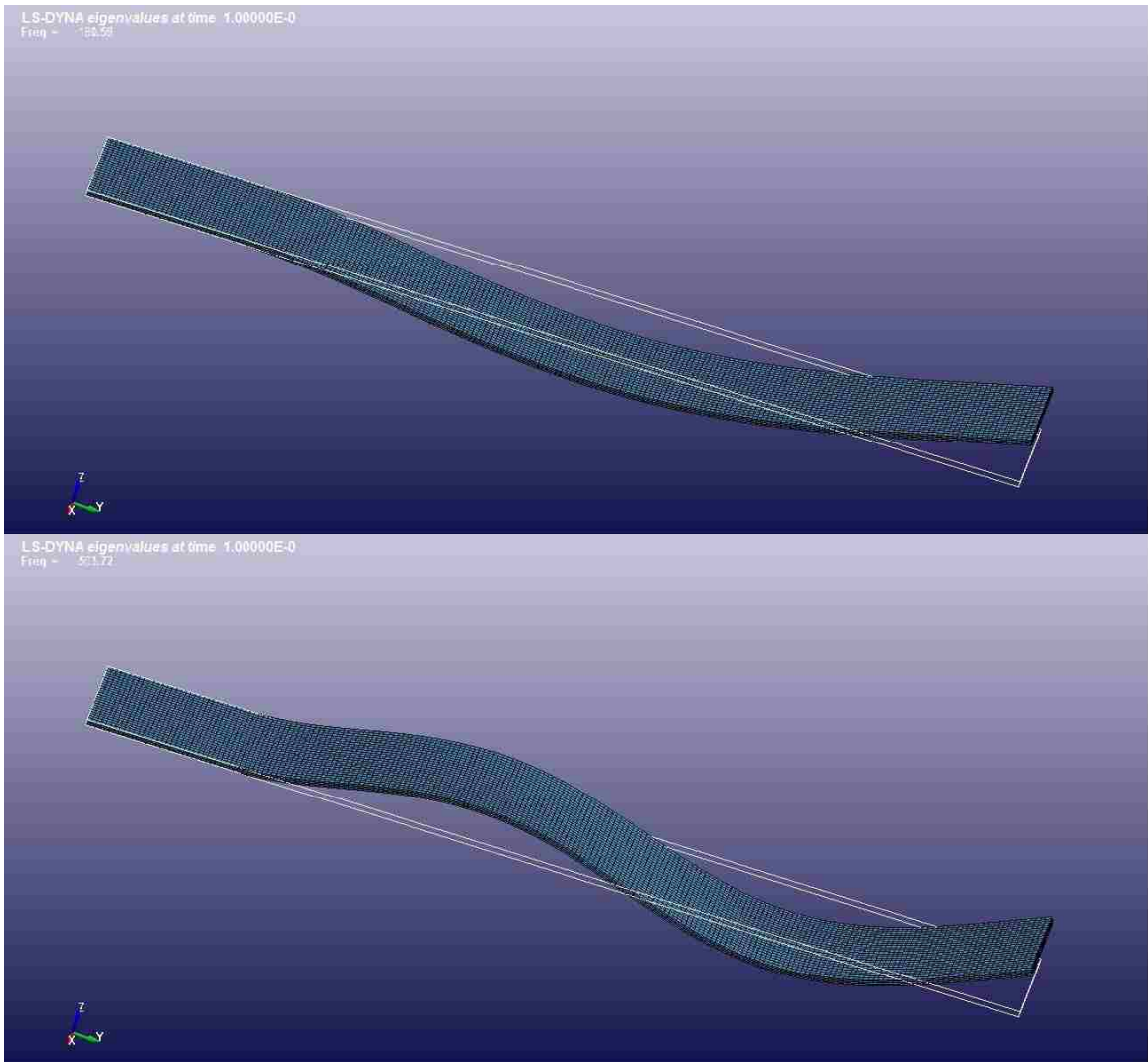
APPENDIX A: MODE SHAPES OF ALUMINUM CANTILEVER BEAM (277, 720,  
1392, 1607, and 2307 Hz)



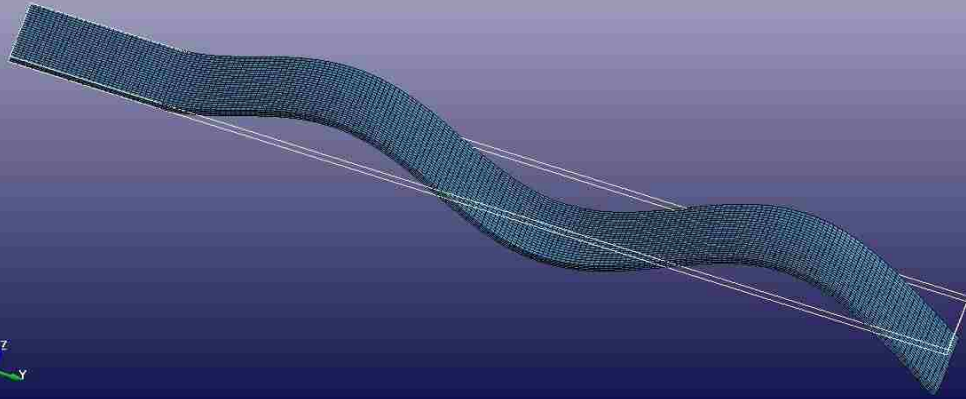


# APPENDIX B: MODE SHAPES OF UNIDIRECTIONAL COMPOSITE

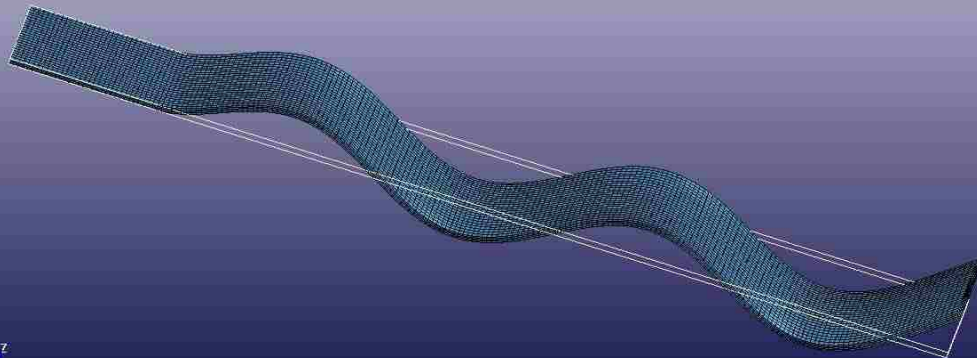
## CANTILEVER BEAM (198, 476, 940, 1514, and 2430 Hz)



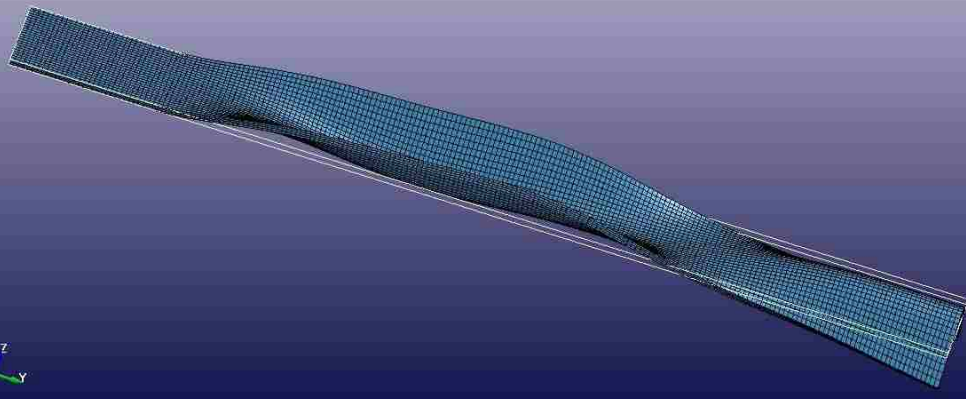
LS-DYNA eigenvalues at time 1.00000E-0  
Freq = 381.64



LS-DYNA eigenvalues at time 1.00000E-0  
Freq = 1511.3

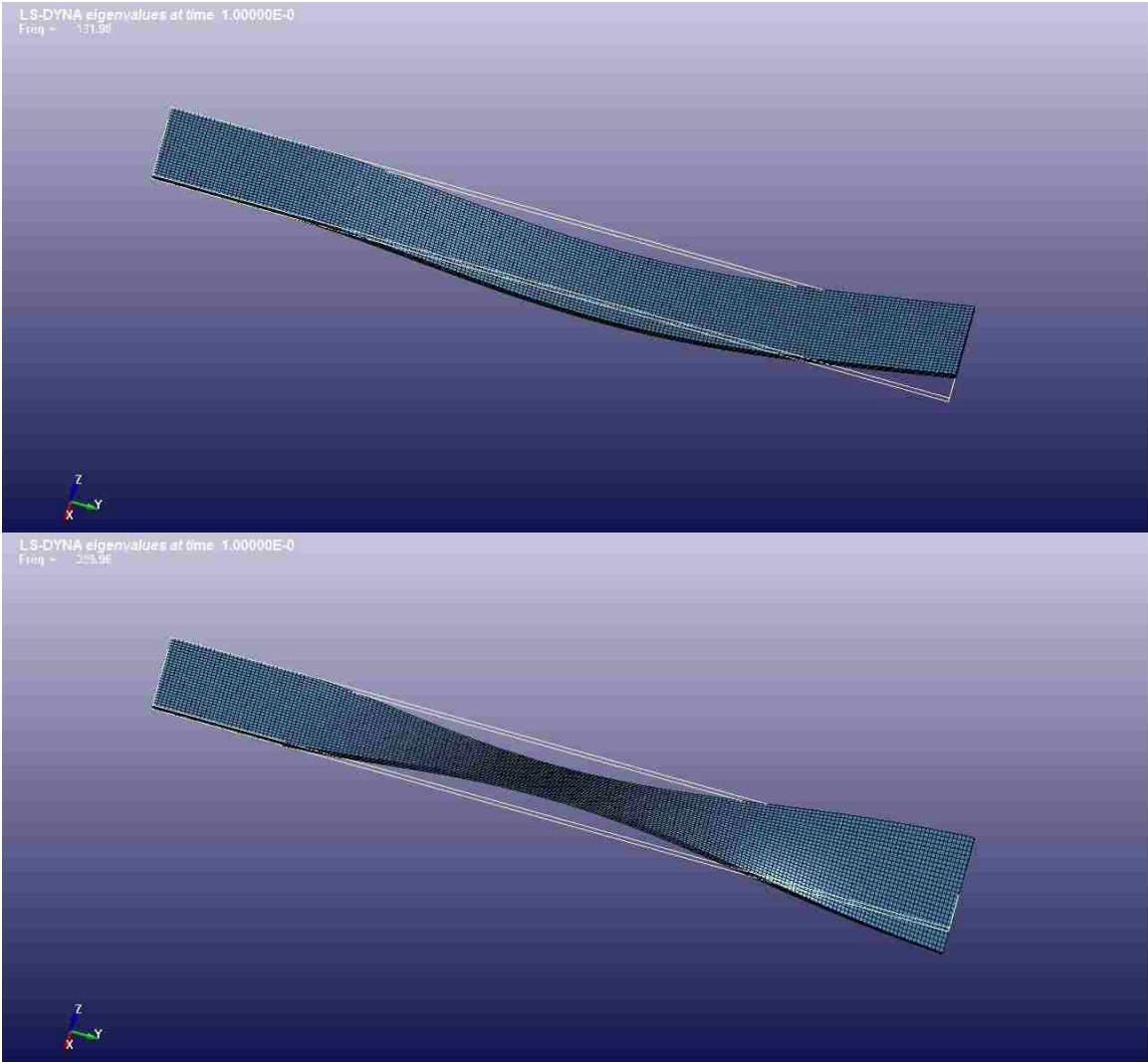


LS-DYNA eigenvalues at time 1.00000E-0  
Freq = 2458.7

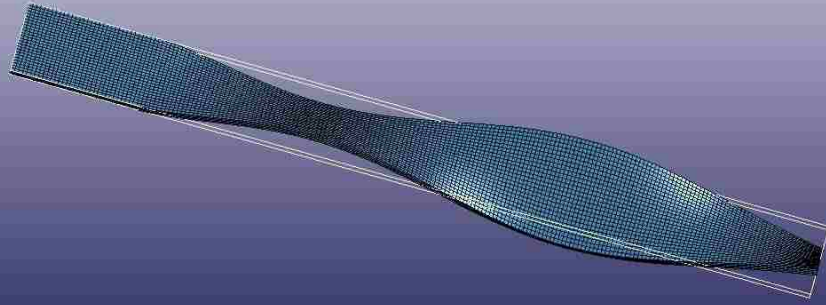


APPENDIX C: MODE SHAPES OF WOVEN FABRIC COMPOSITE CANTILEVER

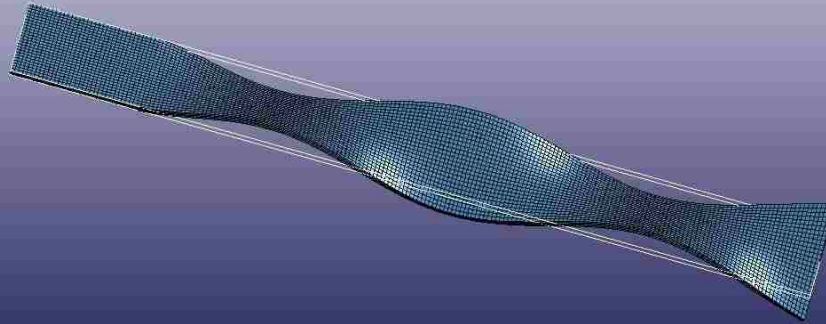
BEAM (137, 330, 647, and 1074 Hz)



LS-DYNA eigenvalues at time 1.00000E-0  
Freq = 1.102

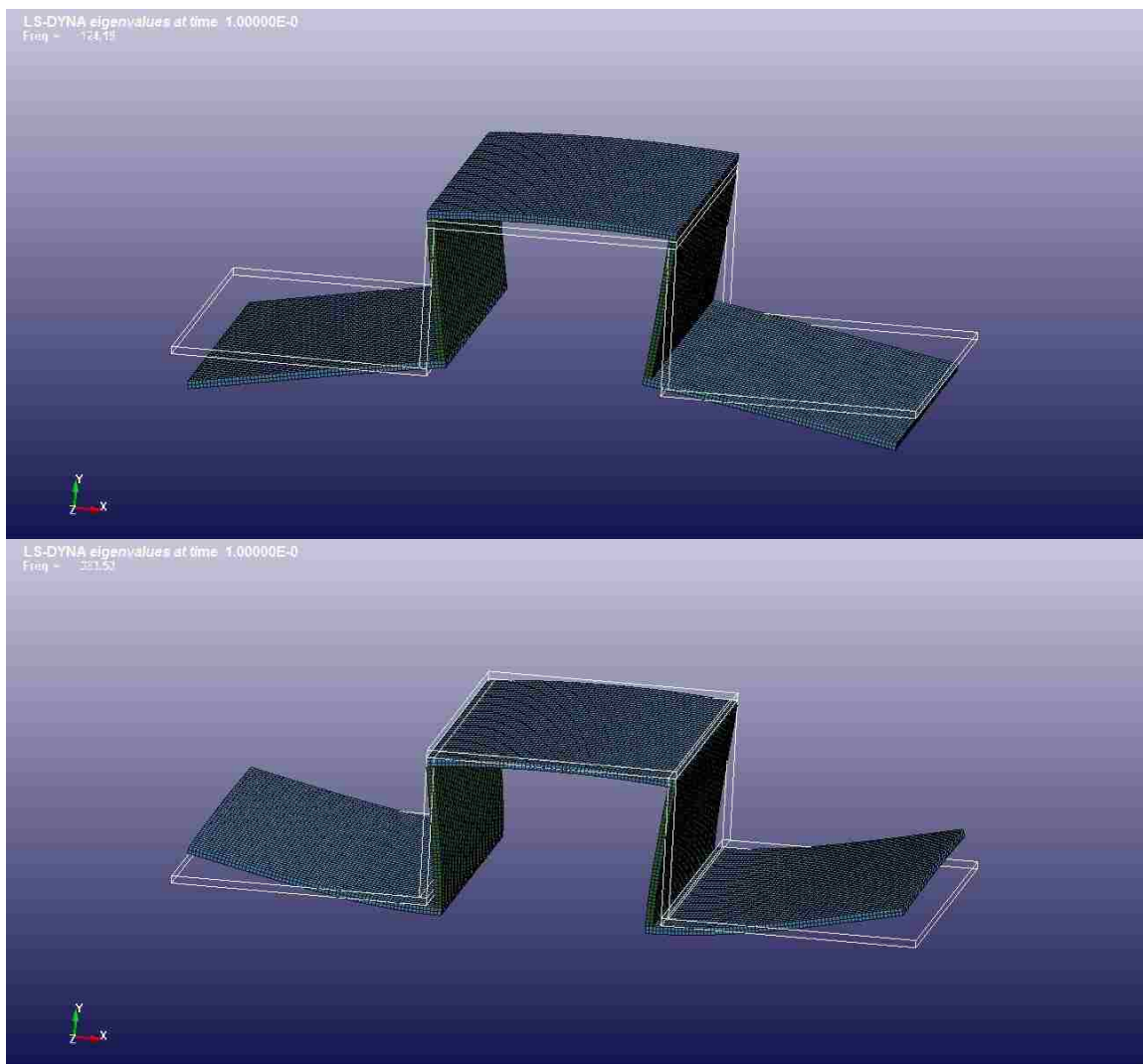


LS-DYNA eigenvalues at time 1.00000E-0  
Freq = 1.447

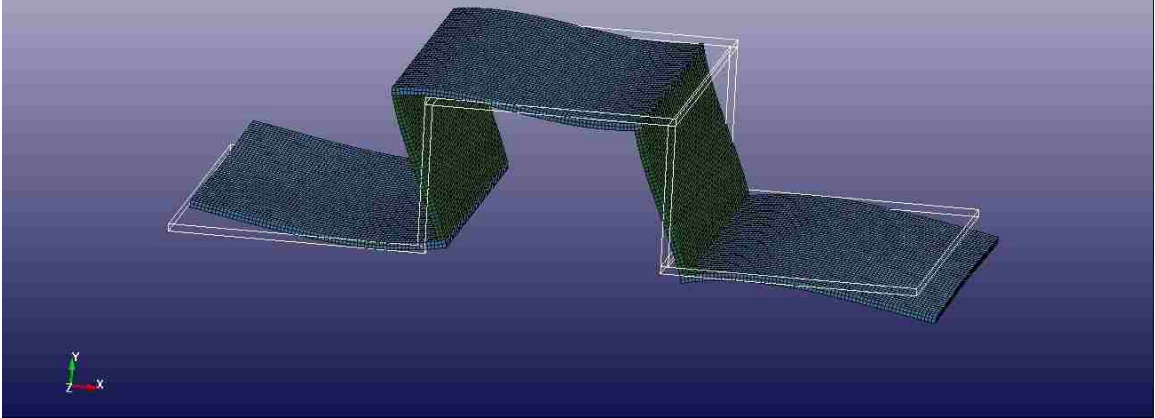




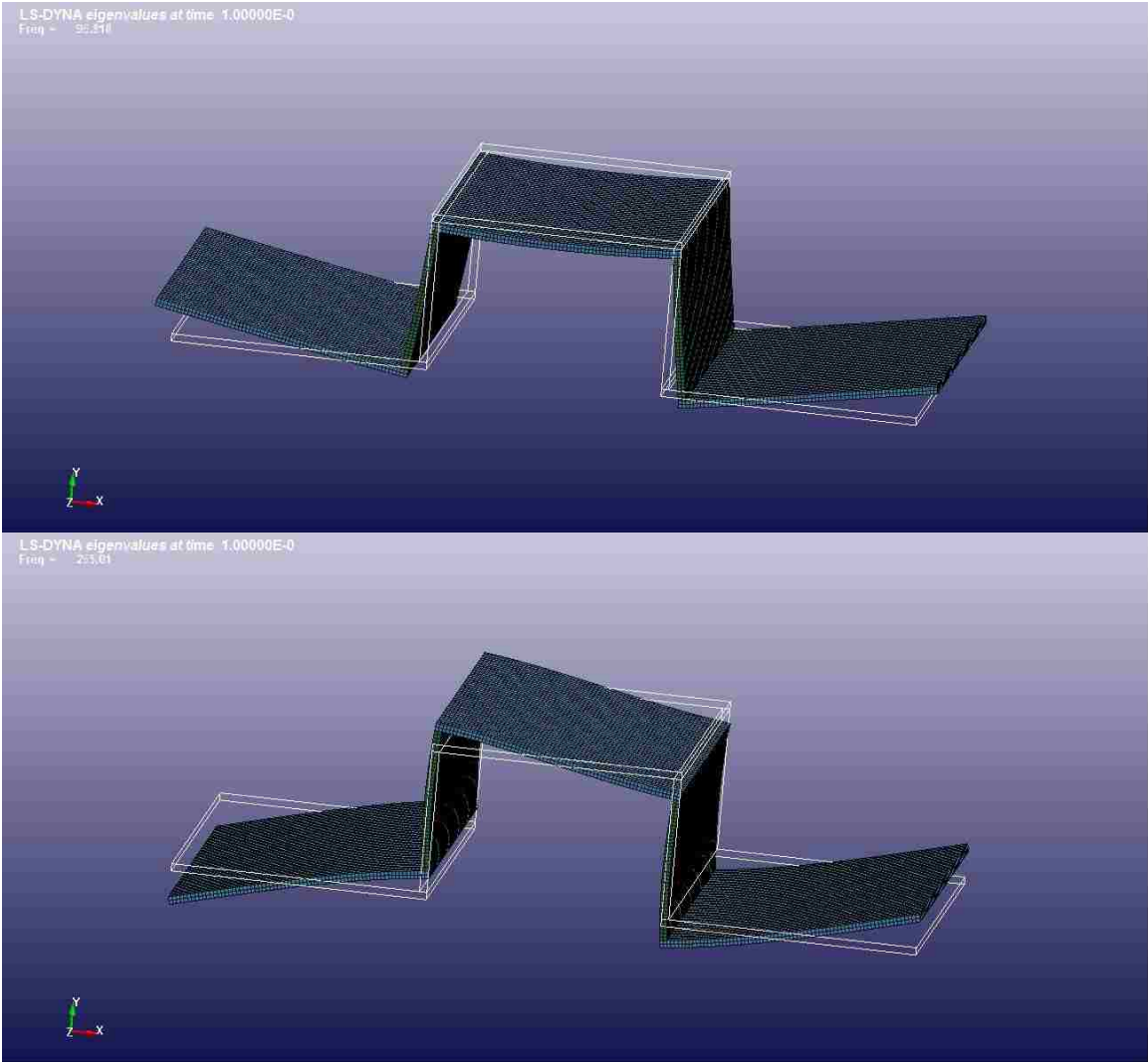
APPENDIX D: MODE SHAPES OF UNIDIRECTIONAL COMPOSITE HAT (127,  
410, and 623 Hz)



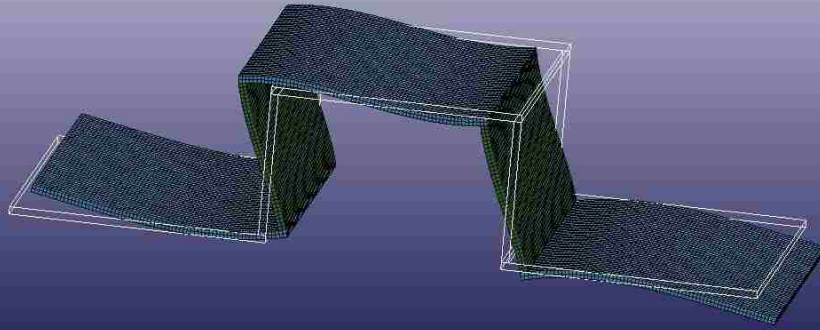
LS-DYNA eigenvalues at time 1.00000E-0  
Freq = #15,63



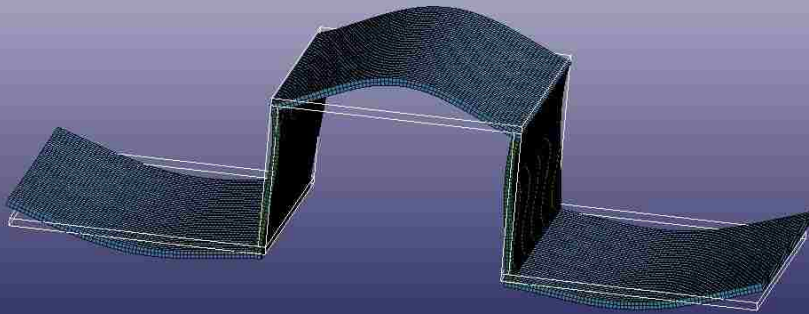
APPENDIX E: MODE SHAPES OF WOVEN FABRIC COMPOSITE HAT (86, 264,  
418, 1149 and 1241 Hz)



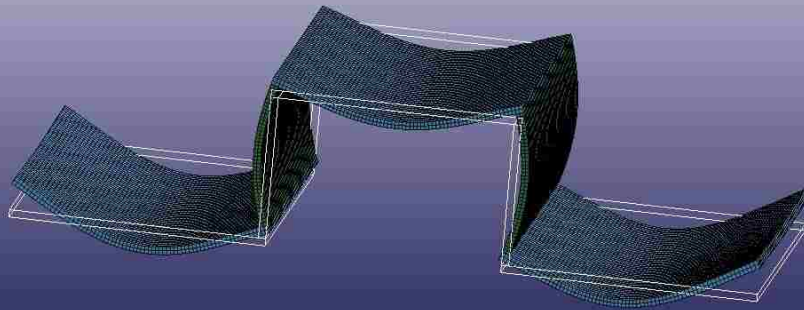
LS-DYNA eigenvalues at time 1.00000E-0  
Freq = 493.3



LS-DYNA eigenvalues at time 1.00000E-0  
Freq = 1217.4



LS-DYNA eigenvalues at time 1.00000E-0  
Freq = 1423.1



## REFERENCES

- [1] Pepper, Darrel W., & Heinrich, Juan C. (2006). *The Finite Element Method: Basic Concepts and Applications* (2<sup>nd</sup> Ed.). Boca Raton, FL: CRC Press.
- [2] Mallik, P.K. (2008). *Fiber-Reinforced Composites* (3<sup>rd</sup> Ed.). Boca Raton, FL: CRC Press.
- [3] Kumarwamy, Karpanan K. (2010). *Experimental and Numerical Analysis of Structures with Bolted Joints Subjected to Impact Load*. (Doctoral Dissertation). University of Nevada Las Vegas
- [4] Doppala, Karthik. (2005). *Experimental and Finite Element Studies of Shock Transmission of Jointed Hat Sections*. (Master's Thesis). University of Nevada Las Vegas
- [5] Fegghi, Masoud. (2007). *Experimental and Finite Element Studies of Shock Transmission Through Bolted Joints*. (Doctoral Dissertation). University of Nevada Las Vegas
- [6] Semke, William H., Bidel, George D., Jerath, Sukhvarsh, Gurav, Sanjay B., & Webster, Adam L. (2006). Efficient dynamic structural response modeling of bolted flange piping systems. *International Journal of Pressure Vessels and Piping*, 83(1), 767-776.
- [7] Kim, Jeong, Yoon, Joo-Cheol, & Kang, Beom-Soo (2007). Finite element analysis and modeling of structure with bolted joints. *Applied Mathematical Modelling*, 31(1), 895-911.
- [8] Stocchi, C., Robinson, P., & Pinho, S.T. (2012). A detailed finite element

investigation of composite bolted joints with countersunk fasteners. *Composites Part A: applied science and manufacturing*.

<http://dx.doi.org/10.1016/j.compositesa.2012.09.013>

- [9] Croccolo, D., De Agostinis, M., & Vincenzi, N. (2011). Failure analysis of bolted joints: Effect of friction coefficient in torque-preloading relationship. *Engineering Failure Analysis*. 18(1), 364-373.
- [10] Ishikawa, T., & Chou, T. W. (1982). Stiffness and strength behavior of woven fabric composites. *Journal of Material Science*. 17(1), 3211-3220.
- [11] Naik, N.K., & Shembekar, P.S. (1992) Elastic Behavior of Woven Fabric Composites: I-Lamina Analysis. *Journal of Composite Materials*. 26(1), 2196-2225
- [12] Hallal, Ali, Younes, Rafic, Fardoun, Farouk, & Nehme, Samer (2012). Improved analytical model to predict the effective elastic properties of 2.5D interlock woven fabrics composite. *Composite Structures*. 94(1), 3009-3028
- [13] Abot, J.L., & Daniel, I.M. (2004). Through-thickness Mechanical Characterization of Woven Fabric Composites. *Journal of Composite Materials*. 38(1), 543-553
- [14] Millet, J.C.F., Bourne, N.K., Meziere, Y.J.E., Vignjevic, R., & Lukyanov, A. (2007). The effect of orientation on the shock response of a carbon fibre-epoxy composite. *Composites Science and Technology*. 67(1), 3253-3260
- [15] Zaretsky, E., deBotten, G., Perl, M. (2004). The response of a glass fibers

- reinforced epoxy composite to an impact loading. *International Journal of Solids and Structures*. 41(1), 569-584
- [16] Lukyanov, A.A. (2010). An equation of state of a carbon-fibre epoxy composite under shock loading. *The European Physical Journal B*. 74(1), 35-45
- [17] Allix, Olivier, Dommangeat, Michel, Gratton, Michel, & Hereil, Pierre-Louis (2001). A multi-scale approach for the response of a 3D carbon/carbon composite under shock loading. *Composites Science and Technology* 61(1), 409-415
- [18] Marshall, I.H., Arnold, W.S., & Wood, J. (1989). Observations on Bolted Connections in Composite Structures. *Composite Structures* 13(1), 133-151
- [19] ASTM Standard D792, 1991, “Density and Specific Gravity (Relative Density) of Plastics by Displacement”, ASTM International, West Conshohocken, PA, 1991, DOI: 10.1520/D0792-08, [www.astm.org](http://www.astm.org).
- [20] Hashin, Z. (1965). On Elastic Behavior of Fiber Reinforced Materials of Arbitrary Transverse Phase Geometry, *Journal of Mechanics of Physical Solids* 13, 119-134
- [21] Bendat, & Piersol (2000). *Random Data Analysis and Measurement Procedures* (3<sup>rd</sup> Ed.). Wiley.
- [22] Livermore Software Technology Co, “LS-DYNA Keyword User’s Manual: Volume 1 Version 971”, Livermore Software Technology Co, May 2007.

VITA

Graduate College  
University of Nevada, Las Vegas

Eldon Goddard

Degrees:

Bachelors of Science, Mechanical Engineering, 2009  
University of Nevada, Las Vegas

Work History:

Test Engineer, November 2013 - Present  
Norgren Kloehn

Graduate Assistant, August 2010 – May 2012  
University of Nevada, Las Vegas

Mechanical Engineering Intern, August 2009 – December 2009  
Arcata Associates

Certifications, Honors, and Awards:

Nevada E.I. Certified  
Member Tau Beta Pi Honors Society  
1<sup>st</sup> Place Senior Design M.E.